The Dissertation Committee for Apolonio Aguilar certifies that this is the approved version of the following dissertation:

The Synthesis and Anion Binding Studies of Scorpiand-Type Calix[5]- and Calix[10]phyrins as well as a Cryptand-Like Bicyclic Calix[15]phyrin System

Committee:

_____
Jonathan L. Sessler, Supervisor

_____
Eric V. Anslyn

_____
Jennifer S. Brodbelt

_____
Rick Russell

_____
Carlton Grant Willson

The Synthesis and Anion Binding Studies of Scorpiand-Type Calix[5]- and Calix[10]phyrins as well as a Cryptand-Like Bicyclic Calix[15]phyrin System

By

Apolonio Aguilar, B.S.; M.A.

Dissertation

Presented to the Faculty of the Graduate School of
The University of Texas at Austin
in Partial Fulfillment
of the Requirements
for the Degree of

Doctor of Philosophy

The University of Texas at Austin

December, 2016

Dedication

To Mom

Acknowledgements

First and foremost, I would like to thank my supervisor Prof. Jonathan L. Sessler for his generous support over the years and for giving me the opportunity to continue this work. It has been a great challenge and it is only because of his moral support that I have been able to reach this point. Jon, I'll always be in your debt!

The Synthesis and Anion Binding Studies of Scorpiand-Type Calix[5]- and Calix[10]phyrins as well as a Cryptand-Like Bicyclic Calix[15]phyrin System

Apolonio Aguilar, Ph.D.

The University of Texas at Austin, 2016

Supervisor: Jonathan Lawrence Sessler

The field of anion recognition in supramolecular chemistry has grown significantly in the past decade. The design challenges that are faced in targeting and sensing anions require a greater level of sophistication than is needed for cations. This reflects the greater diversity in geometry, directionality and lower charge density of the larger anions. Many of the existing systems for anion sensing are designed to wrap around the anion creating many points of contact. Some receptors are preorganized while others are more flexible. Often a balance between competing factors is needed to obtain high specificity. An important aspect of anion recognition is sensing, wherein the binding event triggers a change that can be readily monitored. Having a good receptor is again critical. This dissertation presents a set of pyrrole-based macromolecules related

to the calix[n]phyrins that interact with guest anions via hydrogen bonding interactions that extend beyond one plane, electrostatic attraction from protonation, and pi-anion interactions. Of the anions tested with the hosts reported in this dissertation, the sulfate anion proved to be bound most strongly. It also produced distinct colorimetric changes that were visible to the naked eye.

Table of Contents

List of Tables

List of Figures

Chapter 1: Introduction

1.1 Overview of anion binding challenges

Anion recognition has moved from being solely of academic interest to a fundamental pillar of supramolecular chemistry with applications in many areas, including sensing, extraction, transport through lipid bilayers, molecular assemblies and organocatalysis.[1] The challenges facing anion recognition differ from metal binding in that anions have a greater variation in geometries, with spherical, linear, trigonal planar, tetrahedral and octahedral shaped anions all being known. Anions are also generally larger than the isoelectronic cations and therefore require the design of larger hosts. This also means they have lower charge-to-radius ratios and weaker electrostatic interactions with most hosts. Additionally, anions have relatively high hydration energies. This is reflected in the Hofmeister series[2] which is a ranking based on their effect on the solubility of proteins. This series correlates well with the hydrophobicity of the anions and consequently to the ease with which they dissolve in organic solvents. The least hydrophobic anions in the series are the fluoride and sulfate anions and move down through hydrogen phosphate, acetate, chloride, nitrate, bromide, and perchlorate to name a few. The Hofmeister bias refers to the idea that during extraction from water to an apolar solvent, a poorly solvated anion, such as perchlorate, is more easily extracted than a highly solvated hydrophilic anion, such as sulfate. This creates a greater challenge in the extraction of hydrophilic anions, such as sulfate.

Anion extraction requires an electroneutral process and so charge neutrality must be maintained with co-transfer of a cation, which may be a metal or a proton. Often the hosts act as ditopic receptors that can also complex to a metal ion or which have basic nitrogen atoms that may be protonated.

Variations in properties of anions such as geometry or shape, differences in charge density and even basicity can be used to design selective hosts. Ideally hosts can be prepared that are tuned to a given, targeted anionic guest. To bind anions, the hosts are typically designed to use hydrogen bonding in combination with electrostatics (ion pairing) and anion-π interactions. In addition to binding affinity and selectivity, a signaling unit must be included for the sensing and potentially quantification of anionic guests. The growth of the field has led to the development of several strategies to address these requirements.

1.2. Strategies of recognition of fluoride anion.

Selective sensors for fluoride, a popular anion binding guest, take advantage of the basicity of the anion to form strong hydrogen bonds or deprotonate the host sensor. This can result in a signal in the form of an optical response. Examples of such hosts include the work of Bose and Ghosh who use indole-conjugated urea/thiourea ligands **1-3** (Figure 1.1) as sensors.[3,4] These hosts undergo a deprotonation resulting in an anion that is delocalized along the ligand. Another sensor for fluoride was developed by Davidson; it uses the bis(bora)calixarene **4** as a selective, bidentate, fluorescent fluoride

sensor.[5] Here, the Lewis acidic nature of the boron center and the preorganization of the calixarene results in the selective binding of fluoride.

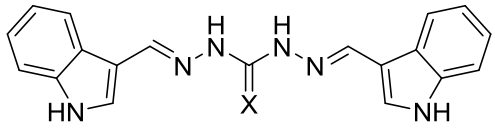

1 X = S
2 X = O
3 X = NH_2Cl

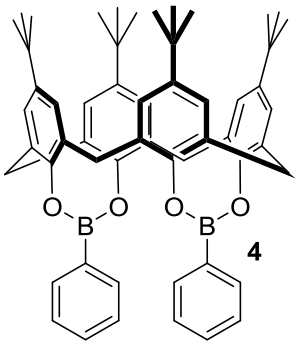

4

Figure 1.1. Sensors for fluoride.

1.3. Strategies for the recognition of phosphate containing anions.

Another strategy has been used by Bencini et al. for the selective binding of the phosphate-containing anions.[6] In competitive experiments at varying pH, the phenanthroline-containing polyammonium receptor **5** (Figure 1.2) was found to bind ATP selectively among other polyphosphate-containing biological molecules. A combination of electrostatic attractions and hydrogen bonding interactions involving the anion and the phenanthroline provided fluorescence signaling for the binding event. Fluorescent imidazolium receptors have also been used as effective sensors for dihydrogenphosphate. Yoon, et al. have used electrostatic attractions between positively charged imidazolium ions and C—H hydrogen bonding in **6** to capture these anions. According to the authors, ab initio calculations provided support for the

conclusion that the binding selectivity toward $H_2PO_4^-$ reflects the rigidity of the framework of the receptor.[7]

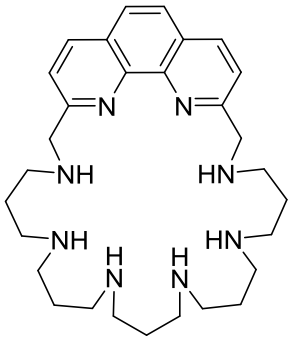

5

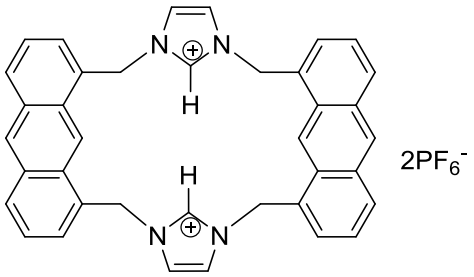

6

Figure 1.2. Binding the phosphate anion through multiple hydrogen bonding and electrostatic interactions.

The work of Espinoza demonstrates a different approach to anion binding. Using an open chain system and strong hydrogen bond donors in the form of urea groups they created bis(carbazolyl)urea receptors such as **7** in Figure 1.3 and showed they permitted the selective recognition of hydrogenpyrophosphate in aqueous media.[8]

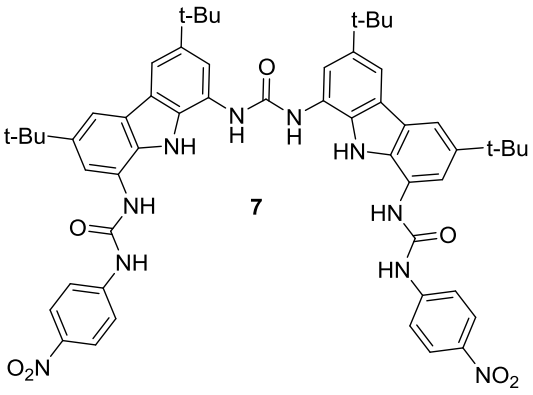

7

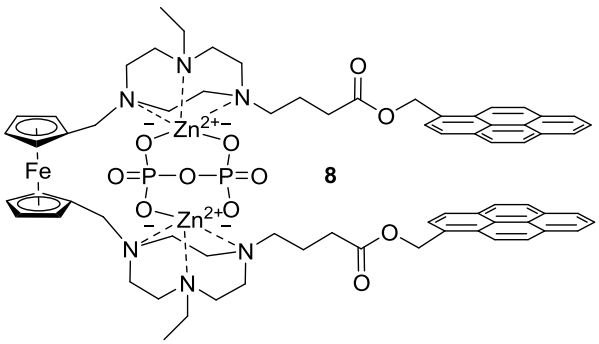

8

Figure 1.3. Binding anions with multiple hydrogen bonds and metal centers.

Another strategy involves including metal centers in the host so as to maintain the charge neutrality of the complex. The ferrocene based receptor **8** functionalized with two Zn^{II}(TACN)(pyrene) subunits (Figure 3), developed by Bond and Spiccia, can bind pyrophosphate and other polyphosphate nucleotides. The binding event gives rise to a conformational change where the two fluorescent pyrene units shift from a trans-like to a cis-like conformation. This promotes interaction between the pyrene units and results in an enhancement in the excimer emission.[9]

1.4. Strategy for the recognition of the nitrate anion.

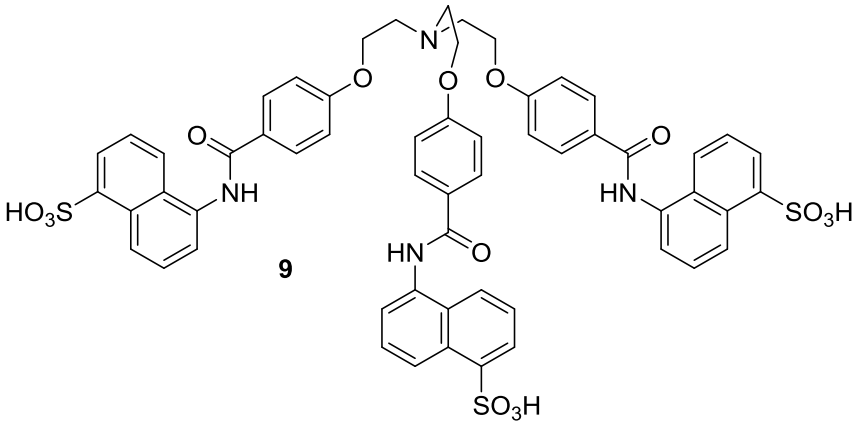

9

Figure 1.4. Tripodal dansyl sensor for nitrate.

One of the few receptors developed for the nitrate anion is a tripodal podand bearing amide functionality **9** developed by Sun.[10] Upon protonation, the tripod adopts in situ a cone-shaped conformation through hydrogen bonding and C—H···π interaction. The preorganized cavity is capable of binding the target nitrate anions through N—H

bonds. The incipient negative charge is accommodated by deprotonation of a dansyl group. The sensing is effected via quenching of the fluorescence emission.

1.5. Strategies using assemblies with a reporter molecule.

An alternative strategy to incorporating a reporter molecule into an anion binding host is to use an indicator that is competitively displaced by the guest anion resulting in an optical signal. This strategy was pioneered by Anslyn and co-workers in the development of an indicator displacement assay (IDA) for citrate using the tripodal receptor **10** containing three guanidinium groups as shown in Figure 5. Displacement of the 5-carboxyfluorescein dye **11** by citrate to form complex **12** resulted in a change in the fluorescence of the displaced dye.[11]

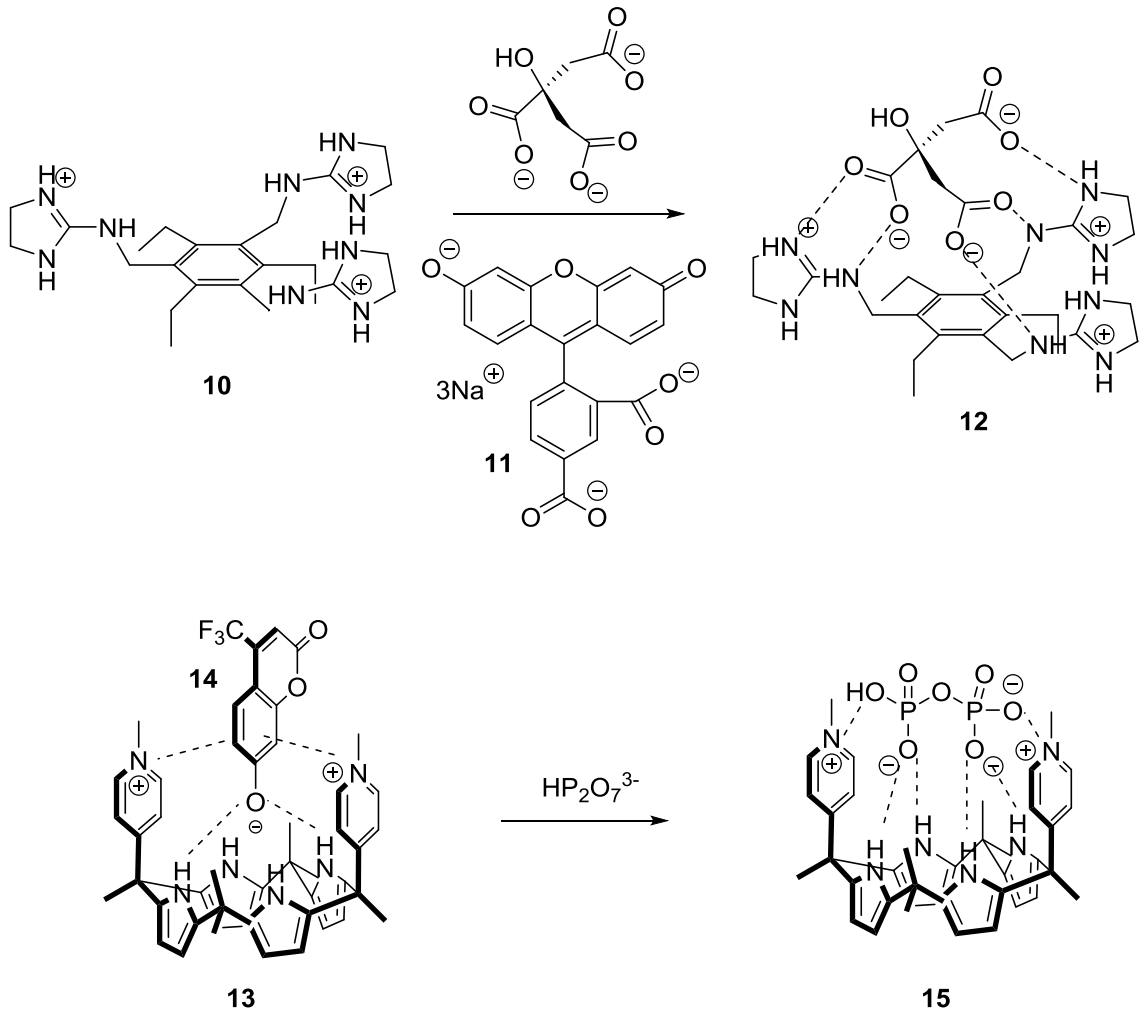

Figure 1.5. Supramolecular assemblies for citrate and pyrophosphate sensing.

Sessler and co-workers reported a similar strategy using a dicationic calix[4]pyrrole derivative **13** for the selective recognition of pyrophosphate using a displacement based assay.[12] The pyrophosphate displaced the anionic dye **14** resulting in increased fluorescence emission. Color changes detectable by the naked eye were also observed.

1.6. Sulfate selective hosts and extractants.

The importance of selective separation of the sulfate anion from nuclear waste has been noted by Moyer and co-workers.[13] Its removal would potentially result in improved vitrification, reduced waste-form volume, higher waste-form performance, all of which would lead to potential cleanup schedule acceleration and cost savings. The liquid-liquid extraction of sulfate is especially challenging given the high hydration energy of this dianion (-1090 kJ/mol). By way of reference, the hydration energies of the nitrate and chloride anions are -306 kJ/mol and -374 kJ/mol respectively.[14] As noted above, this difference is qualitatively reflected in the Hofmeister bias, an effect that correlates with the hydrophobicity of most anions.[2]

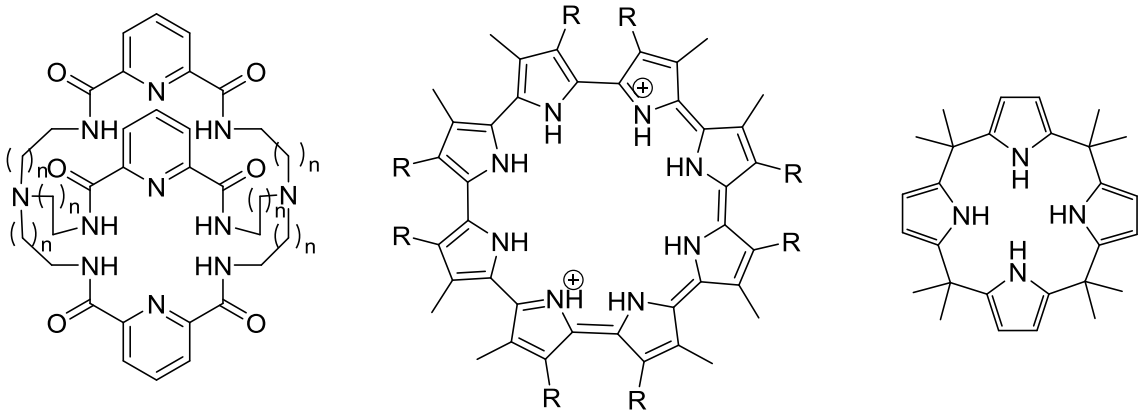

16
n = 2

17a R = C_2H_5
17b R = $C_{11}H_{20}$

18

Figure 1.6. Cryptand and macrocycles for sulfate binding.

Sulfate binding requires a relatively large number of hydrogen bond donors and benefits from electrostatic stabilization that can be achieved by protonation of a basic

unit on the host. Two major classes of hosts have emerged that can meet these requirements. The two groups are 1) macrocyclic polyaza and polyamide receptors and 2) calixpyrroles and polypyrrole macrocycles.[13] Figure 1.6 shows representative members of these two receptor classes. The diprotonated bicyclic host **16** can encapsulate the sulfate anion and crystallizes as the sulfate salt with seven hydrogen bonds to the sulfate. The binding is higher than for its smaller analogues presumably because of the larger more flexible cavity.[15] The cyclo[8]pyrrole **17a** very neatly forms eight hydrogen bonds to sulfate but it suffers from poor solubility in organic solvents. The analogue **17b** has much better solubility and can extract sulfate from solution but it suffers from slow exchange kinetics.[16] The calixpyrrole **18** was shown to crystallize with tetramethylammonium sulfate where there are four hydrogen bonds from the pyrroles to one of the sulfate oxygen atoms. There is, however, extra stabilization of the complex resulting from interactions of the tetramethylammonium ion with the cone-like portion of the calixpyrrole.[17]

Subsequent work using calixpyrroles resulted in improvements in sulfate binding and extraction. As a general rule, these advances came from appending additional hydrogen bonding units to the core to create receptors such as the bipyrrole strapped calixpyrrole **19**.[18] A highly efficient sulfate extractant was developed by Wu using the tripodal hexaurea **20**.[19] The crystal structure of the latter sulfate complex revealed that all six ureas are hydrogen bonded to the sulfate anion to give a total of twelve hydrogen bonds.

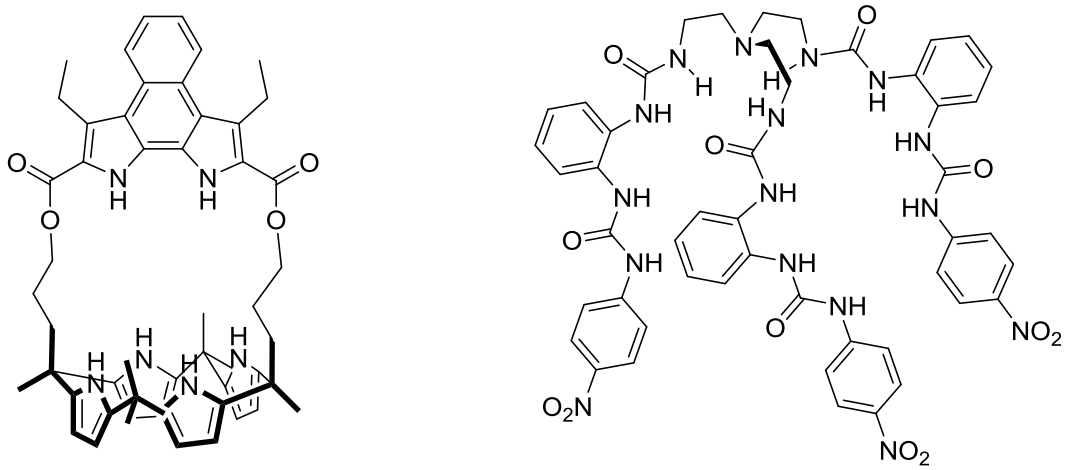

19 **20**

Figure 1.7. Strapped calixpyrrole and a tripodal hexaurea for sulfate binding.

1.7. Calixphyrins and anion binding.

A relatively unexplored class of pyrrole macrocyclic compounds are the so-called calix[n]phyrins. These are a hybrid of the calixpyrroles containing sp^3 hybridized *meso*-carbons and the porphyrins that have sp^2 hybridized *meso*-carbons. Nomenclature includes the number of pyrrole rings in the macrocycle, n, in square brackets such as calix[n]phyrin.[20] This is followed by a set of numerals in brackets. The number of numerals refers to the number of pyrroles in the macrocycle. Each individual number indicates the amount of *meso*-atoms. One starts with the highest order sp^2-center and continues in the direction of in which the nearest sp^2-center lies. Bold numbers designate sp^2 hybridised *meso*-carbons, whereas italicized numbers refer to the sp^3 centers. Examples are given in the Figure 1.8.

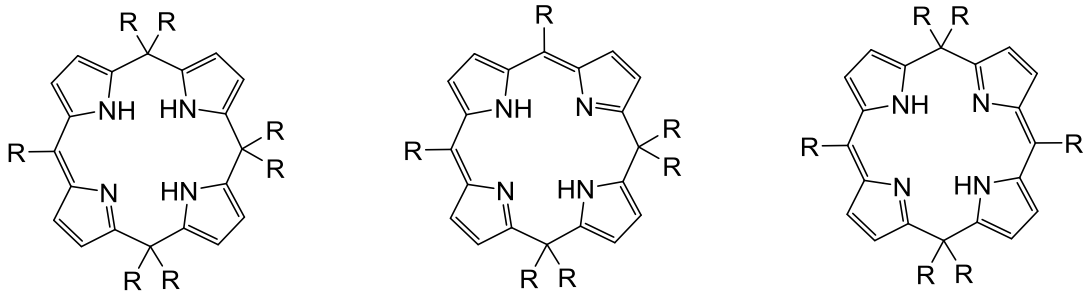

Figure 1.8. Examples of calix[n]phyrin nomenclature.

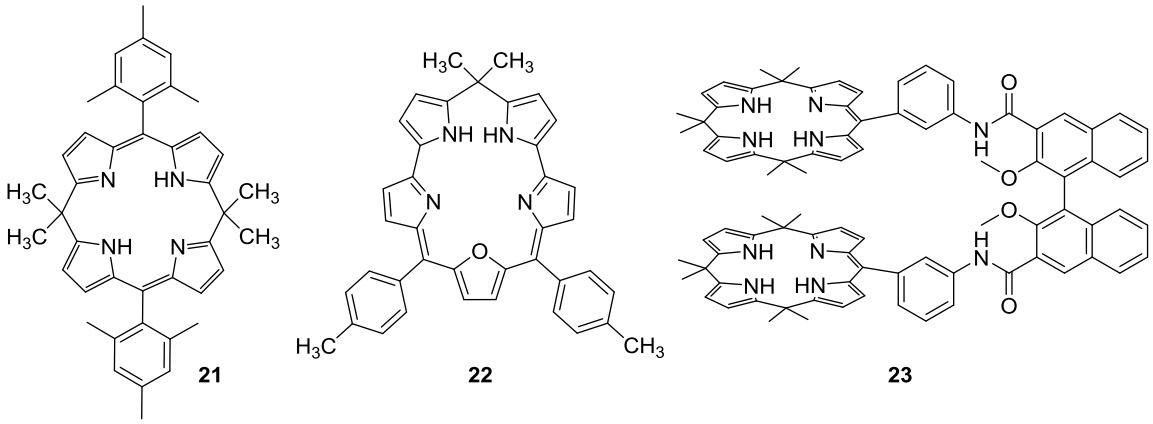

Figure 1.9. Cailx[n]phyrins developed for anion binding.

It was reported by Sessler and co-workers that the calixphyrin **21** was able to bind anions when treated with tetrabutylammonium salts as inferred from changes in the UV-vis spectra in dichloromethane.[21] Another calixphyrin, the calixoxasmaragdyrin **22**, exhibited specific sensing ability for the hydrogen sulfate anion in chloroform.[22] This receptor showed selectivity over other anions. In contrast the corresponding calixthiasmaragdyrin was not effective in binding anions. A chiral calix[4]phyrin **23** was synthesized by Bernatkova et al. Potentiometric studies revealed moderate

discrimination between the poly-oxygenated D and L enantiomers of malic acid.[23] It is the view of the author that anion binding properties of the calix[n]phyrins warrant further investigation since there may be opportunities to improve their anion recognition capabilities by appending additional anion binding groups to the ring structures.[24]

1.8. Cryptands and anion binding.

Cryptands are three dimensional topographically non-planar structures that have long been of interest due to their ability to achieve high specificities and substrate binding affinities due to extensive receptor-substrate contacts. Ideally, cryptands can "sense" variations in the molecular size, shape, and architectures of the targeted substrates. These properties may be synthetically fine-tuned by varying of the cryptand. If cryptand-like receptor molecules are membrane soluble, they may even serve as carrier molecules, rendering membranes permeable to various charged guests.[25]

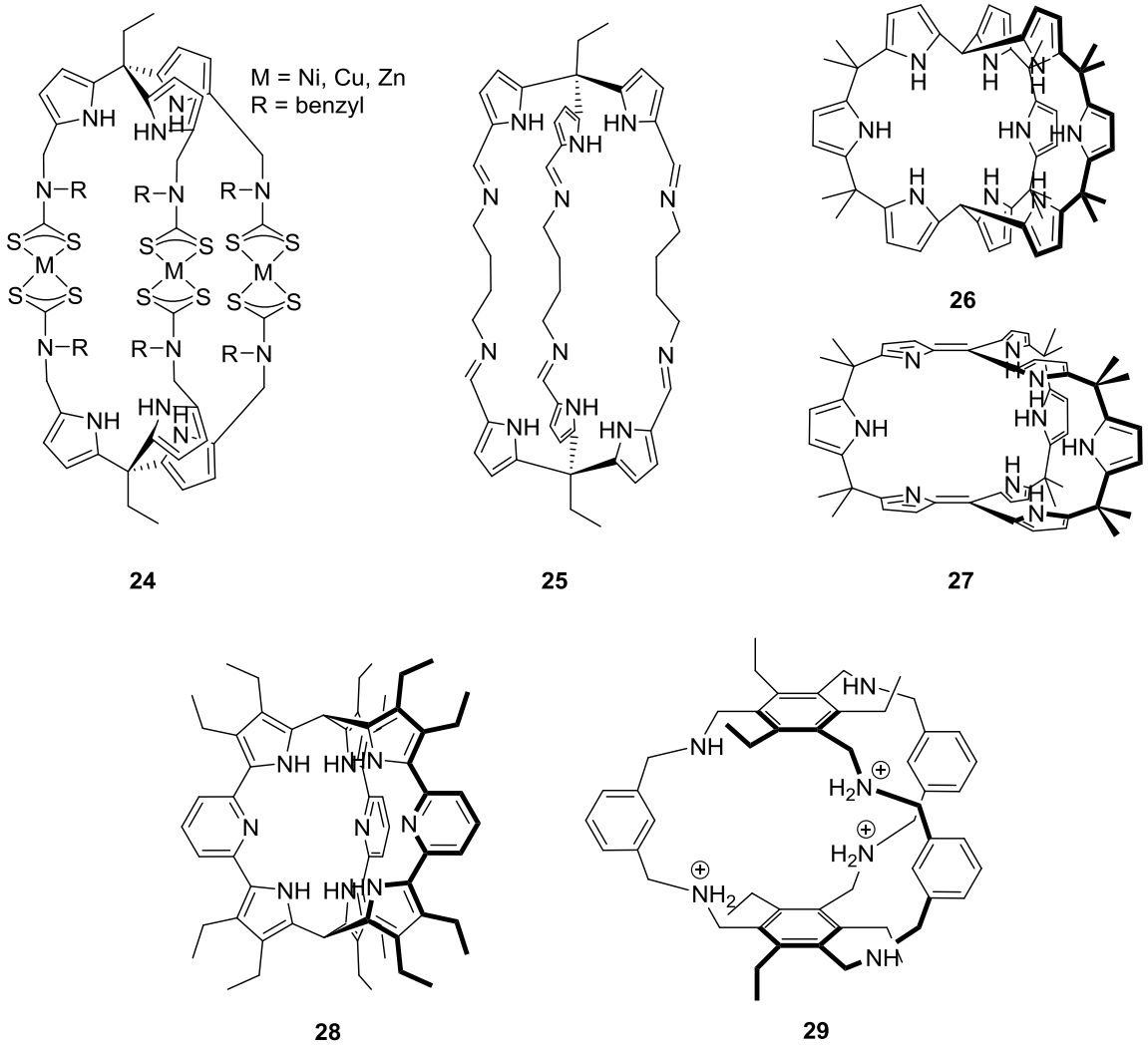

Figure 1.10. Cryptands and anion binding.

Some pyrrole based cryptands such as **24** rely on a tripyrrolylmethane subunit as a precursor.[26] Early examples of such cryptands were found to interact with anions, something that could be followed using cyclic voltammetry. Interactions were observed with benzoate, chloride and dihydrogen phosphate. Unfortunately, the ^{1}H NMR spectra for the metallo-cryptands of structure **24** proved complex and very broad, making this technique unsuitable for measuring the binding constants. Moreover, characterization

was only accomplished using high resolution mass spectrometry. The same tripyrrolylmethane was used in the synthesis of the bis(tripyrolyl) cryptand **25**.[27] The synthesis of these iminic cryptands involved the condensation of the triformyl derivative of the tripyrrolylmethane and various diaminoalkanes. The diaminic precursors were encapsulated in the cavities as was seen in the crystal structures of the complexes. The tripyrrolyl methane has also been used in the Sessler group to synthesize a cryptand analogue of calixpyrrole. The species in question, compound **26**, was found to bind fluoride, albeit not completely within the cavity. In fact, only two of the bridging cryptand arms were found to coordinate the fluoride anion (via six N-H hydrogen bonds), while three of the remaining pyrroles were uninvolved in binding, at least in the solid state.[28] Subsequently, cryptand **26** was treated with DDQ to obtain the oxidized compound **27**, shown in Scheme 9.[29] The dipyrrylpyridine-derived cryptand **28** demonstrated homotropic positive allostery in the binding of carboxylic acids, presumably due to changes in basicity and acidity of the adjacent pyridine and pyrrole moieties upon binding. [30] The hexaazacryptand **29** was synthesized by Delgado and co-workers and was shown to encapsulate sulfate within the cavity.[31]

1.9. Intended approach to anion binding.

In general, topographically non-planar structures are useful in molecular recognition. This principle is well established in the case of charged anion receptors thanks to seminal early contributions by Lehn,[32-37] Martell,[33,38,39] and Schmidtchen.[40-42] It is less established for neutral receptors. Existing anion receptors are structurally linear

or tripodal compounds. They can encapsulate their guests while benefitting from some structural preorganization. Most cyclic hosts are not fully planar and often use appended groups to improve the interaction with the guests. Our work builds on the results of calix[n]phyrins and cryptands for binding anions.

Chapter 2

2.1. Cryptand Precursors.

The tripyrrolylmethane building block was envisioned as a good precursor for cryptand-like molecules. These potential intermediates may be obtained by the reaction of pyrroles with an orthoester. Preliminary experiments revealed that β-substituted pyrroles were too sterically hindered to form the desired tripyrrolylmethane product. Consequently, β-unsubstituted pyrroles were used in this work. These kinds of pyrroles were thus condensed with triethyl orthorformate and triethyl orthopropionate; however, both resulting products (**30a** and **30b**, respectively c.f. Figure 2.1), proved to have poor solubility upon subsequent formylation. Trimethyl orthovalerate provided a butyl group at the bridging carbon and the resulting formylated tripyrrolyl compound was found to have adequate solubility in organic solvents. Formylation at the α-positions was effected using Vilsmeier-Haak conditions giving 5,5',5''-(pentane-1,1,1-triyl)tris(1H-pyrrole-2-carbaldehyde) **30c** as a specific product.

The objective of this work was the design of a chemosensor that could selectively bind to an anionic guest molecule while at the same time give a colorimetric indication of the binding event that is visible to the naked eye. For this purpose, the α,α-linked oligopyrroles serve as useful building blocks for cryptand-like structures. Based on the design, these products were not expected to be aromatic. However, they

were expected to retain conjugation giving rise to absorbance in the visible region of the electromagnetic spectrum.

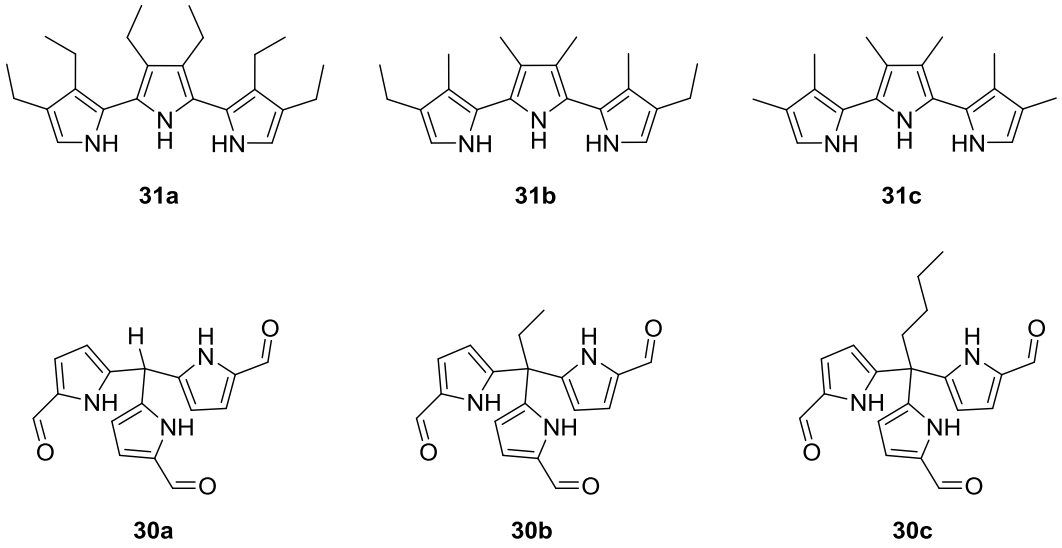

Figure 2.1. Trialdehyde and terpyrrole precursors.

α,α-Linked terpyrroles were envisioned as the other set of building blocks. These linear fragments were expected to react with the trialdehyde **30c** to yield conjugated systems containing at least five pyrroles. Initially the all β-ethyl substituted (**31a**) and methyl ethyl substituted (**31b**) terpyrroles were used. This relatively high degree of substitution imparted greater solubility to the precursors and to the products. However, it also increased the complexity of the ^{1}H-NMR spectra of the products and made characterization more difficult. Since characterization ultimately proved to be one of the greatest challenges of the project, a decision was made to use 3,3',3'',4,4',4''-hexamethyl-1H,1'H,1''H-2,2':5',2''-terpyrrole **31c** as the key terpyrrole precursor despite its relatively poor solubility.

2.2. Condensation of terpyrrole with trialdehyde.

The overarching goal of this project was to prepare the topographically non-planar cryptand-like structure **32**. In theory, this target would have the ability to encapsulate guests selectively within the three pentapyrrolic bridging arms. A total of nine hydrogen bond donors and six potential protonation sites would be available to accommodate and stabilize anions in non-polar solvents.

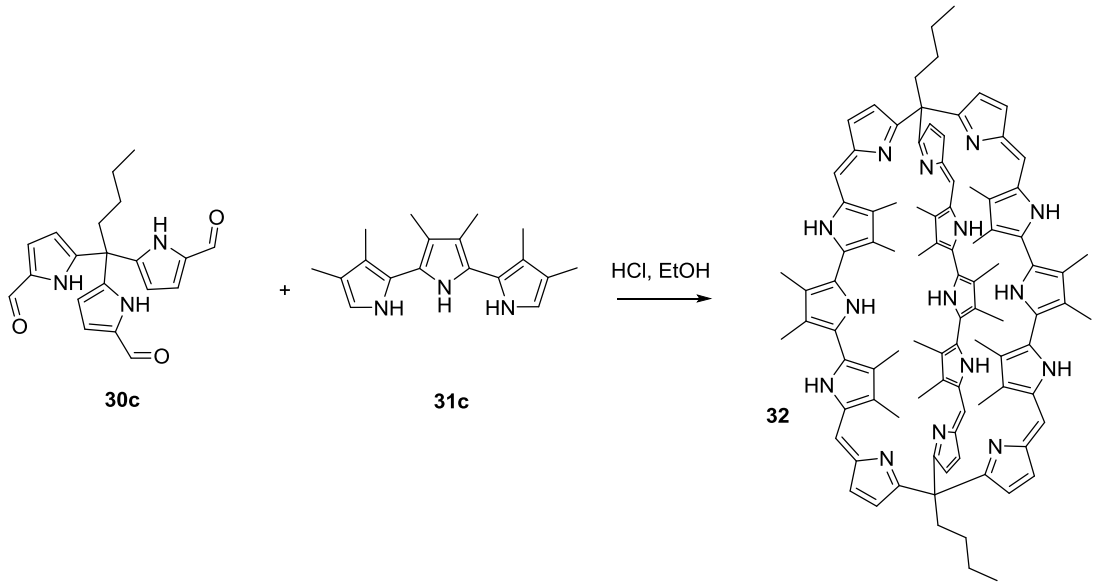

Figure 2.2. Reaction of trialdehyde **30c** with terpyrrole **31c** to form cryptand **32**.

The reagent stoichiometry expected to favor formation of compound **32** is a 1.5:1 (terpyrrole **31c** to trialdehyde **30c**) ratio. Both reagents were dissolved with stirring in ethanol that had been bubbled with nitrogen for two hours to make a 1 mmol solution of the terpyrrole **31c** and 0.67 mmol of trialdehyde **30c**. Because of solubility considerations, the trialdehyde **30c** was first dissolved in a minimum amount of

dichloromethane. This solution was then added to ethanol. The concentrated hydrochloric acid (used as a catalyst) was added dropwise to the reaction mixture to make a 0.05 M solution in ethanol and stirred at room temperature for 2 hours. Upon addition of the acid catalyst, the reaction mixture turned very dark blue. Mass Spectrometric analysis of the crude mixture revealed the formation of the desired product as the major ion peak in the spectrum.

2.3. Identification, isolation and purification of products.

Motivated by the mass spectrometric result, the mixture was taken through purification procedures on silica gel with traditional eluent systems including ethyl acetate / hexanes, methanol / dichloromethane. However, no success in separation was obtained due to the dark coloration of the material and broad streaking over the column. The use of neutral and basic alumina, as well as spiking of the eluent with triethylamine as a means of avoiding protonated mixtures of the compounds did not lead to effective separation. Silica gel based preparatory plates were also tried. Initially this latter method appeared to have separated darker bands of material from the reaction mixture. These bands were collected and extracted. Unfortunately, the ^{1}H-NMR spectra in chloroform-*d* and pyridine-d_5 revealed no discernible peaks. Instead broad bands were observed in the expected spectral regions. In DMSO-d_6 two signals ascribable to the β-hydrogens were discernible along with the broad features. However, variable temperature NMR spectral studies in DMSO at 27 °C and 100 °C did not result in resolution of the ^{1}H-NMR signals.

Despite the challenges in using ^{1}H-NMR spectroscopy, analytical LCMS and high resolution mass spectrometry of the fractions isolated from flash chromatography on silica gel allowed for the identification of three fractions with m/z = +1438.82, two of which were confirmed by HRMS and one fraction of m/z = +1193.66. The LCMS profile in Figure 2.3 shows the distribution of components with the indicated masses.

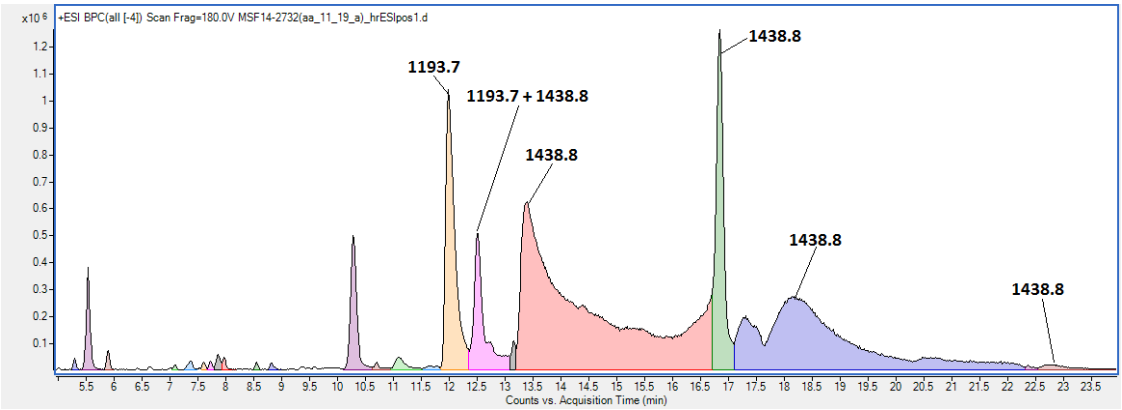

Figure 2.3. LCMS profile of the crude reaction products from reaction attempt aa_11_19 showing all ion peaks.

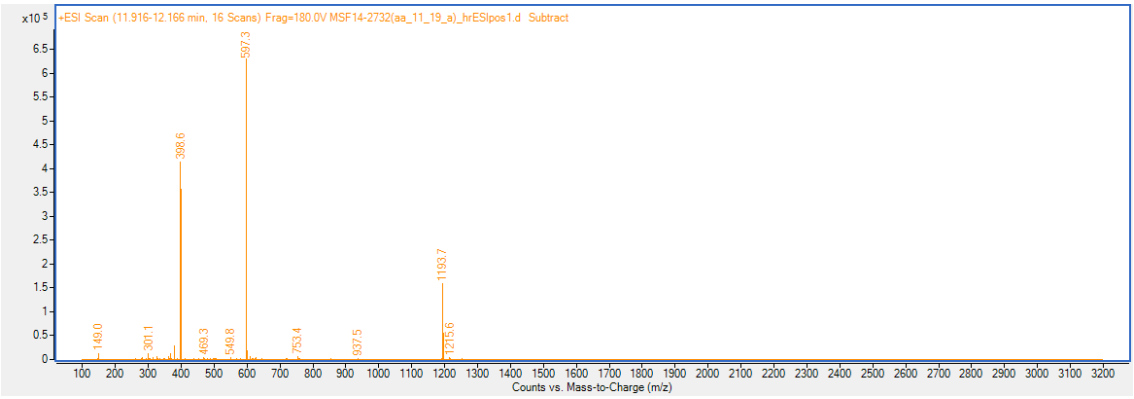

Figure 2.4. The peak highlighted in orange (elution time 11.916-12.166 min) contains a compound of mass 1193.7, a value that corresponds to a [2+2] adduct. Note that $[MH]^{+}$ = 1193.7, $[MH_2]^{2+}$ = 597.3, and $[MH_3]^{3+}$ = 398.6.

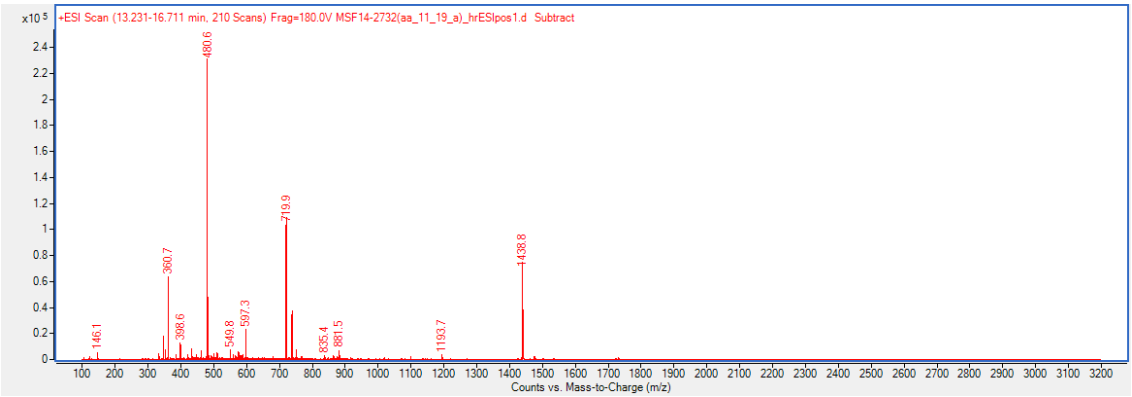

Figure 2.5. The region highlighted in pink (elution time 13.231-16.711 min) contains a compound of mass 1438.8, a value that corresponds to a [3+2] adduct. Note that $[MH]^{+}$ = 1438.8, $[MH_2]^{2+}$ = 719.9, and $[MH_3]^{3+}$ = 480.6.

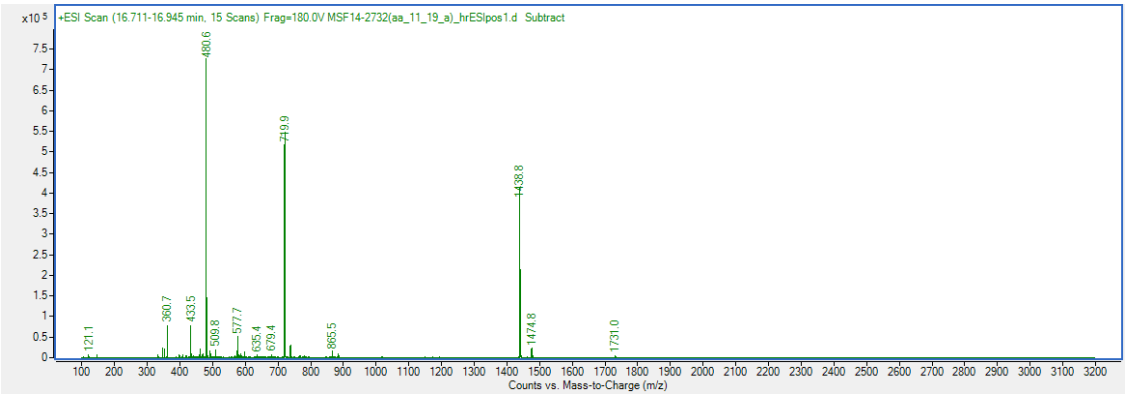

Figure 2.6. The region highlighted in green (elution time 16.711-16.945 min) contains a compound of mass 1438.8, a value that corresponds to a [3+2] adduct. Note that $[MH]^{+}$ = 1438.8, $[MH_2]^{2+}$ = 719.9, and $[MH_3]^{3+}$ = 480.6.

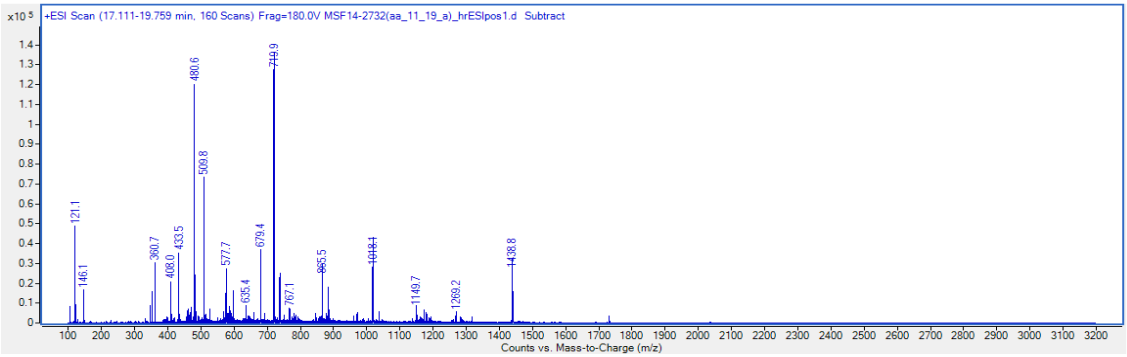

Figure 2.7. The region highlighted in blue (elution time 17.111-19.759 min) contains a compound of mass 1438.8, a value that corresponds to a [3+2] adduct. Note that $[MH]^{+}$ = 1438.8, $[MH_2]^{2+}$ = 719.9, and $[MH_3]^{3+}$ = 480.6. This fraction has more impurities.

Consequently, high performance liquid chromatography using a reverse phase (C-18) column was employed in an effort to purify the crude mixture. The neutral mixture had low solubility in acetonitrile/water, which limited the sample loading size. Additionally, there was no discrete separation of compounds observed on the HPLC trace due to streaking and overlap of compounds, something that could be observed even on analytical HPLC. As a result, large amounts of material were lost during these attempts at purification.

A recently introduced technology, recycling preparatory gel permeation chromatography HPLC was then tried. Chloroform was used as the eluent. The high solubility of the various products in chloroform and the differences in size between the discrete adducts and the presumed larger polymeric compounds allowed for effective separation using this new approach. Additionally, the method gave qualitative information on the relative sizes of the products and allowed for easier identification.

Using the recycling prep GPC-HPLC, we could separate out four major identifiable adducts of the reaction mixture in the form of their hydrochloride salts.

For the sake of convenience these will be referred to as [m+n] using the condensation ratio of terpyrrole **31c** (m) to trialdehyde **30c** (n) to define specific adducts. The purified adducts were identified by ESI positive mass spectrometry as the [6+4], [3+2], [2+2], and [1+1] products. The [6+4] and [3+2] gave rise to ions of m/z = +1438.8 corresponding to their $(MH_2)^{2+}$ and $(MH)^{+}$ ions, respectively, as confirmed by high resolution mass spectrometry. The product with an m/z = +1193.7 was identified as the $(MH)^{+}$ of the [2+2] adduct, while the fraction giving an MS peak at m/z = +597.3 corresponded to the $(MH_2)^{2+}$ ion of the [2+2] and the $(MH)^{+}$ ion of the [1+1] adducts. Proposed structures for these adducts are shown in Figures 2.8 and 2.10.

As can be seen by inspection of Figure 2.8, there are two possible isomers for the [3+2] adduct, the cryptand like structure **32** labelled [3+2]a, and a tethered bicyclic structure **33** labelled as [3+2]b. It can be reasonably proposed, by a cursory look at the products, that condensation of one terpyrrole with one trialdehyde results in an initial product that has two competing pathways to products. The first is an intramolecular condensation to afford the [1+1] product **35** and the second is an intermolecular reaction with either another terpyrrole or trialdehyde that can then proceed to give the [2+2] addition product **34**. The [1+1] and [2+2] adducts in solution can then serve as precursors to the two isomeric [3+2] adducts. Reaction of the [2+2] adduct with another

terpyrrole precursor affords the cryptand-like [3+2]a adduct **32**. Condensation of two of the [1+1] adducts with a terpyrrole would then be expected to give a [3+2]b adduct **33**.

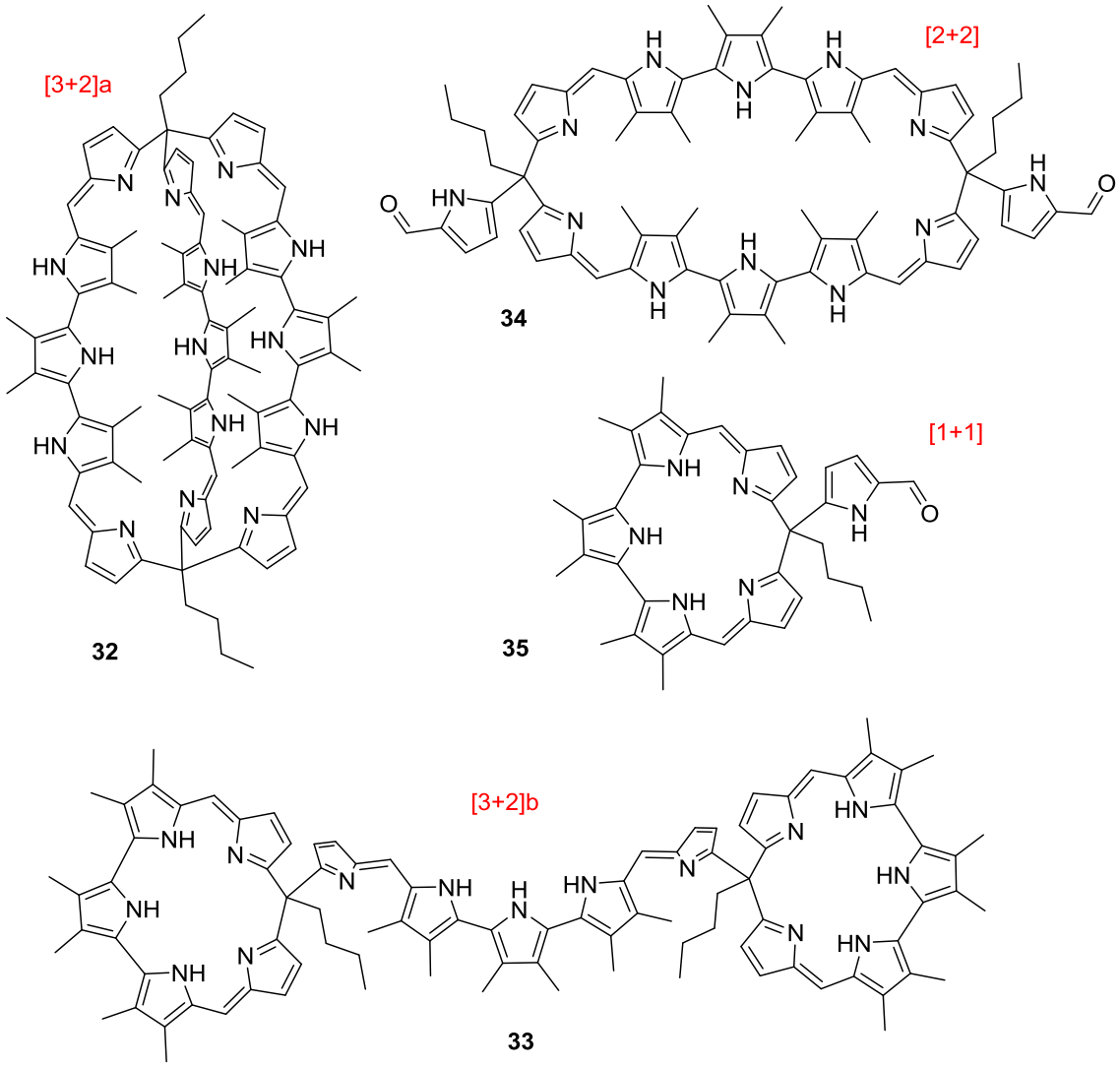

Figure 2.8. Proposed adducts obtained from the condensation of **30c** with **31c**.

In addition to the products shown in Figure 2.8, size exclusion chromatography revealed that some [6+4] adduct was formed. This adduct was isolated during the purification process and high resolution mass spectrometric analysis revealed what

could be its $(MH_2)^{2+}$ ion shown in Figure 2.9. The ^{1}H-NMR spectrum of the hydrochloride salt of this material contained discrete proton signals in the expected regions. However, these peaks come on top of poorly resolved bands, which might reflect fast conformational exchange. Two of several possible isomers for this adduct are shown in Figure 2.10 as [6+4]a derived from a [2+2] building block, and [6+4]b derived from a [1+1] building block. The relatively large [6+4] adduct may have interesting supramolecular properties. However, it has not yet been subject of study. Rather an effort was made to explore the features of the smaller adducts.

MS Spectrum Peak List

Obs. m/z	Calc. m/z	Charge	Abund	Formula	Ion/Isotope	Tgt Mass Error (ppm)
559.51720			140710.52			
1438.83110	1438.82810	2	3895.25	C188H198N30	(M+2H)+2	-2.12
1439.33510	1439.32960	2	6558.35	C188H198N30	(M+2H)+2	-3.85
1439.83310	1439.83110	2	8335.51	C188H198N30	(M+2H)+2	-1.35
1440.33670	1440.33270	2	5242.09	C188H198N30	(M+2H)+2	-2.82
1440.83810	1440.83420	2	3492.66	C188H198N30	(M+2H)+2	-2.68
1441.34440	1441.33570	2	1651.71	C188H198N30	(M+2H)+2	-6.03
1441.84340	1441.83730	2	984.22	C188H198N30	(M+2H)+2	-4.28

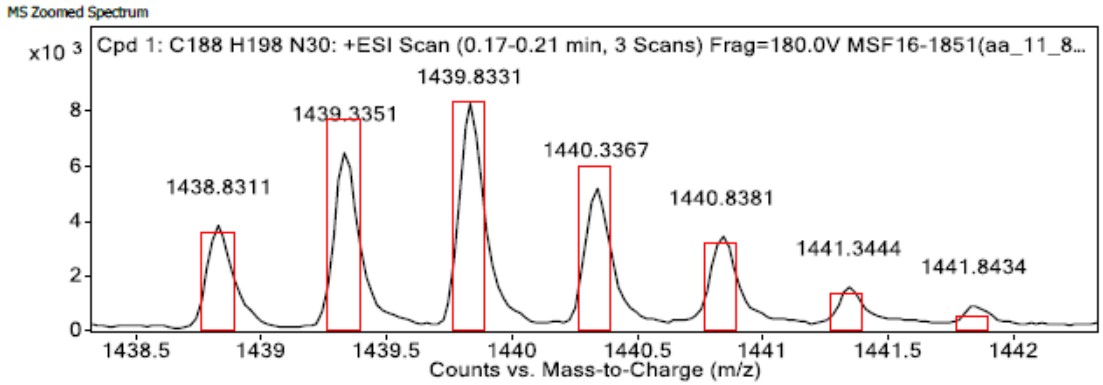

Figure 2.9. High resolution mass spectrometric results that provide support for the formation of a [6+4] adduct.

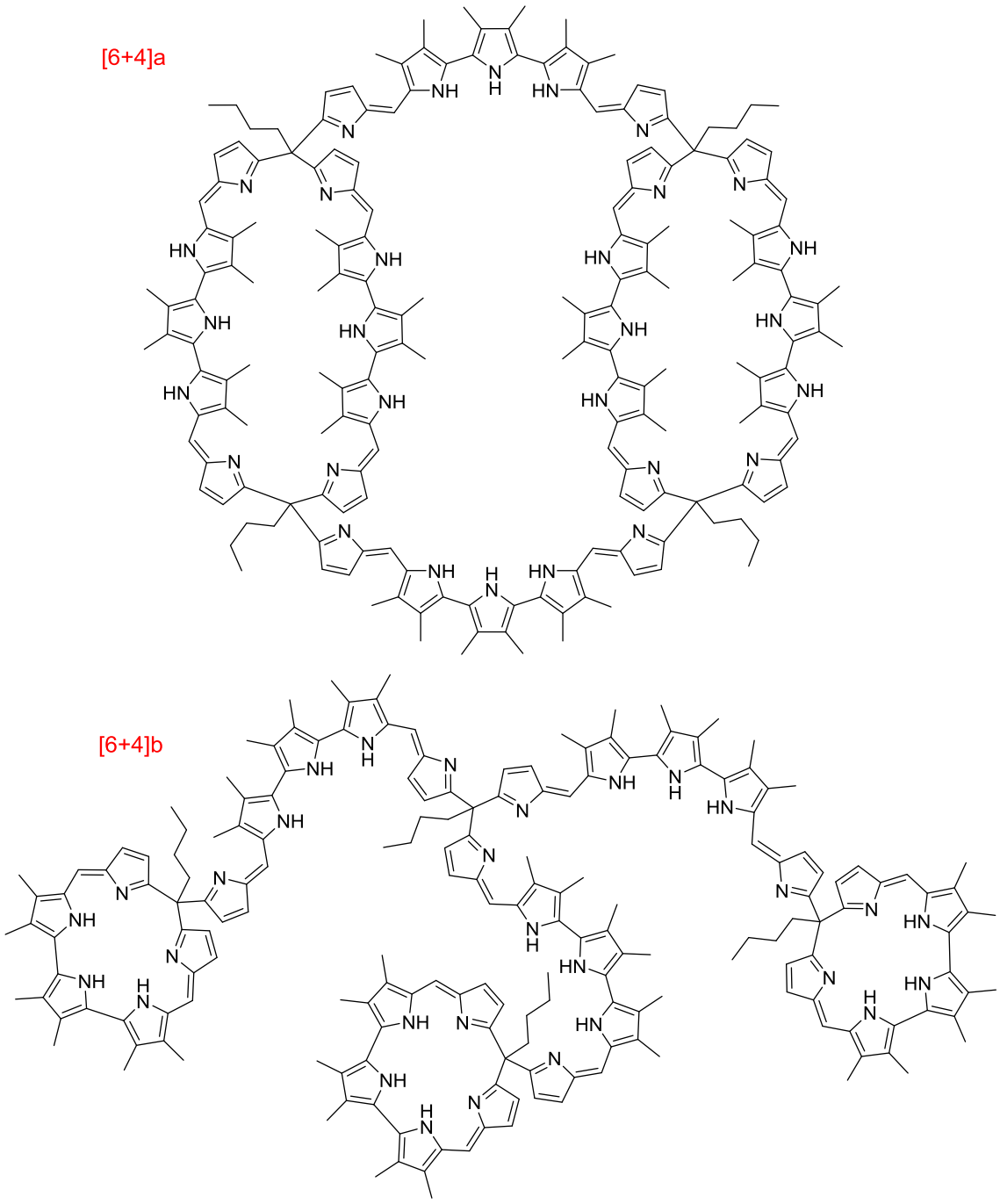

Figure 2.10. Two proposed isomers of the [6+4] adduct identified in the reaction between **30c** and **31c**.

The initial reaction conditions produced two isomers of the [3+2] adduct that proved challenging to separate due to their similarities in size. However, in due course, the reaction conditions could be optimized to produce the [2+2] adduct needed to synthesize the cryptand-like [3+2]a adduct **32** while avoiding the concurrent synthesis of large quantities of the [3+2]b adduct. Once this was done, this latter species could be removed as an impurity using the prep GPC-HPLC.

2.4. Characterization of the [1+1] adduct: a scorpiand-type calix[5]phyrin.

Each of the adducts was isolated as its hydrochloride salt when obtained in pure form from the recycling preparatory GPC-HPLC separation protocol using chloroform as the solvent. The [1+1] adduct was isolated in 4% yield. The ^{1}H-NMR spectrum proved consistent with a symmetrical molecule with protonation of the two azafulvene-type nitrogens and a total of 6 N-H protons. On the other hand, the ^{1}H-NMR spectrum of the neutral [1+1] product is characterized by a broadening of the N-H proton signals due to hydrogen bonding. In fact, only two N-H signals are visible. The UV-vis absorption spectrum for the hydrochloride salt has a band at λ_{max} = 460 nm while the neutral compound has a band at λ_{max} = 425 nm. Molecular modeling suggests that the protonated molecule is symmetrical (Figure 2.11A), while the neutral macrocycle supports hydrogen bonding between the exocyclic pyrrole N-H protons and one of the azafulvene nitrogen atoms (Figure 2.11B).

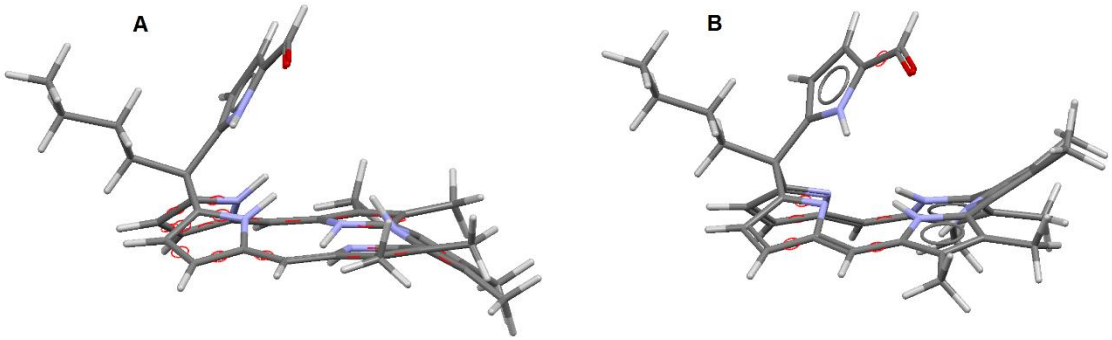

Figure 2.11. Molecular modeling studies of the [1+1] adduct. (**A**) [1+1]·2HCl, (**B**) [1+1].

2.5 Characterization of the [2+2] adduct: A scorpiand-type calix[10]phyrin.

The hydrochloride salt of the [2+2] adduct was isolated in 15% yield. The ^{1}H-NMR spectrum of the hydrochloride salt is consistent with a tetra-protonated structure with protons on each of the four azafulvene-like nitrogens. There are 6 sets of N-H protons, 1 set of aldehyde protons, 6 sets of pyrrole β hydrogens and 2 sets of meso-bridging methylene protons. This leads the author to suggest that the molecule has C2 symmetry in solution. Single crystal X-ray diffraction analysis of a single crystal of the [2+2]·4HCl grown in deuterated dichloromethane layered with pentane revealed pseudo-C2 symmetry in the solid state (Figure 2.12). A top view of the structure reveals that the molecule adopts a figure eight conformation. This creates two cavities into which anions might potentially bind. In fact, in the X-ray structure of [2+2]·4HCl, four chloride anions are encapsulated within the two cavities being held in place by apparent hydrogen bonds as well as electrostatic interactions, as discussed further below. Side views show that there are two parallel layers for each of the cavities that encapsulate two chloride

anions, one at each level (Figure 2.13). In the solid state, the pyrroles on the meso bridges are aligned. This breaks the C2 symmetry but presumably to enhance the stability by allowing dipole alignment of the aldehydes. The pyrrole and butyl groups on the bridging meso carbons provide an apparent locking mechanism that avoids the dynamic twisting seen in other figure eight polypyrrolic structures, such as in the cyclo[6]pyridine[6]pyrrole synthesized in this group, which lacks meso bridges.[43]

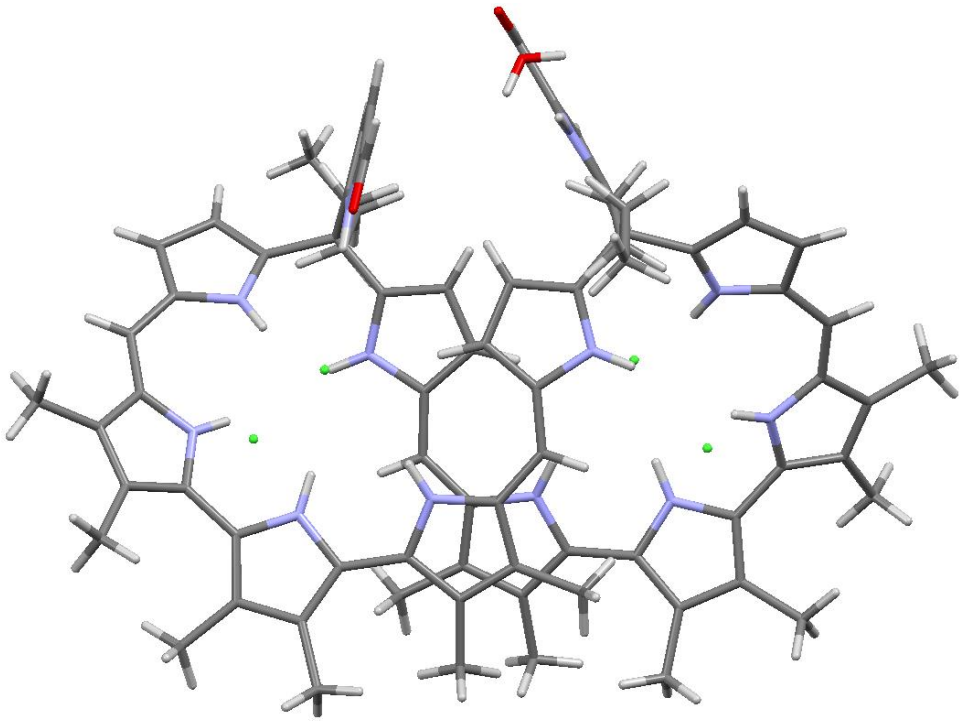

Figure 2.12. Single X-ray crystal structure of the [2+2] adduct as its tetrahydrochloride salt.

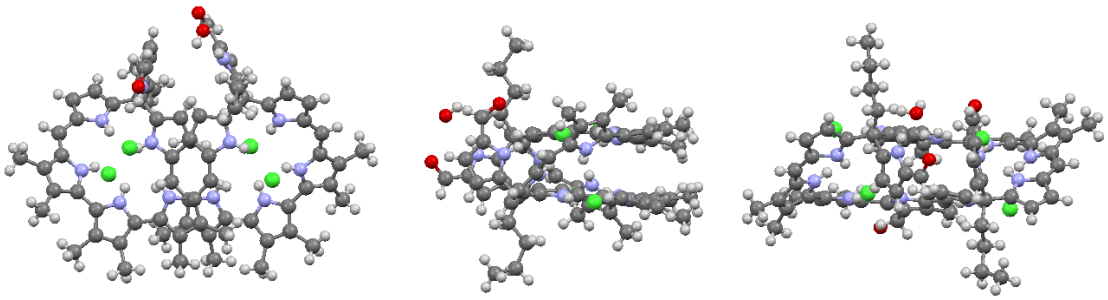

Figure 2.13. Top, side, and front views of the [2+2] adduct as its tetrahydrochloride salt.

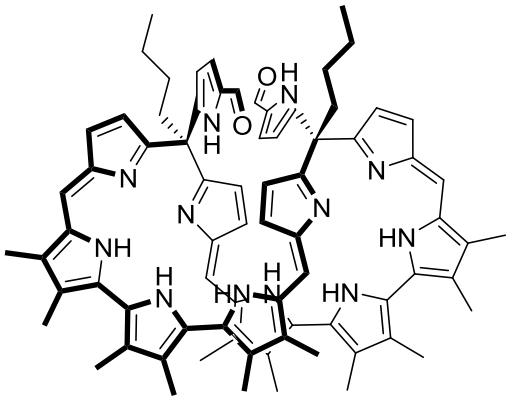

Figure 2.14. Skeletal structure of the free base form of the [2+2] adduct based on the single X-ray analysis of the tetrakis HCl complex.

The four chloride anions in [2+2]·4HCl interact with the host in two ways. Two of the chloride anions are encapsulated within the cavity and held in place via hydrogen bonds (5 total) involving the host (4 N-H, 1 C-H or 3N-H, 2C-H). The difference in the types of hydrogen bond is due to the alignment of the pyrroles on the meso-position. As a consequence of this latter orientation, there is an N-H bond hydrogen bond donor that

faces into one cavity and a C-H bond that stabilizes an anionic chloride bound in the adjacent cavity. The chloride on the left in Figure 2.15 has four N-H bonds and one C-H bond with the β hydrogen of a pyrrole in the macrocycle. The N-H proton from that same pyrrole is involved in a hydrogen bond to the chloride on the right side that is further stabilized by hydrogen bonds to two N-H protons and one meso-carbon C-H proton on meso carbon. Both 'outer' chloride anions appear bound by 3 hydrogen bonds to the host (2 N-H, 1 C-H).

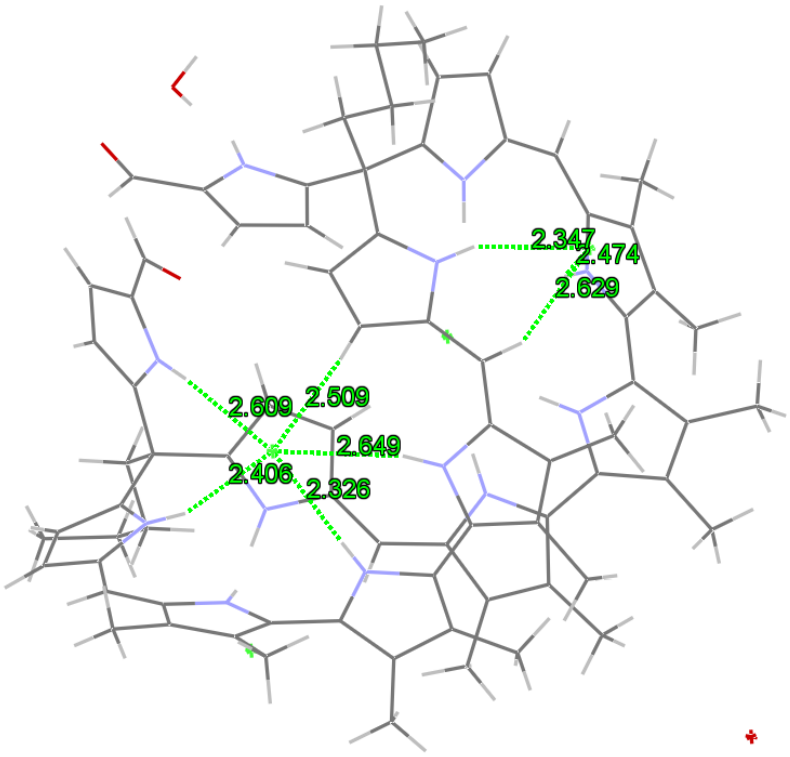

Figure 2.15. View of the X-ray structure of [2+2]·4HCl showing the two types of hydrogen bonding interactions between the [2+2] host and chloride.

It is also important to note that the [2+2]·4HCl complex is chiral and crystallizes with a pair of enantiomers in the unit cell. The design of these receptors was intended for binding simple anions, however the resulting products show potential for more complex applications. The two aldehydes on the host can act as handles for appending chiral molecules that may form diastereomeric species with chiral (racemic) guests. These aldehydes could also potentially serve as handles for attachment of the receptor to solid supports and for tethering the core system to other recognition units to obtain, e.g. ditopic receptors.

The neutral [2+2] adduct was obtained by dissolving the [2+2]·4HCl in ethyl acetate and washing with saturated sodium bicarbonate. The ^{1}H-NMR spectrum recorded in chloroform showed that the structure adopts a symmetrical conformation in solution. This is ascribed to the presence of two perpendicular internal mirror planes, which results in convergence to a much simpler ^{1}H-NMR spectrum than would otherwise be expected.

2.6. Characterization of the major [3+2] adduct: Confirmation of structure.

Two isomeric [3+2]·6HCl adducts were isolated from the mixture by prep GPC-HPLC. One was the major product. The other was obtained in amounts too small to characterize. Using size exclusion chromatography, the [3+2] adduct was isolated as the major product as its HCl salt following the elution of the [6+4] adduct and higher molecular weight products. The ^{1}H-NMR spectrum of this material revealed a total of 33 proton signals resonating upfield of 5.0 ppm. This corresponded to what would be

expected for a [3+2] adduct: 12 β hydrogens, 6 meso methylene hydrogens, and if completely protonated, 15 N-H proton signals. This gives a total of 33 protons as expected. Interestingly, this hydrochloride salt displays individual signals for each of the protons resonating above 5 ppm indicating that it has little overall symmetry. Due to the complexity of the ^{1}H-NMR spectrum, it was not possible to make individual assignments except for identification of the N-H protons through deuterium exchange using deuterated methanol. Without proper assignment of the various proton signals, the NOESY data could not be used to determine the structure. No solid state structure could be obtained. It was thus an open question whether the major [3+2] adduct was the cryptand like structure [3+2]a or the tethered bicyclic compound [3+2]b.

The solid state confirmation of the [2+2] structure gave us the opportunity to determine the structure of the dominant [3+2] adduct through chemical means. Specifically, the [2+2] adduct was treated with terpyrrole. This reaction resulted in the formation of higher molecular weight products, including a [6+4] and a [3+2] adduct. The ^{1}H-NMR spectrum of the [3+2] adduct obtained from this reaction matched that obtained as the [3+2]a product from the main reaction mixture. This result thus provided evidence that the main [3+2] adduct in the reaction is the cryptand-like structure [3+2]a shown in Figure 2.16.

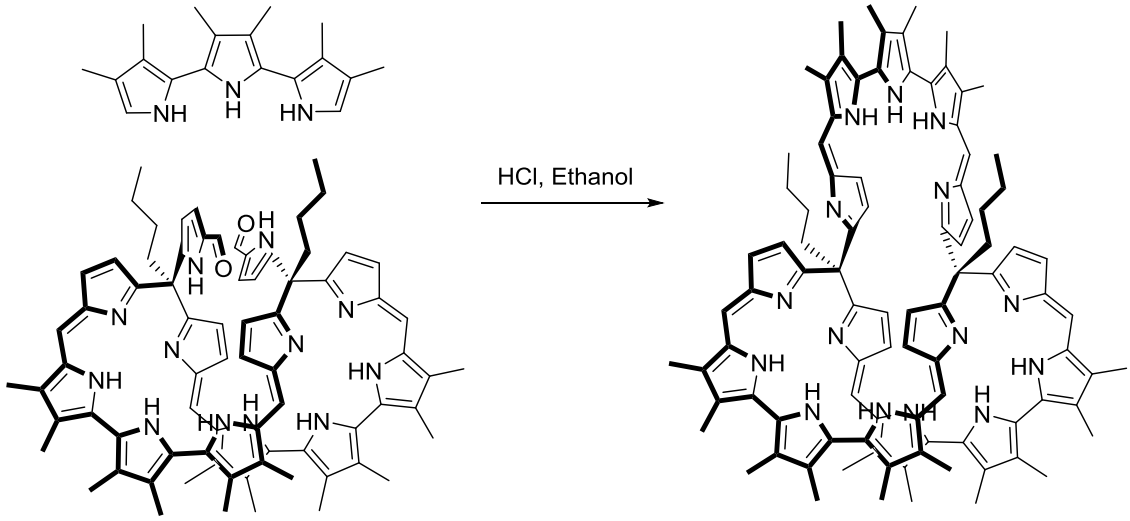

Figure 2.16. Reaction of the [2+2] adduct with terpyrrole to yield a species identical to the dominant [3+2] adduct obtained from the crude reaction mixture of 30c and 31c. This finding was taken as a confirmation of a cryptand-like structure.

2.7. Optimization of reaction conditions for synthesis of [2+2] and [1+1] adducts and purification.

The original reaction conditions involving a 1.5:1 mixture of the terpyrrole **31c** and trialdehyde **30c** resulted in production of the [3+2]b product that proved difficult to separate from the major [3+2]a adduct. To optimize the yield of the [2+2] adduct, conditions were then modified such that a 1:1 ratio of terpyrrole and trialdehyde were used. In this modified procedure, the terpyrrole was added dropwise via an addition funnel over a period of one hour to a stirred solution of the trialdehyde in ethanol containing a catalytic amount of hydrochloric acid. This resulted in a modest increase in the yield of the [2+2] and [1+1] products from 15% to 25% and from 4% to 7%,

respectively. A corresponding decrease in the amounts of the larger molecular weight products was observed. It is interesting to note that carrying out the reaction in chloroform resulted in an increase in the yield of the [1+1] adduct. However, this actual increase remained unquantified since a significant amount of insoluble polymeric material was also produced which made it difficult to isolate the desired [1+1] product.

The above 1:1 stoichiometric reaction conditions yielded a mixture of products that were identified by mass spectrometric analysis as the [1+1] and [2+2] adducts as well as new products identified as a [1+2] and a [2+3] adduct. Fortunately, these conditions yielded the [2+2] as the major product. Using less of the terpyrrole meant that the starting trialdehyde **30c** remained in the reaction mixture. Unfortunately, size exclusion chromatography failed to separate the starting trialdehyde **30c** from the [1+1] adduct. Despite being a very powerful method for separating the components of the given reaction mixture by recycling of the material through the system for 15-25 cycles, the [3+2] and [2+2] adducts were isolated with co-eluting impurities. As a consequence, the isolated reaction products all retained some impurities.

To complement the size exclusion chromatography, preparatory reverse phase (C-18) HPLC was used in an effort to remove the remaining impurities. In these experiments, the impure [1+1] and [2+2] fractions collected from the recycling preparatory GPC-HPLC were then concentrated in vacuo to obtain the respective hydrochloride salts. These samples were then prepared for the reverse phase HPLC purification by dissolving in 50:50 acetonitrile:water. These two hydrochloride salts (and

the attendant impurities) were somewhat soluble in acetonitrile but very soluble in the 1:1 acetonitrile:water mixture. A solvent gradient from 40% to 99% acetonitrile in water was used as the eluent. Acetic acid, 0.1% v/v, was present in both the water and acetonitrile.

Unfortunately, the desired products eluted over roughly a 10-minute time span in the case of each sample, an effect ascribed to the presence of multiple protonation states. However, purification could be accomplished by discarding fractions containing the impurities. This exclusion resulted in a loss of product. However, it achieved greater purity. The product fractions were combined, diluted into ethyl acetate and neutralized with sodium bicarbonate before being concentrated in vacuo. The solids obtained in this way were dissolved in ethanol and converted to the presumed hydrochloride salts by treating with concentrated hydrochloric acid and then taken to dryness in vacuo. Both the [1+1] and [2+2] hydrochloride salts could be stored safely for weeks without appreciable decomposition.

Chapter 3

3.1. Optical properties of [1+1], [2+2], and [3+2] adducts.

The three products, namely the [1+1], [2+2], and [3+2] adducts (Figure 3.1) were assessed for their ability to bind various test anions. Each of the products was characterized by absorption features in the visible region of the spectrum in their neutral form. Relative to the neutral forms, the hydrochloride salts of each adduct were characterized by absorption bands that were red shifted. Key Λ_{max} values are given in Table 3.1.

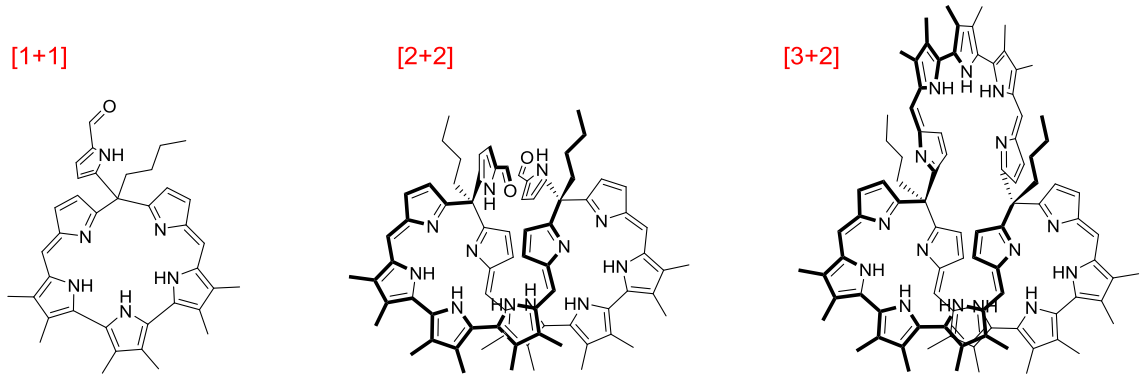

Figure 3.1 Adducts tested for their ability to bind anions.

Adduct	Λ_{max}
[1+1] in chloroform	301 nm, 425 nm
[1+1].2PF_6 in chloroform	296 nm, 463 nm
[2+2] in dichloroethane	300 nm, 468 nm
[2+2].4HPF_6 in dichloroethane	295 nm, 539 nm, 612 nm
[3+2] in dichloroethane	512 nm

Table 3.1 Absorbance maxima for the neutral and protonated forms of the [1+1], [2+2] and [3+2] adducts.

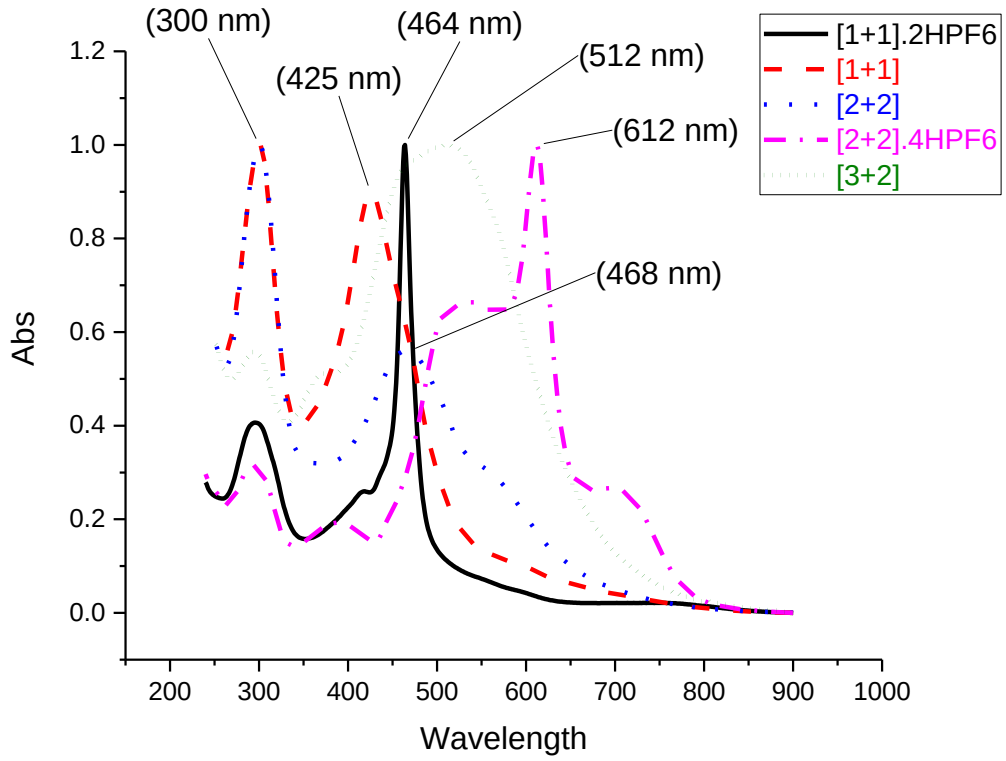

Figure 3.2 Overlay of UV-vis spectra of the neutral and protonated forms of the [1+1], [2+2] and [3+2] adducts.

The normalized absorption spectra for each of the neutral and protonated adducts is shown in Figure 3.2. Both the [1+1] and [2+2] neutral adducts have two main absorption peaks that are ascribed to the bridgehead formyl pyrrole moieties and the conjugated pentapyrrolic subunits. Protonation of these two systems using HPF_6 results in quenching of the absorbance assigned to the formyl pyrrole and an increase in intensity and a bathochromic shift in the absorbance feature ascribed to the pentapyrrolic portion of the system. The propensity of these systems to respond to changes in their environments allowed their interactions with selected anionic species to be quantified.

3.2. Anion binding titrations of the [1+1] adduct.

[1+1]

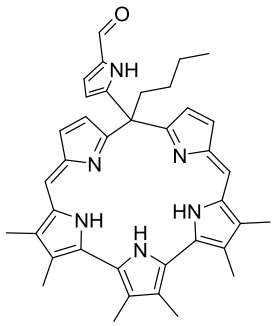

The [1+1] adduct is a pentapyrrolic macrocycle (calix[5]phyrin) with five pyrroles in conjugation and with an sp^3 bridging carbon that bears a 5-formyl pyrrole. This compound bears resemblance to scorpiand molecules wherein a group appended to a macrocycle can be directed toward the inner cavity created by the ring to interact with a bound guest. The [1+1] adduct possesses four hydrogen bond donors (the pyrrolic N-H

protons), and three hydrogen bond acceptors in the form of 2 azafulvene nitrogens within the ring and one formyl oxygen atom. The two azafulvene nitrogens also make the macrocycle susceptible to double protonation.

Treatment of the neutral [1+1] adduct with selected anions did not produce any change in the absorption spectrum as can be seen in Figure 3.3 for spherical, trigonal planar, tetrahedral, or octahedral anions.

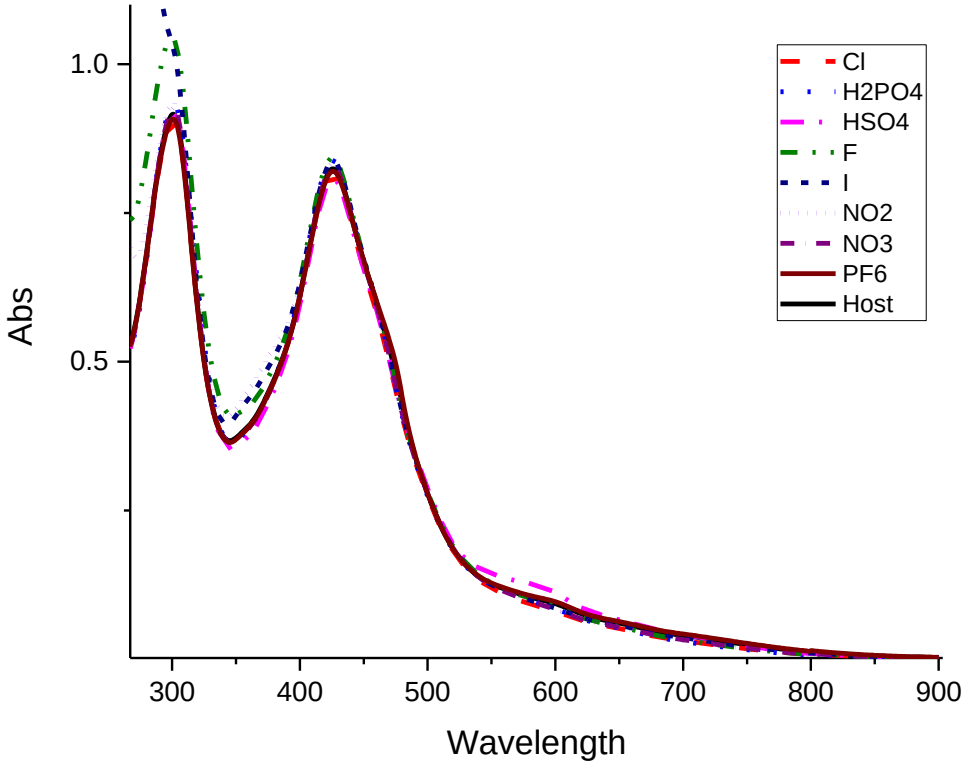

Figure 3.3. [1+1] adduct treated with the tetrabutylammonium salts of selected anions.

A dilution experiment carried out in methanol provided evidence that the [1+1] adduct aggregates in chloroform and is not monomeric at the concentrations used for the titration experiments ($K = 2.0 \times 10^4 \pm 5 \times 10^3$ M^{-1} in methanol).

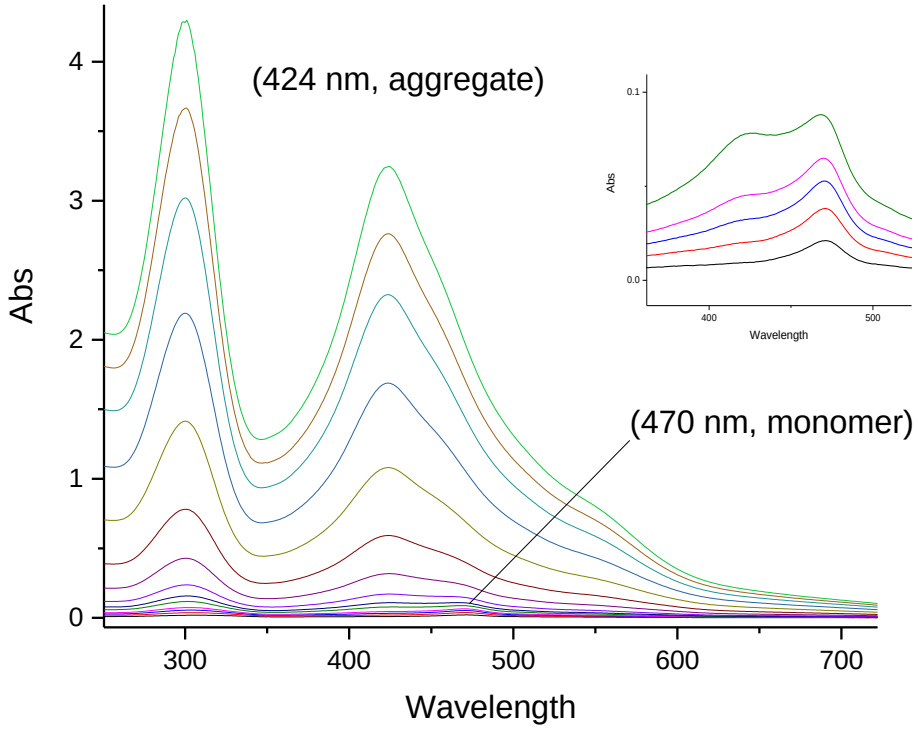

Figure 3.4. UV-vis spectra of the [1+1] adduct in methanol used to quantify the extent of aggregation.

The [1+1] adduct was converted to its HPF_6 salt. The neutral [1+1] adduct was dissolved in ethyl acetate and washed with a 0.5 M HPF_6(aq) solution. The anion binding affinity of this protonated form was then tested in chloroform using the tetrabutylammonium salts of selected anions. The results obtained from UV-vis

spectroscopic titrations are shown in Table 3.2. The strongest binding was observed with TBABr with a 1:2 host:guest binding stoichiometry as determined using the Thordarson fitting program.[44,45] The stoichiometry was determined by a best fit comparison of 2:1, 1:1, and 1:2 host:guest models using global fitting of 2-4 UV-vis data sets. Dihydrogenphosphate and hydrogen sulfate which are larger tetrahedral anions showed lower binding affinities and appeared to form 1:1 complexes. Figure 3.5 shows the UV-vis spectra obtained for the various titration experiments. These spectral results provide support for the conclusion that for all tested anions, with the exception of dihydrogenphosphate, there was a bathochromic shift in the absorbance of the complex. In the case of dihydrogenphosphate, it is thought that the observed spectral changes reflect an acid base reaction wherein deprotonation of the host occurs.

Host	Solvent	Guest	K_1 (M^{-1})	% Error	K_2 (M^{-1})	% Error
[1+1]·2HPF_6	chloroform	TBACl	3.1E+06	13	2.2E+04	5
[1+1]·2HPF_6	chloroform	TBABr	1.9E+07	24	2.9E+05	11
[1+1]·2HPF_6	chloroform	TBAI	1.6E+06	6	3.5E+04	5
[1+1]·2HPF_6	chloroform	$TBAH_2PO_4$	1.0E+05	6	x	
[1+1]·2HPF_6	chloroform	$TBAHSO_4$	7.1E+05	30	x	

Table 3.2. Best fit derived binding constants for the titration of selected anions with the HPF_6 salt of the [1+1] adduct in chloroform using global fitting of 2 or 3 different wavelength data sets with the Thordarson online software obtained from supramolecular.org.

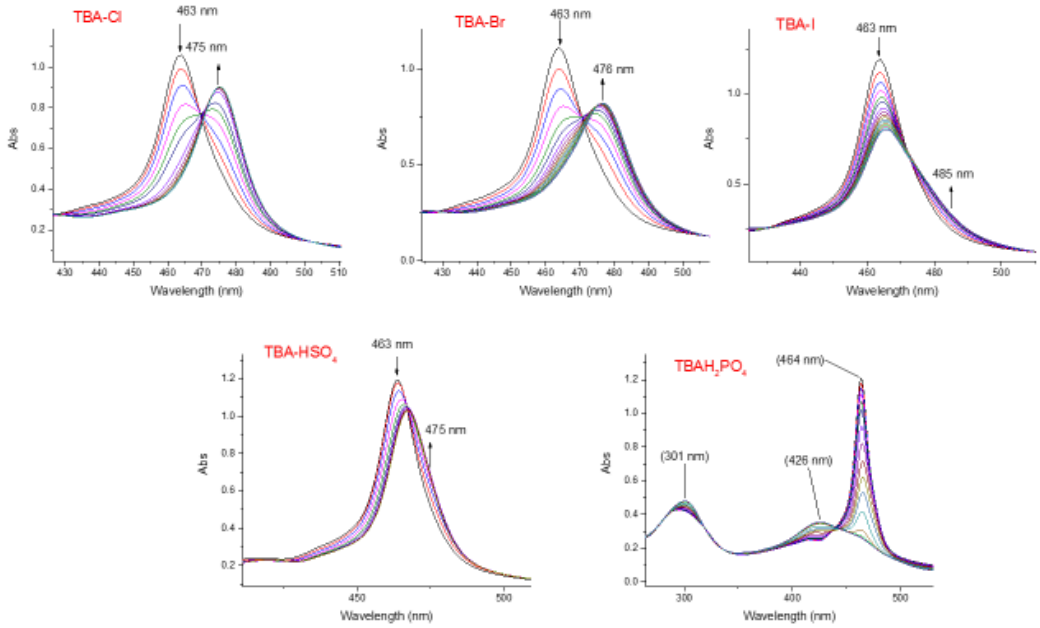

Figure 3.5. UV-vis spectra corresponding to binding titrations of the [1+1] adduct in chloroform with the tetrabutylammonium salts of selected anions.

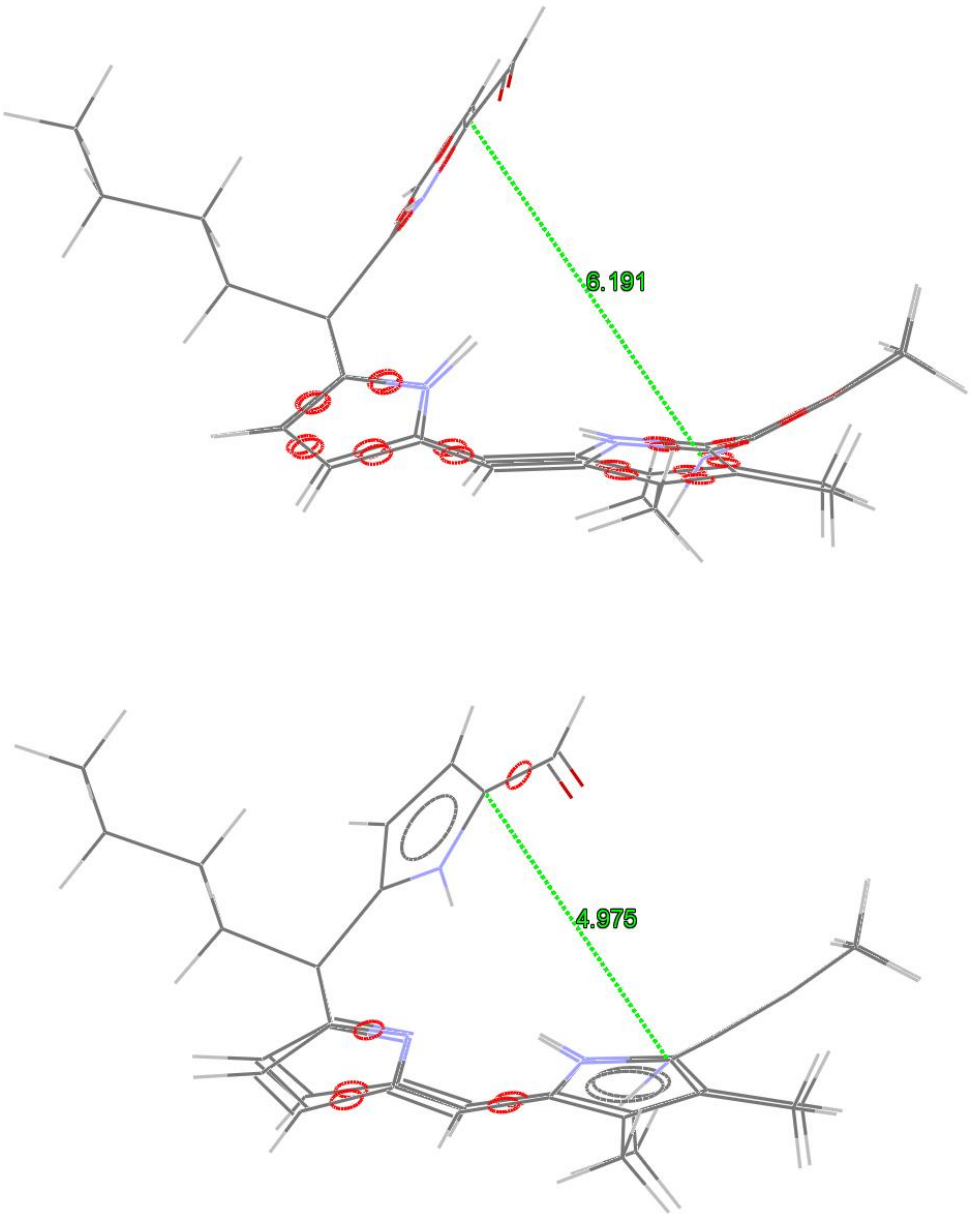

Figure 3.6. Molecular model of the protonated (top) and neutral (bottom) forms of the [1+1] adduct showing how intramolecular hydrogen bonding interactions in combination with aggregation may preclude binding to anionic guests.

Comparison of the molecular models for the neutral and protonated forms of the [1+1] adduct leads to the suggestion that there are intramolecular hydrogen bonding interactions in the neutral form that serves to accommodate the binding cavity this blocking interactions with anionic guests (Figure 3.6). This internal steric effect, in addition to aggregation, may explain the lack of response of the neutral form of the [1+1] when exposed to the tetrabutylammonium salts of the test anions used in this study.

3.3. Anion binding titrations of the [2+2] adduct in 1,2-dichloroethane.

The [2+2] adduct displayed a spectral response when its neutral form was exposed to certain salts. For instance, a significant and immediate color was seen when treated with the tetrabutylammonium (TBA^+) salts of sulfate and hydrogen sulfate anions compared to the other anion containing salts in 1,2-dichloroethane. However, after a period of 48 hours, a slight change in color was observed for all the tested anions as their TBA^+ salts (Figure 3.7).

Figure 3.7. Results of treating solutions of the [2+2] adduct in 1,2-dichloroethane with an excess of the tetrabutylammonium salts of selected anions and photographed after 48 hours. From left to right: sulfate, hydrogen sulfate, chloride, bromide, iodide, dihydrogen phosphate, pyrophosphate and perchlorate.

Host	Solvent	Guest	K_1 (M^{-1})	% Error	K_2 (M^{-1})	% Error
[2+2]	1,2-dichloroethane	TBA_2SO_4	2.4E+07	180	3.5E+03	8
[2+2]	1,2-dichloroethane	$TBAHSO_4$	1.2E+07	85	6.4	14
[2+2]	1,2-dichloroethane	TBACl	3.1E+06	27	3.1E+06	22
[2+2]	1,2-dichloroethane	TBABr	2.4E+06	44	2.4E+05	25
[2+2]	1,2-dichloroethane	TBAI	2.7E+05	22	2.2E+05	32
[2+2]	1,2-dichloroethane	$TBA_3HP_2O_7$	5.3E+06	28	1.0E+06	21
[2+2]	1,2-dichloroethane	$TBAClO_4$	3.4E+02	6	x	

Table 3.3. Best fit derived binding constants for the titration of selected anions as their TBA salts with the [2+2] adduct in 1,2-dichloroethane using global fitting of 3 or 4 different wavelength data sets with the Thordarson online software obtained from supramolecular.org.

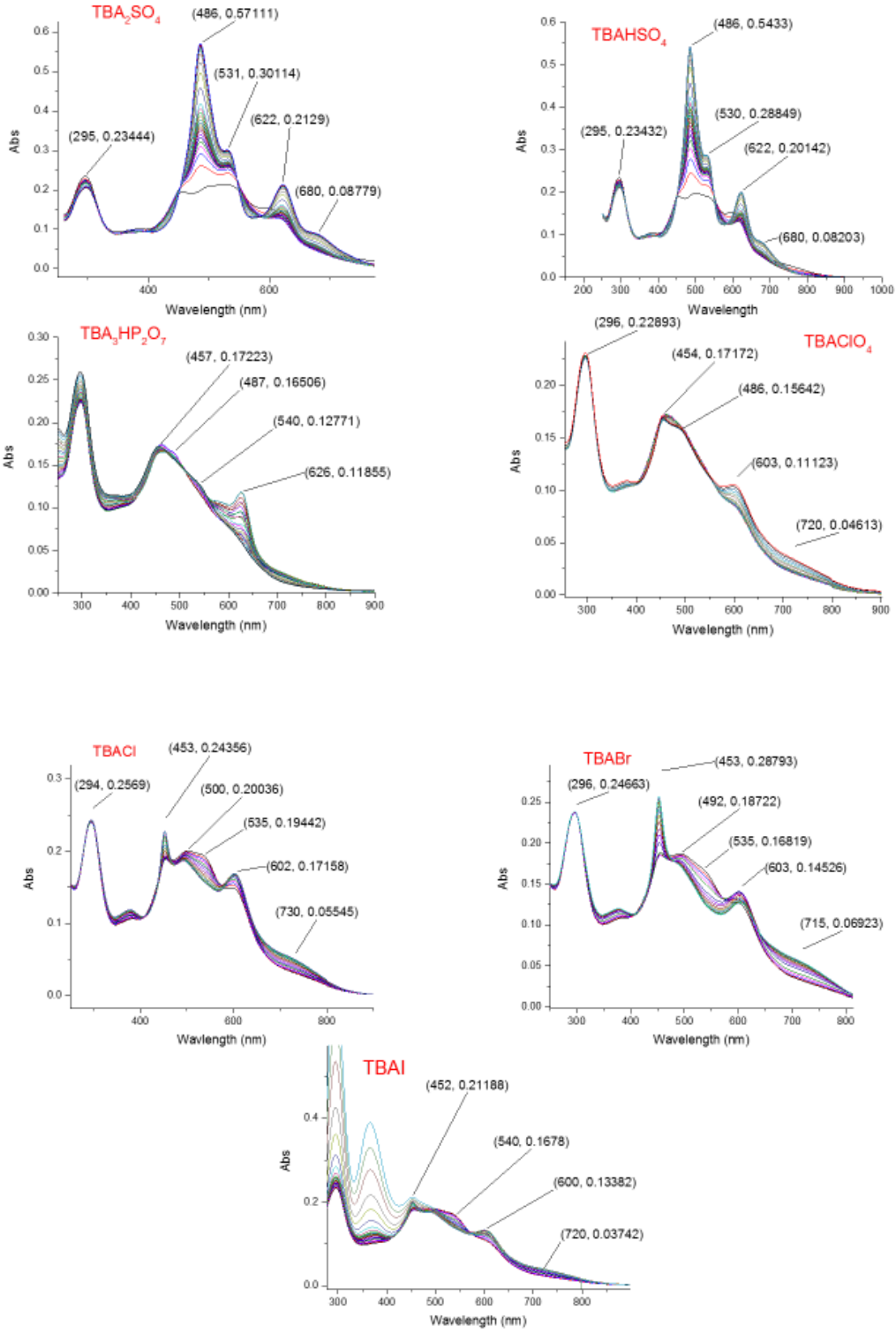

Figure 3.8. UV-vis spectra corresponding to binding titrations of the [2+2] adduct in dichloroethane with the tetrabutylammonium salts of selected anions.

The strongest binding was observed in the case of the sulfate anion (Table 3.3). A 1:2 binding stoichiometry gave the best curve fits. This proved to be true for most other anions as well. An exception is the perchlorate anion which showed the weakest binding and data that fit best to a 1:1 binding stoichiometry. These results are supported by the fact that the solid-state crystal structure of [2+2] has a figure eight conformation that establishes two cavities suitable for binding. The only anions that gave rise to a significant spectral change that is also visible to the naked eye proved to be the sulfate and hydrogen sulfate anions (Figures 3.7 and 3.8). The observed large spectral change in the iodide titration was from absorbance of the tetrabutylammonium salt in dichloroethane.

The solution of the [2+2] adduct was also prepared in 1,2-dichloroethane and treated with the acetate and cyanide anions to see how basic anions interact with this particular receptor. After 12 days of maturing it was observed that these two basic anions also produce a color change, although quite different from that seen with the sulfate/hydrogen sulfate anions and the halides (Figure 3.9).

Figure 3.9 Results of treating solutions of the [2+2] adduct in 1,2-dichloroethane recorded 12 days after exposure to an excess of the tetrabutylammonium salts of selected anions. From left to right: free [2+2], sulfate, hydrogen sulfate, chloride, bromide, acetate, cyanide, and nitrate.

3.4. Anion binding titrations of the [2+2] adduct in methanol.

The anion binding ability of the neutral [2+2] adduct was then assessed in the polar protic solvent methanol to determine whether the binding would be significant in a solvent that interferes with the hydrogen bonding between the host and the anion. An initial assessment in methanol demonstrated that, just as in 1,2-dichloroethane, both sulfate and hydrogen sulfate produce a significant color change (Figure 3.11) and increase in absorption upon binding, while the other anions tested resulted in quenching (Figure 3.10).

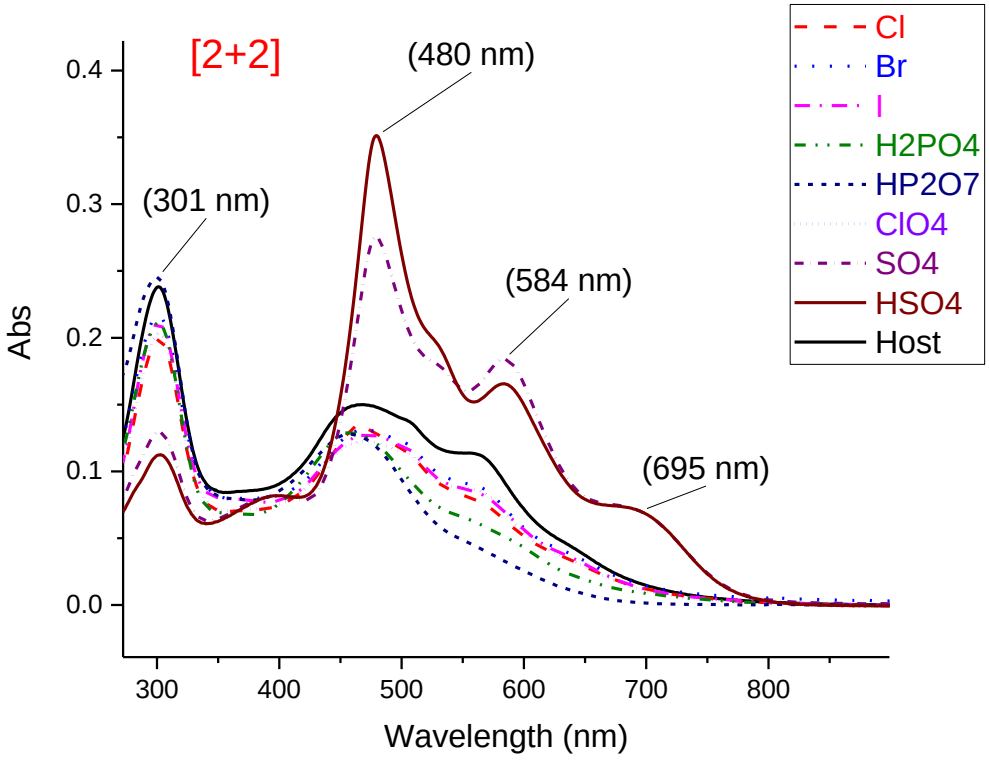

Figure 3.10. Overlay of the UV-vis spectra of the [2+2] adduct in methanol recorded upon treatment with selected anions in methanol.

Figure 3.11. Colors observed for the [2+2] adduct in methanol upon exposure to excess tetrabutylammonium anions. From left to right: Host only, sulfate, hydrogen sulfate, chloride, bromide, acetate, cyanide, nitrate, and dihydrogen phosphate.

Host	Solvent	Guest	K_1 (M^{-1})	% Error	K_2 (M^{-1})	% Error
[2+2]	methanol	TBA_2SO_4	7. 7E+04	8	7.7E+04	8
[2+2]	methanol	$TBAHSO_4$	3.6E+04	3	150	1

Table 3.4. Binding constants for the interaction of selected anions with the neutral form of the [2+2] adduct in methanol as derived from a global fitting of 3 or 4 different wavelength data sets using the Thordarson online software available at supramolecular.org.

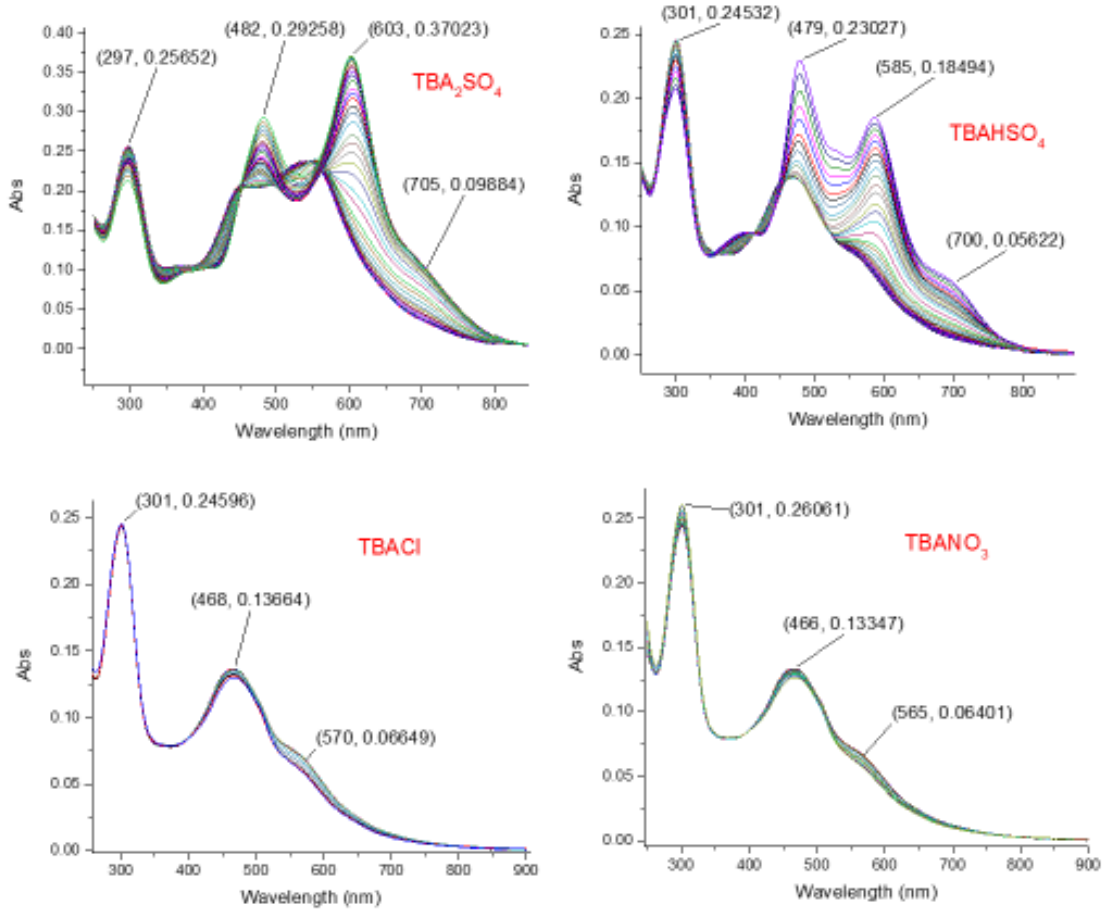

Figure 3.12. Results of binding titrations of the [2+2] adduct with the tetrabutylammonium salts of selected anions as recorded in methanol.

It was determined that for the four anions assessed, the data could be best fit to a 1:2 host:guest binding stoichiometry. This [2+2] adduct binds the first equivalent of sulfate and hydrogen sulfate well (large K_1), however the K_2 value is high for sulfate and very small for hydrogen sulfate, reflecting little affinity for the second anion in the latter case. For the sulfate anion, the specific K_1 and K_2 values suggest positive cooperativity as per equation 1 ($\alpha = 4.02$).[44]

$$\alpha = \frac{4K_2}{K_1} = \frac{4(7.72\times10^4)}{7.67\times10^4} = 4.0 \qquad \text{(Eq. 1)}$$

The other anions induced a decrease in absorbance of the host as can be seen in Figure 3.12. The fitting gave the best results for a 1:2 host:guest stoichiometry for both chloride and nitrate. However, the quality of the fit was too low to be reliable.

The neutral form of the [2+2] adduct was prepared by washing a solution of the hydrochloride salt in ethyl acetate with saturated sodium bicarbonate. While this simple washing process was expected to deprotonate the host, it may still encapsulate an anionic guest which might prevent complete deprotonation. It is also possible the host exists in a conformation that stabilizes the binding of an anion. These or other effects could account for the observed spectral changes for methanolic solutions with time.

3.5. Anion binding titrations of the [2+2] adduct in 1 mM HPF_6 in methanol.

To test whether the protonated host would display greater affinities for anionic guests than the neutral form, the [2+2] adduct was dissolved in methanol to produce a 7.5 $x10^{-6}$ M solution that was also 1mM in HPF_6 and titrated against TBACl. The experimental data could be fit to a 1:2 binding stoichiometry with K_1 =7.7 $x10^3$ ± 6% (M^{-1}) and K_2 = 3.1 $x10^3$ ± 1% (M^{-1}). Interestingly, in methanol the protonated host showed positive cooperativity for the chloride anion in contrast to the neutral host.

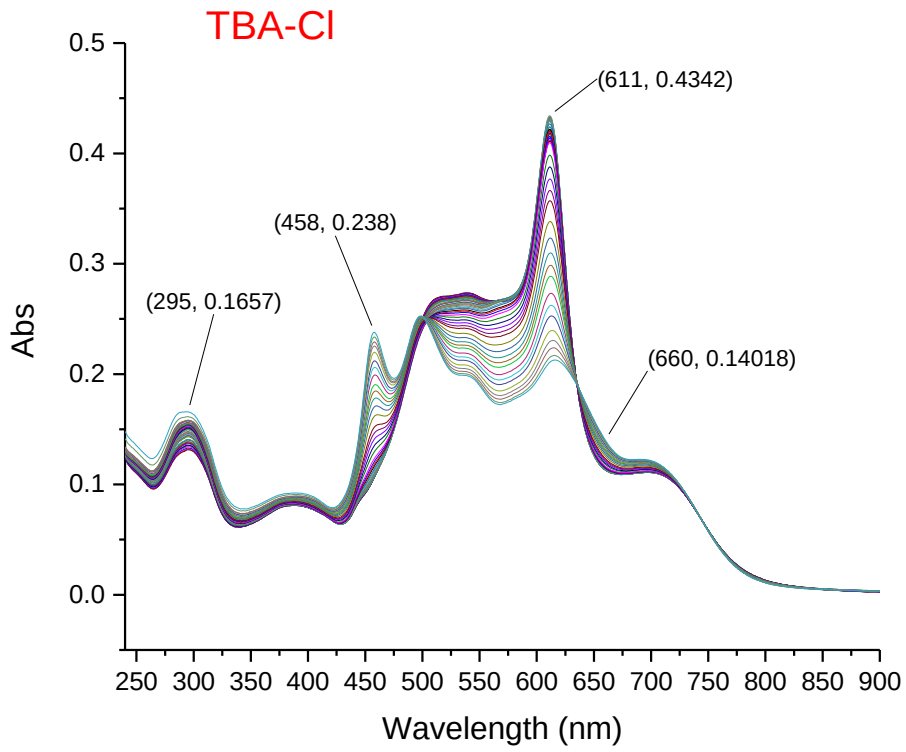

Figure 3.13. Spectral changes seen when the neutral form of the [2+2] adduct in 1 mM HPF_6 in methanol is titrated with TBACl.

The spectral changes observed in the [2+2] adduct with both sulfate and hydrogen sulfate in dichloroethane and methanol were significant and could be attributed to a few possibilities (Figure 3.14). The conjugated pentapyrrolic bridges of the [2+2] adduct are susceptible to multiple protonation at the two azafulvene-type nitrogen atoms. The two azafulvene-type atoms may also be involved in tautomerization. The conformation observed in the tetrahydrochloride salt of the [2+2] adduct may be significantly different from what exists for the neutral [2+2] in solution.

The sulfate and hydrogen sulfate anions could potentially induce a dramatic conformational change in the host to result in a better and more defined conjugation pathway. These effects, alone or in combination, may account for the observed changes in the spectral properties of the host upon addition of sulfate or hydrogensulfate.

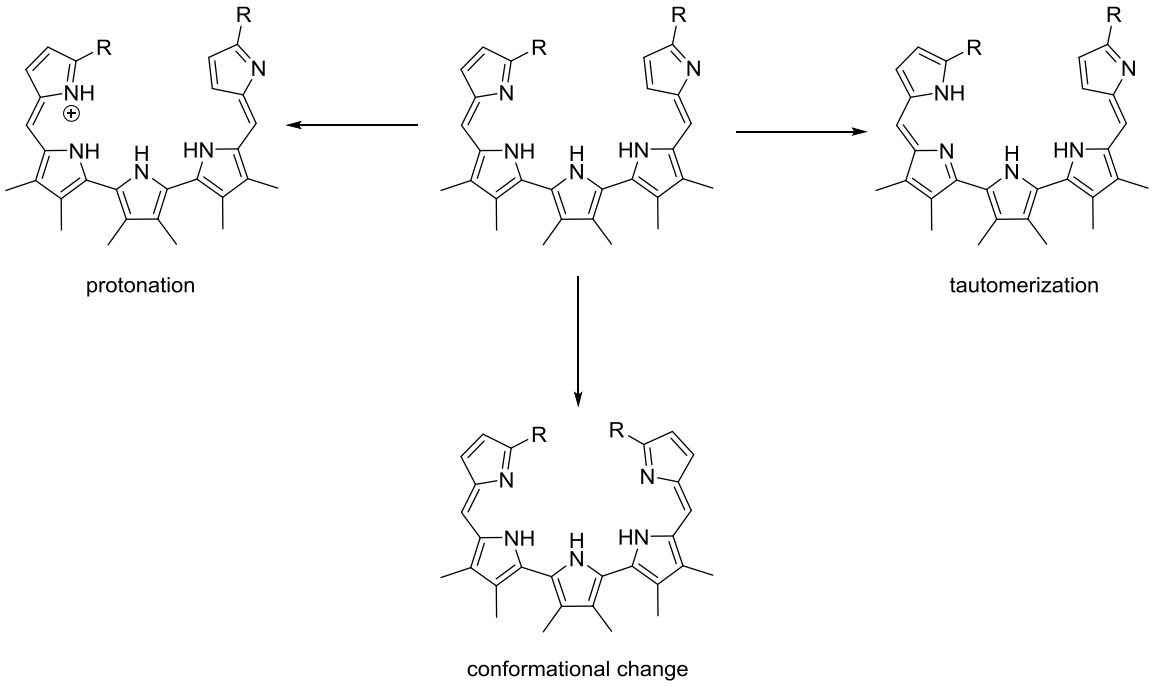

Figure 3.14. Conjugated pentapyrrolic bridge shown with changes that could have an effect on the spectral properties of the [2+2] adduct.

To test whether acid-base chemistry is contributing to the change, two solutions containing the host exposed to excess tetrabutylammonium sulfate and tetrabutylammonium chloride in methanol were each treated with dropwise addition of 1 M sulfuric acid and 1 M hydrochloric acid in water, respectively. In the case of the sulfate anion, the solution became a brighter purple, while in the case of chloride, addition of the hydrochloric acid resulted in a dark grey solution. It can be inferred that

the color change observed in the sulfate is not solely the result of acid-base chemistry. The change in color upon addition of sulfuric acid to a brighter purple color indicates that the acid results in further protonation. This leaves the possibility that tautomerization may have a role in the observed spectral changes.

Further titration experiments at different host concentrations need to be performed to assess the possibility of aggregation influencing anion binding along with a complementary dilution experiment. Additionally, insight into the effect of protonation can be gained by running the titrations experiments in the presence of excess acid containing a non-coordinating anion. The excess of an acid will minimize the effect of potential deprotonation by any introduced anion and eliminate the effects of tautomerization.

3.6. Anion binding titrations of the [3+2] adduct in 20% dichloromethane in methanol and in 1,2-dichlroethane.

The binding affinity of the neutral [3+2] cryptand-like adduct was also assessed. The solubility of the neutral adduct was low in methanol. Thus, the spectroscopic binding titrations were carried out in a mixture of 20% dichloromethane in methanol. In this solvent mixture, both chloride and bromide anions demonstrate stronger first binding constants than does the sulfate anion. However, the second is bound more strongly in the case of the sulfate and bromide anions compared to what is seen for chloride.

As expected, the binding constant for sulfate was higher in pure dichloroethane than in the 20% dichloromethane in methanol mixture. Comparison of the results of fitting to a 1:2 binding model revealed that the sulfate anion is bound more strongly to this host than bromide. A higher K_2 was seen in the case of sulfate than for fluoride or bromide (Table 3.5).

[3+2]

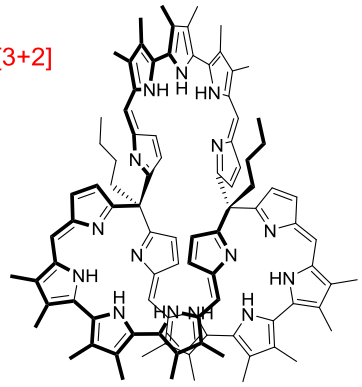

Host	Solvent	Guest	K_1	% Error	K_2	% Error
[3+2]	20%dichloromethane in methanol	TBA_2SO_4	4.2E+04	6	2.5E+03	4
[3+2]	20%dichloromethane in methanol	TBACl	2.2E+05	17	130	6
[3+2]	20%dichloromethane in methanol	TBABr	1.2E+05	9	3.0E+03	7
Host	Solvent	Guest	K_1	% Error	K_2	% Error
[3+2]	dichloroethane	TBA_2SO_4	2.6E+05	13	3.3E+03	3
[3+2]	dichloroethane	TBAF	7.4E+05	14	68	7
[3+2]	dichloroethane	TBABr	3.0E+04	14	130	5

Table 3.5 Binding constants (K_a, M^{-1}) for the [3+2] adduct interacting with various anions as obtained from global fittings of 3 or 4 different wavelength data sets to the Thordarson online software found at supramolecular.org.

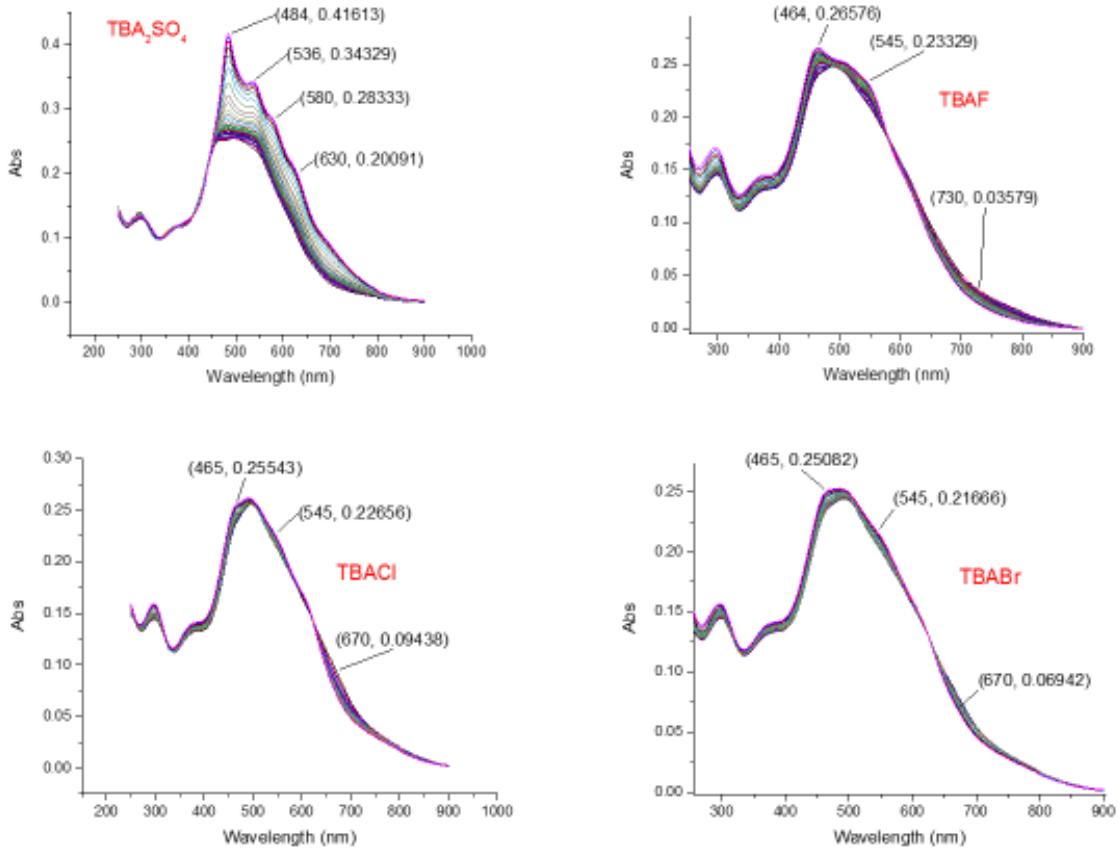

Figure 3.15. UV-vis spectra obtained from binding titrations of the neutral form of the [3+2] adduct in dichloroethane in with the tetrabutylammonium salts of selected anions.

3.7. Comparison of [2+2] and [3+2] binding to sulfate.

In the case of both the [2+2] and [3+2] adducts a color change was observed upon addition of the sulfate anion in either 1,2-dichloroethane or methanol. The [2+2] however was demonstrated to have selectivity for the sulfate and hydrogen sulfate anions and to bind two equivalents of the sulfate anion.

UV-vis spectra recorded during the course of titrations involving the tetrabutylammonium salts of selected anions revealed that the sulfate and hydrogen sulfate produced the greatest spectral changes (Figure 3.15).

Host	Solvent	Guest	K_1	% Error	K_2	% Error
[2+2]	Methanol	TBA_2SO_4	7.7E+04	8	7.7E+04	8
[3+2]	20% dichloromethane in methanol	TBA_2SO_4	4.2E+04	6	2.5E+03	4
[2+2]	Dichloroethane	TBA_2SO_4	2.4E+07	180	3.5E+03	8
[3+2]	Dichloroethane	TBA_2SO_4	2.6E+05	13	3.3E+03	3

Table 3.6 Binding constants for the interaction between the [2+2] and [3+2] adducts and the sulfate anion as determined in different solvents.

3.8. Solid to liquid extraction and anion exchange using [2+2]·4HCl in magnesium sulfate.

The [2+2] adduct demonstrated a significant change in the UV-vis absorption when exposed to the tetrabutylammonium salt of sulfate and hydrogen sulfate compared to other tested anions. The affinity for sulfate was then tested using the hydrochloride salt of the [2+2] adduct by testing exchange of the presumably complexed

chloride counter anion for sulfate by exposing to solid magnesium sulfate. The precise experimental conditions are outlined below.

A 6.5 mg sample of the hydrochloride salt of the [2+2] adduct was stirred in a 2.5 mL suspension of 20% methanol in dichloromethane containing 50 mg of powdered magnesium sulfate for a period of 15 h to see if there would be any anion exchange from chloride to sulfate. Displacement of chloride by sulfate in the [2+2] adduct could not be confirmed by mass spectrometry. However, the ^{1}H-NMR spectrum of the compound after filtration and concentration in vacuo was different from at the outset of the experiment. Downfield shifts were observed for six of the N-H proton signals and for the aldehyde proton, while the β and meso hydrogen signals shifted upfield, except for those at δ 7.11 and 6.81 ppm as seen in Table 3.7. Figure 3.16 is the overlay of the two proton NMR spectra with the largest differences in the chemical shifts indicated with arrows. While these results are not conclusive proof of anion exchange, the change in the chemical shifts is consistent with a stronger interaction occurring between the host and the bound anionic guest. Such a finding could reflect sulfate anion binding.

[2+2]·4HCl (δ)	[2+2]·2H_2SO_4 (δ)	Δδ	Type of Proton
13.92	13.98	+0.06	-N-H
13.06	13.16	+0.10	-N-H
13.04	13.08	+0.04	-N-H
12.05	12.15	+0.10	-N-H
11.80	11.78	-0.02	-C-H
10.29	10.27	-0.02	-C-H
9.40	9.41	+0.01	-CHO
9.27	9.34	+0.07	-N-H
8.48	8.50	+0.02	-N-H
7.26	7.24	-0.02	-C-H
7.11	7.11	0.00	-C-H
6.81	6.81	0.00	-C-H
6.55	6.54	-0.01	-C-H
6.35	6.34	-0.01	-C-H
5.35	5.28	-0.07	-C-H

Table 3.7. ^{1}H NMR (400 MHz, methylene chloride-d_2) spectral shifts for the [2+2] adduct as the hydrochloride salt and what is presumed to be the sulfuric acid salt after stirring with magnesium sulfate. See text for details.

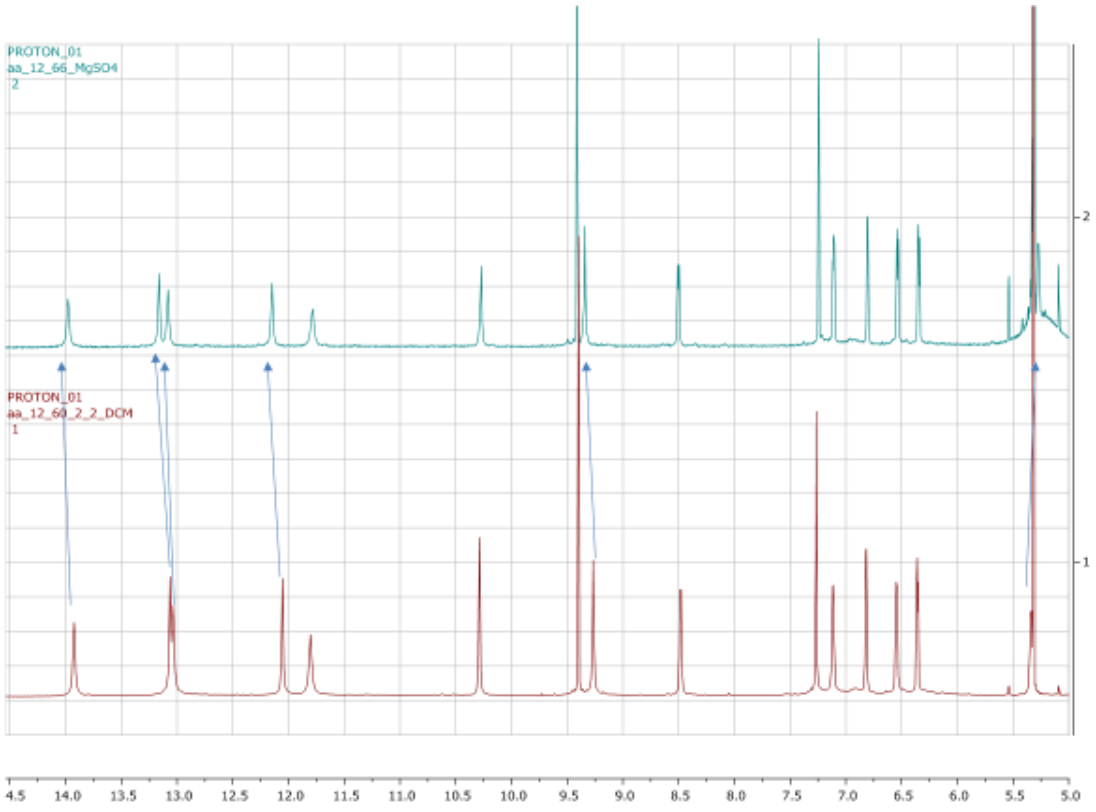

Figure 3.16. Overlay of the ^{1}H-NMR spectra of the tetrahydrochloride salt of the [2+2] (bottom) with the product obtained after stirring in methanol/dichloromethane for 15 hours in the presence of suspended solid magnesium sulfate (top). Arrows show the largest chemical shifts.

3.9. Derivatization of [2+2] with diamines and sulfate complexation.

Attempts were made to functionalize the neutral [2+2] adduct at the aldehyde positions. Toward this end, this adduct was exposed to the chiral diamine (1R,2R)-(-)-1,2-diaminocyclohexane (DA). This was done by dissolving the [2+2] adduct and the chiral diamine in dichloromethane followed by the addition of powdered magnesium sulfate as a dehydrating agent and catalyst with stirring overnight. Mass Spectrometric analysis provided evidence for imine formation. However, the result of the reaction was

not cyclization. Instead two separate diamines were found to have added, one to each of the two aldehydes (Table 3.8). The mass spectrometric analysis (ESI+) provided evidence that the product formed in this way stabilizes a complex with two sulfate anions that is stable enough to be detectable as a positive ion. Major ion peaks were observed for the $([2+2]+2DA+2H_2SO_4+2H)^{2+}$ followed by $([2+2]+2DA+2H_2SO_4+3H)^{3+}$, $([2+2]+2DA+H_2SO_4+2H)^{2+}$, $([2+2]+2DA+3H)^{3+}$. No evidence of cyclization (i.e. reaction involving one diamine and the two aldehydes) was observed (Figure 3.16)

Starting Material	Complex	m/z
[2+2]	$([2+2]+2DA+2H_2SO_4+2H)^{2+}$	791.5
	$([2+2]+2DA+H_2SO_4+2H)^{2+}$	742.8
	$([2+2]+2DA+H_2SO_4+3H)^{3+}$	495.4
	$([2+2]+2DA+3H)^{3+}$	462.8
[2+2]·4HCl	$([2+2]+DA+H_2SO_4+H)^{+}$	1369.4
	$([2+2]+DA+H)^{+}$	1271.5
	$([2+2]+DA+H_2SO_4+2H)^{2+}$	685.3
	$([2+2]+DA+2H)^{2+}$	636.3
	$([2+2]+2DA+3H)^{3+}$	462.9
	$([2+2]+DA+3H)^{3+}$	424.7

Table 3.8. Low resolution ESI+ mass spectrometric data for the diamine adducts of [2+2].

The crystal structure of the hydrochloride salt of the [2+2] adduct (Figure 2.12) shows that the two aldehyde subunits reside near one another in the solid state. The neutral compound may have a conformation that does not favor the cyclization, resulting in two of the chiral diamines adding to the two aldehydes. Consequently, the reaction was repeated using the hydrochloride salt under the same conditions. In this case, mass spectrometric analysis (ESI+) revealed peaks consistent with cyclization as can be seen from Table 3.8 and Figure 3.18.

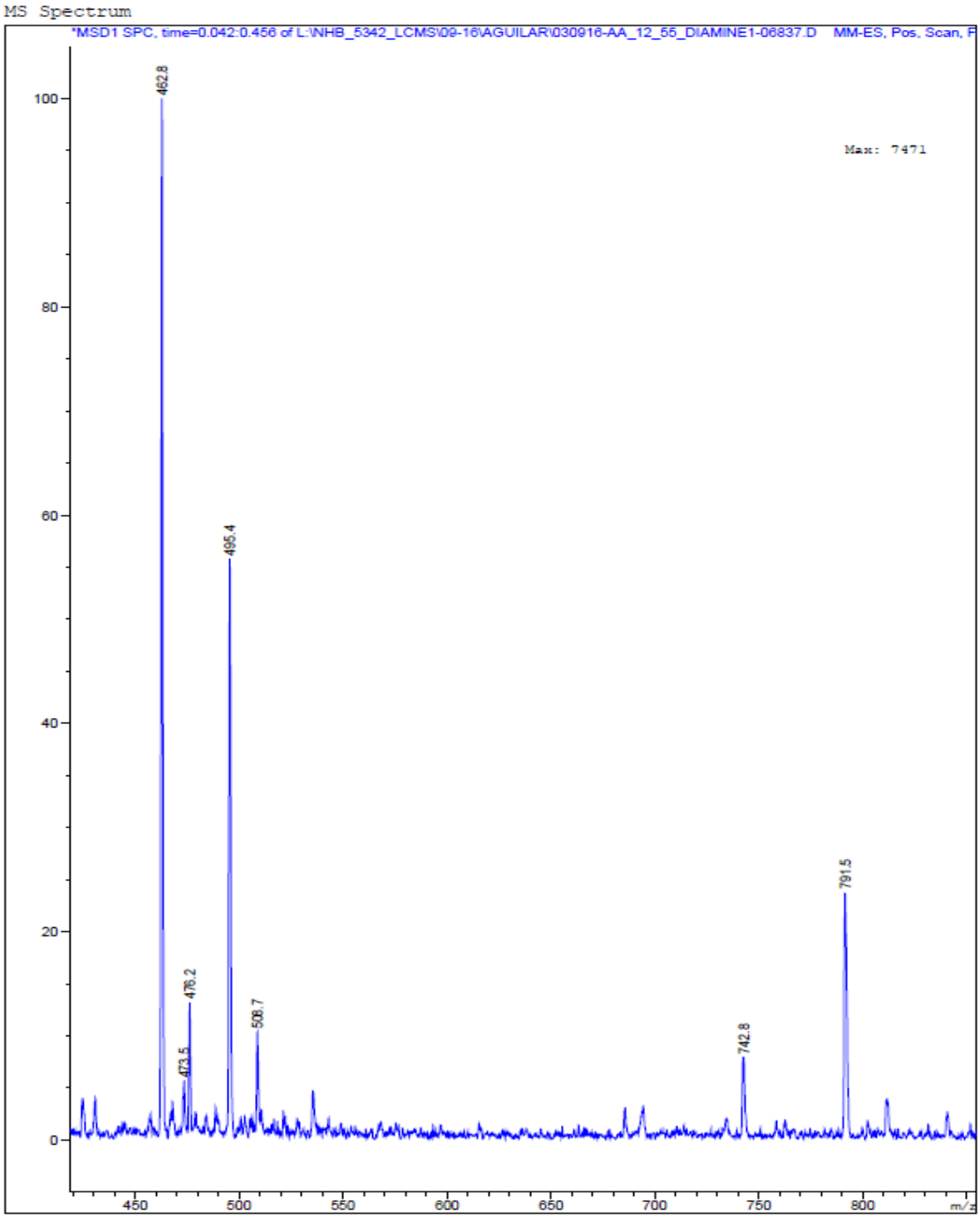

Figure 3.17. Low resolution ESI+ mass spectrum of the presumed product [2+2]+2DA+2H_2SO_4.

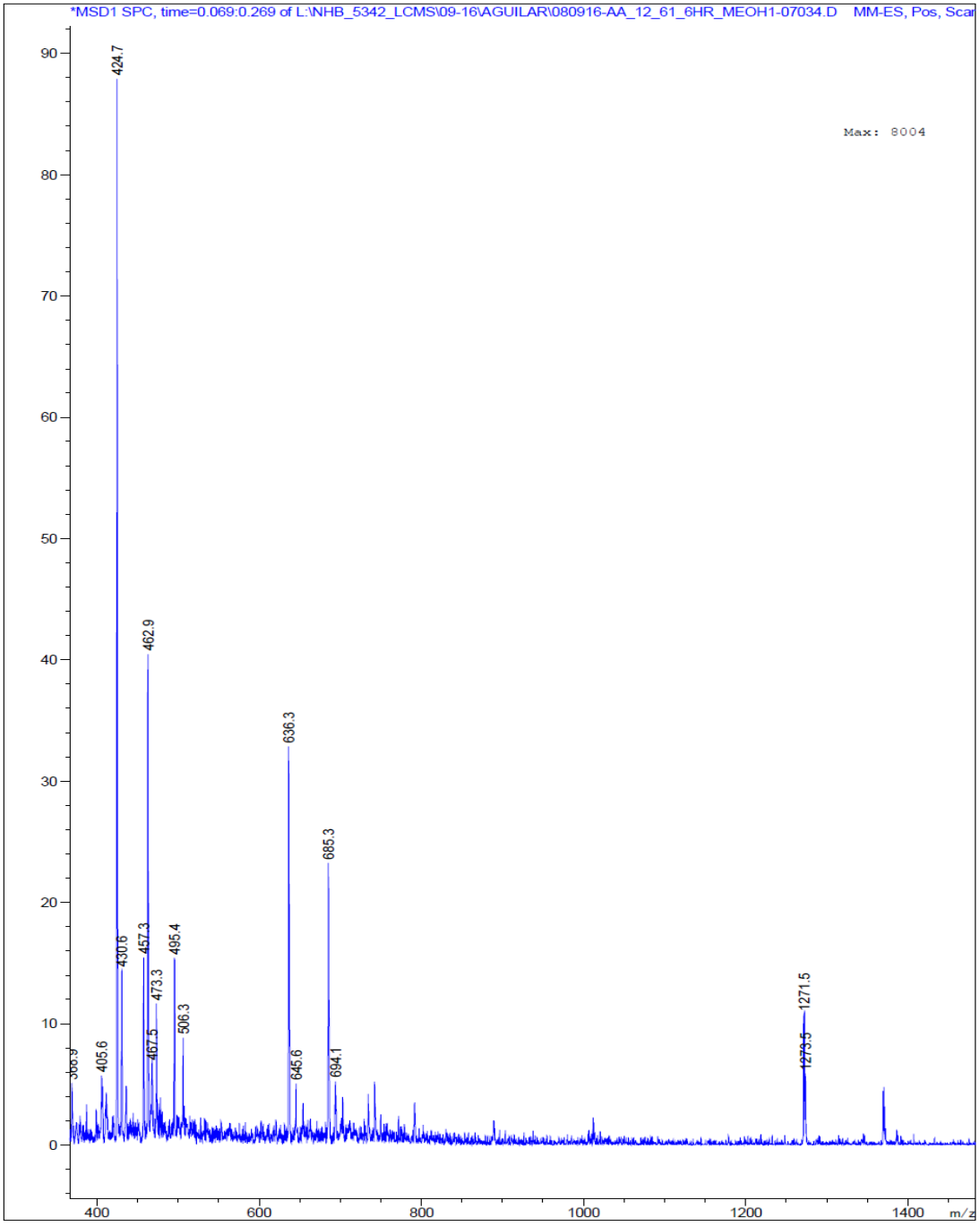

Figure 3.18. Low resolution ESI+ mass spectrum of the presumed product of [2+2]+ DA+H_2SO_4.

The ^{1}H-NMR spectrum of this putative cyclization products is shown in Figure 3.20 (top). This spectrum is consistent with a degree of symmetry in the products presumable reflecting a C2 axis of rotation as is seen in the crystal structure of the HCl salt (Figure 2.12). This leads the author to suggest that the compounds produced via this condensation contain two cavities that each hold a sulfate anion within a chiral environment induced by the diamines.

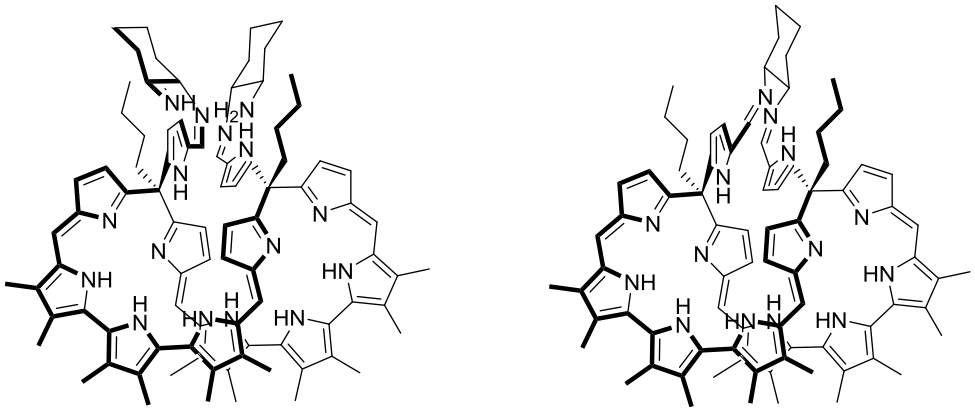

Figure 3.19. Proposed structures for the macrocyclic products obtained when the [2+2] adduct is allowed to react with (1R,2R)-(-)-1,2-diaminocyclohexane (DA). [2+2]+2DA is used to designate the product formed from the neutral adduct, whereas [2+2]+DA denotes the product obtained starting from the hydrochloride salt of the [2+2] adduct.

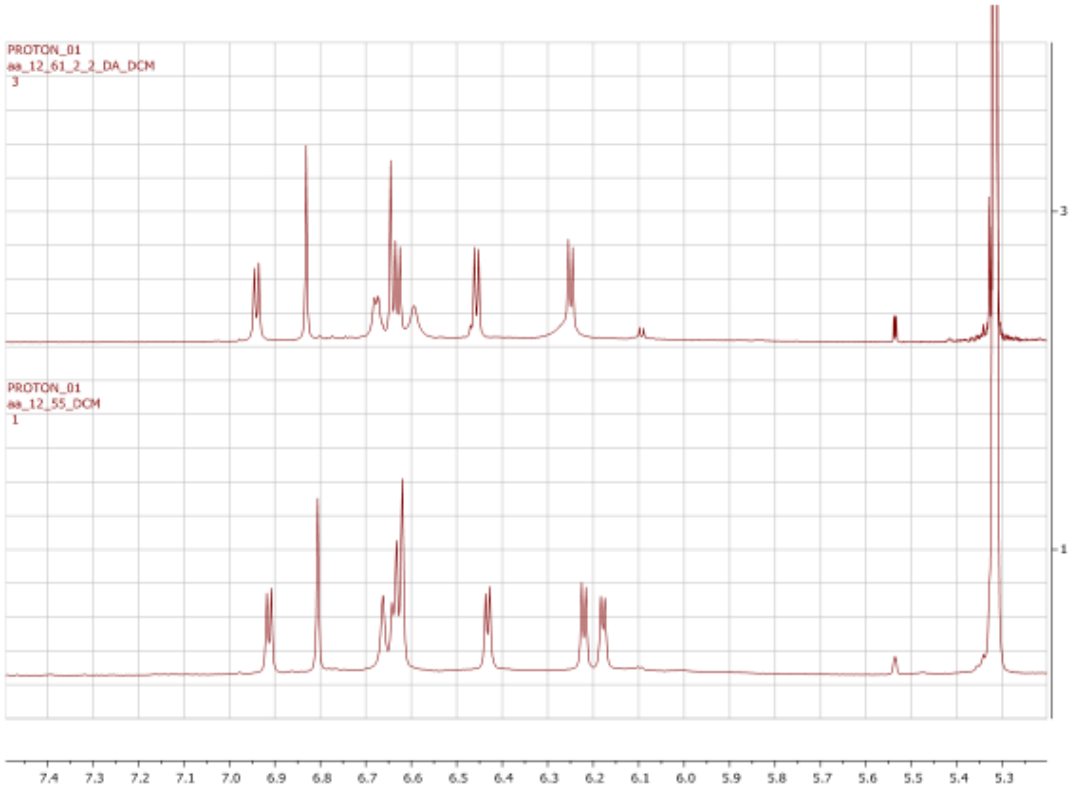

Figure 3.20. ^{1}H-NMR spectra of [2+2]+2DA (bottom) and [2+2]+DA (top).

3.10. Future Directions.

The aldehyde handles on the [1+1] and [2+2] adducts may allow access to ditopic receptors by appending functionality, such as crown ethers for binding metals. These moieties may also allow preparation of chiral sensors for biologically relevant anions. In the case of both the [1+1] and [2+2] adducts, the aldehyde moieties may permit reaction with chiral diamines to create cavities that discriminate between chiral guests. The aldehydes might also provide a handle that would allow the adducts to be attached to solid supports. The cryptand like adduct [3+2]a, if it adopts a conformation similar to

the [2+2] adduct, may exist as a mixture of enantiomers (Figure 3.21) that could be resolved and serve as chiral hosts or sensors or both.

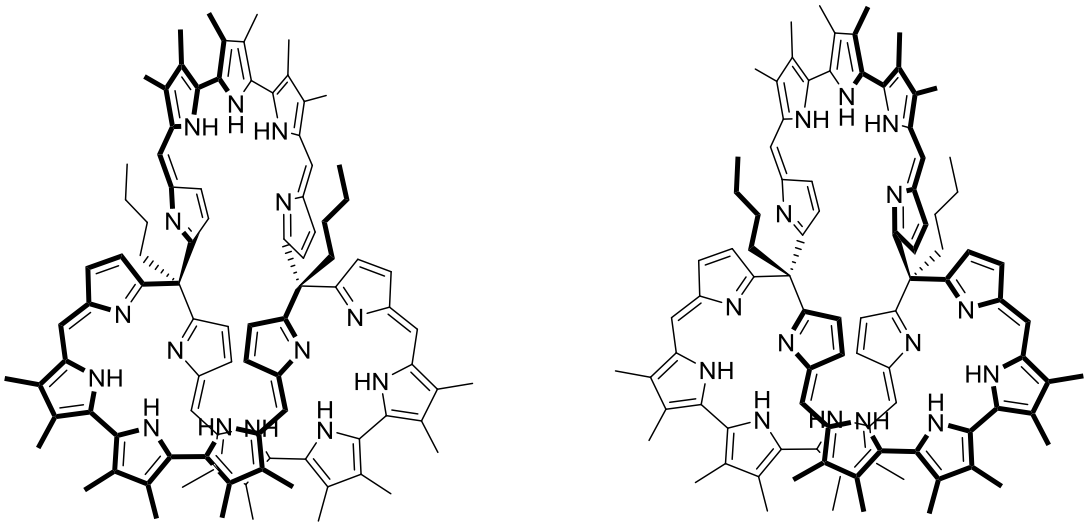

Figure 3.21. Enantiomers of [3+2] adduct.

It would be interesting to study the metal coordination chemistry of the [1+1], [2+2] and [3+2] adducts since several related macrocycles exhibit rich metalation chemistry. Each adduct also contains multiple dipyrromethene subunits that could be converted to BODIPY-like BF_2 entities to permit fluorescence based recognition studies.

Chapter 4:

Experimental

General: ^{1}H and ^{13}C NMR spectra were measured at 25 ºC on a Varian DirectDrive 400 MHz, UV/Vis spectra were recorded on Carey 500 spectrophotometer. Low resolution CI mass spectra were obtained on an Agilent Technologies 6120 Quadrupole LC/MS. High resolution mass spectra were obtained on Agilent QTof mass spectrometer. Purification was done on JAI (Japan Analytical Industry Co., Ltd. Recycling Preparative HPLC LC-92XXII NEXT series. Reverse phase HPLC was performed on Dionex UltiMate 3000 using Hypersil Gold (250 mm x 21.2 mm). Unless otherwise noted, solvents and reagents were reagent-grade and were used without further purification. Tetrahydrofuran (THF) was dried by passage through two columns of activated alumina. Dimethylformamide (DMF) was dried by passage through two columns of activated molecular sieves. Chemical shifts are reported in parts per million (ppm, δ) and are referenced to the residual solvent. Coupling constants are reported in Hertz (Hz). Spectral splitting patterns are designated as s: singlet, d: doublet, t: triplet, q:quartet, m: multiplet (chemically equivalent H's), and comp: complex multiplet (chemically non-equivalent H's), br: broad.

General reaction:

To a two necked 1L round bottom flask equipped with an addition funnel was added 600 mL of ethanol and bubbled with nitrogen gas for two hours. The trialdehyde **30c**

351.4 mg (1 mmol) was dissolved in 2 mL of dichloromethane and this solution was poured into the stirring ethanol. To 100 mL of ethanol that was bubbled for 2 hours with nitrogen was added 281.4 mg (1 mmol) of the terpyrrole **31c**. This terpyrrole solution was placed in the addition funnel and the entire system was flushed with nitrogen. To the stirring solution of trialdehyde **30c** in ethanol was added 70 drops of concentrated hydrochloric acid. The terpyrrole solution was then added dropwise over a period of one hour. After this time, the reaction mixture was concentrated in vacuo and taken to dryness on high vacuum.

Purification:

The crude solid was dissolved in 15 mL of chloroform and filtered through filter paper. This solution was then filtered through a PTFE disc and injected in three portion into the recycling prep GPC-HPLC (2HH + 2.5HH columns). The fractions with retention times less than 36 minutes were drained (higher molecular weight) and fractions with retention time 36-40 minutes were recycled (contain the [3+2] and [2+2] adducts) while fractions with retention time 41-43 minutes (contain the [1+1] adduct). Fractions containing the [3+2] and [2+2] adducts were recycled 15 times and collected. The isolated [1+1] and [2+2] fractions were concentrated in vacuo and taken to dryness.

Each sample was dissolved in 5 mL acetonitrile followed by 5 mL water and the 10 mL solution was filtered through a PTFE disc. The solutions were injected in 5 mL portion and run using a solvent gradient with acetonitrile (1% acetic acid v/v) and water (1% acetic acid v/v) as follows: 50% to 90% acetic acid in water over 30 minutes, 90% to

99% in 10 minutes, 99% to 99% for 20 minutes. Mass Spectrometric analysis was used to identify impurities and fractions containing only product were collected and combined. The combined fractions were dissolved in ethyl acetate and washed with sodium bicarbonate, concentrated in vacuo and redissolved in ethanol. To the ethanolic solutions were added 4 drops of concentrated hydrochloric acid and taken to dryness in vacuo.

Estimation of binding constants:

All binding constants were estimating using the online software available at www.supramolecular.org. Host concentrations were 18.3 mM for the [1+1] adduct and 5 mM for the [2+2] and [3+2] adducts. Masses were measured at thee significant figures (reliable at 2 significant figures). Two to four data sets (different wavelengths) were used from each titration for global fitting to 2:1, 1:1, and 1:2 host guest models. The model with the best fit was used. The reported percent error on the linear regression analysis is based on asymptotic standard error which is then used to calculate 95% intervals (which can be approximated as the 2x the standard error). This error is only approximate as it relies on a few key assumptions regarding the non-linear regression process, including that the error is only a result of the physical property being measured (absorbance). It ignores uncertainties in the concentrations of the host and guest (the quantities that form the x-axis in the fitting process.[44]

Tris(pyrrole-2-carbaldehyde) ^{1}H-NMR

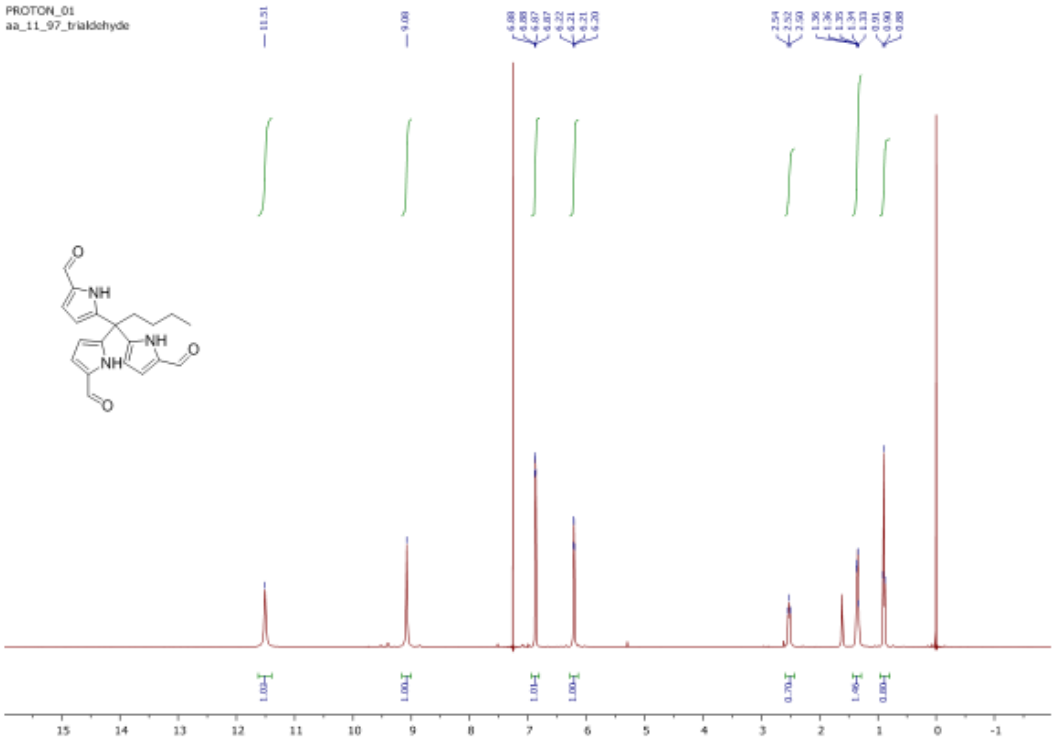

^{1}H-NMR (400 MHz, $CDCl_3$) δ 11.51 (3H, s), 9.08 (3H, s), 6.87 (3H, dd), 6.21 (3H, dd), 2.52 (2H, t), 1.38-1.30 (4H, m), 0.90 (3H, t).

^{13}C-NMR (400 MHz, $CDCl_3$)

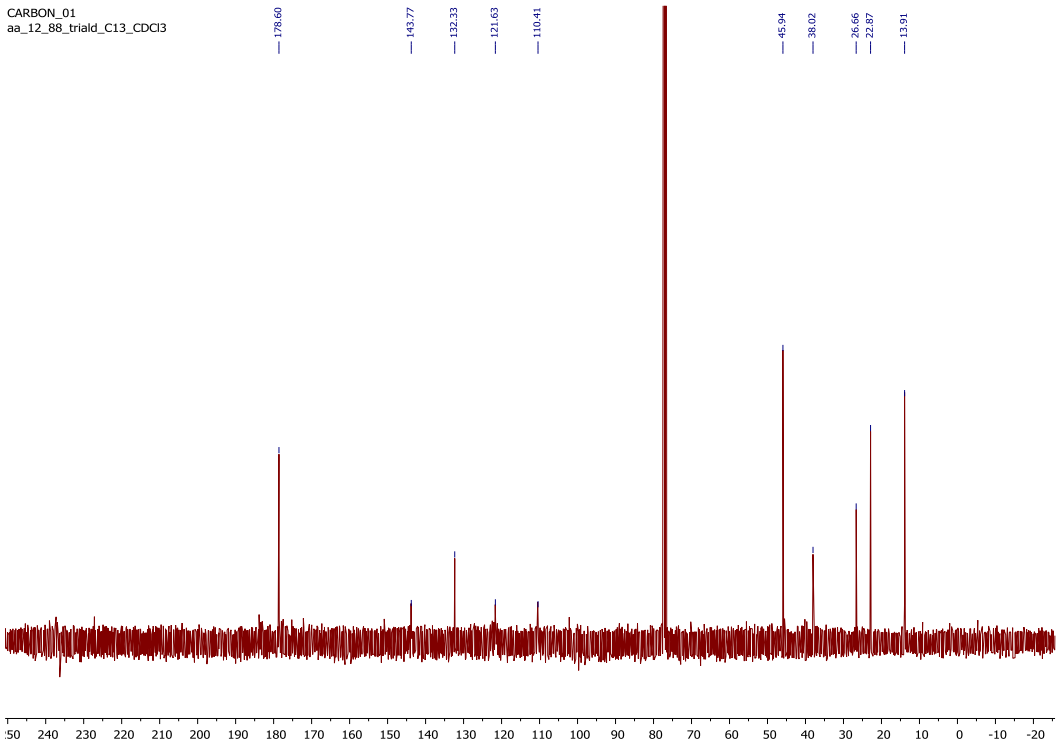

^{13}C NMR (101 MHz, Chloroform-*d*) δ 178.60, 143.77, 132.33, 121.63, 110.41, 77.33, 45.94, 38.02, 26.66, 22.87, 13.91.

[1+1] Neutral adduct (CD_2Cl_2) ^{1}H-NMR

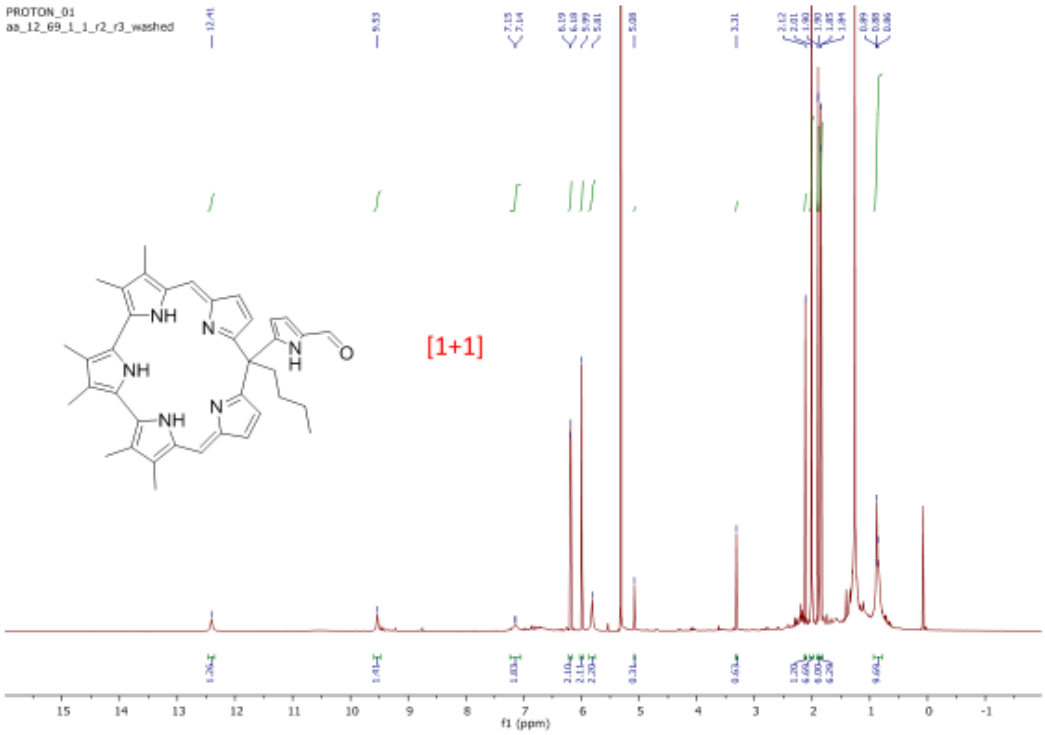

^{1}H-NMR (400 MHz, CD_2Cl_2) δ 12.43 (1H, s), 9.53 (1H, s), 7.23-7.05 (1H, m), multiplet 6.7, 6.19 (2H, d), 5.99 (2H, s), 5.81 (2H, br s), 5.03 (?H, s), 3.31 (?H, s), 2.12 (2H, s), 2.01 (6H, s), 1.90 (6H, s), 1.85 (6H, s), 1.36-1.28 (4H, under grease), 0.90-0.85 (3H, under grease).

[1+1] neutral adduct (CD_2Cl_2) ^{13}C-NMR

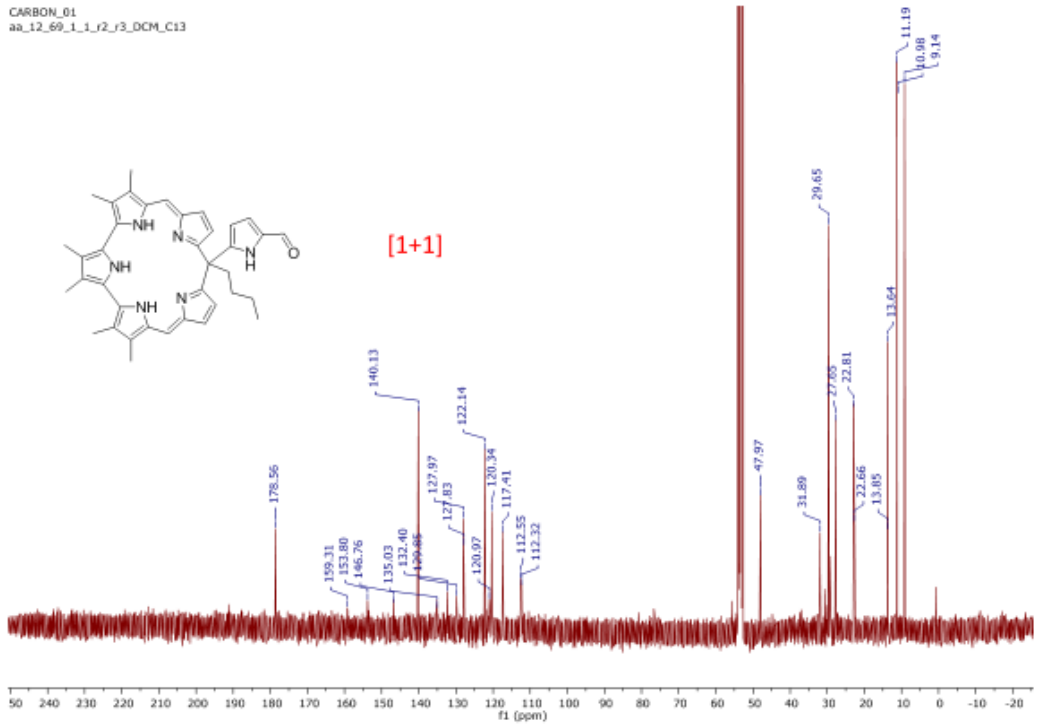

^{13}C-NMR (400 MHz, CD_2Cl_2) δ 178.56, 159.31, 153.80, 146.76, 140.13, 135.03, 132.40, 129.85, 127.97, 127.83, 122.14, 120.97, 120.34, 117.41, 112.55, 112.32, 47.97, 31.89, 27.66, 22.81, 13.64, 11.19, 10.98, 9.14 ppm.

[1+1]·2HCl adduct ^{1}H-NMR $CDCl_3$

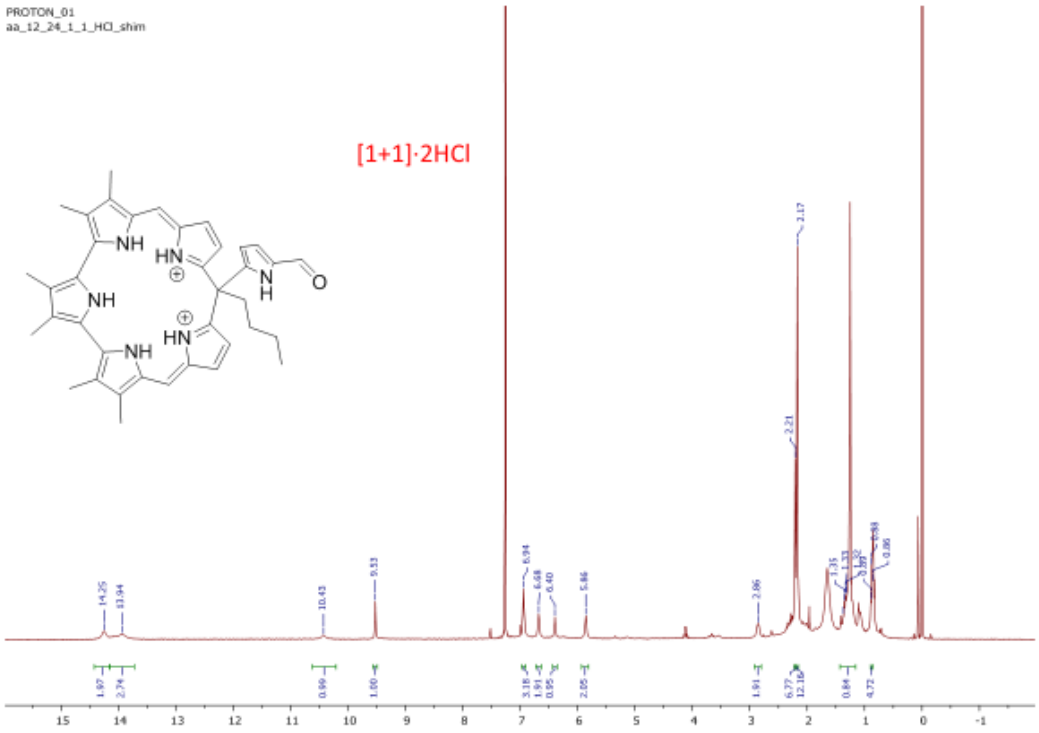

^{1}H-NMR (400 MHz, $CDCl_3$) δ 14.25 (2H, s), 13.94 (3H, m), 10.43 (1H, s), 9.53 (1H, s), 6.94 (3H, s), 6.68 (2H, s), 6.40 (1H, s), 5.86 (2H, s), 2.86 (2H, s), 2.21 (6H, s), 2.17 (12H, s), 1.42-1.28 (4H, m, under ethanol), 0.88 (3H, t under grease)

[1+1]·2HCl adduct ^{1}H-NMR CD_2Cl_2

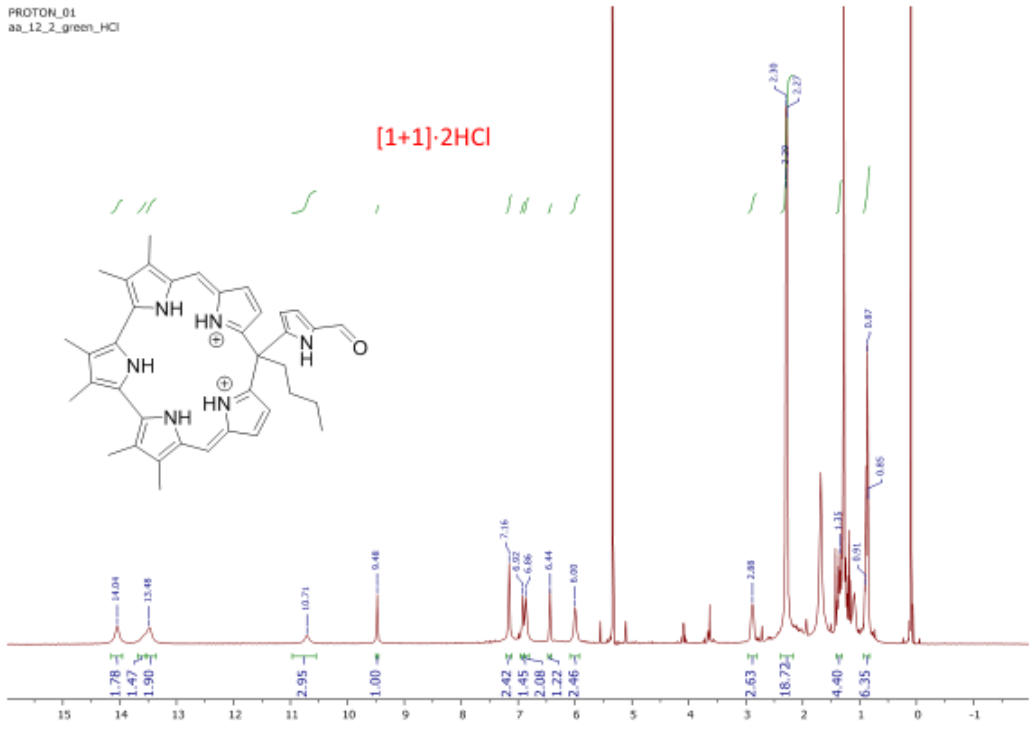

^{1}H-NMR (400 MHz, CD_2Cl_2) δ 14.04 (1H, 2H, br s), 13.48 (3H, br s), 10.71 (1H, br s), 9.48 (1H, s), 7.16 (2H, s), 6.92 (1H, s), 6.86 (2H, s), 6.44 (1H, s), 6.00 (2H, s), 2.88 (2H, s), 2.29 (18H, m), 1.41-1.30 (4H, m under grease), 0.92-0.87 (3H, m under grease).

[2+2] Neutral adduct ^{1}H-NMR (400 MHz, $CDCl_3$) (12/69)

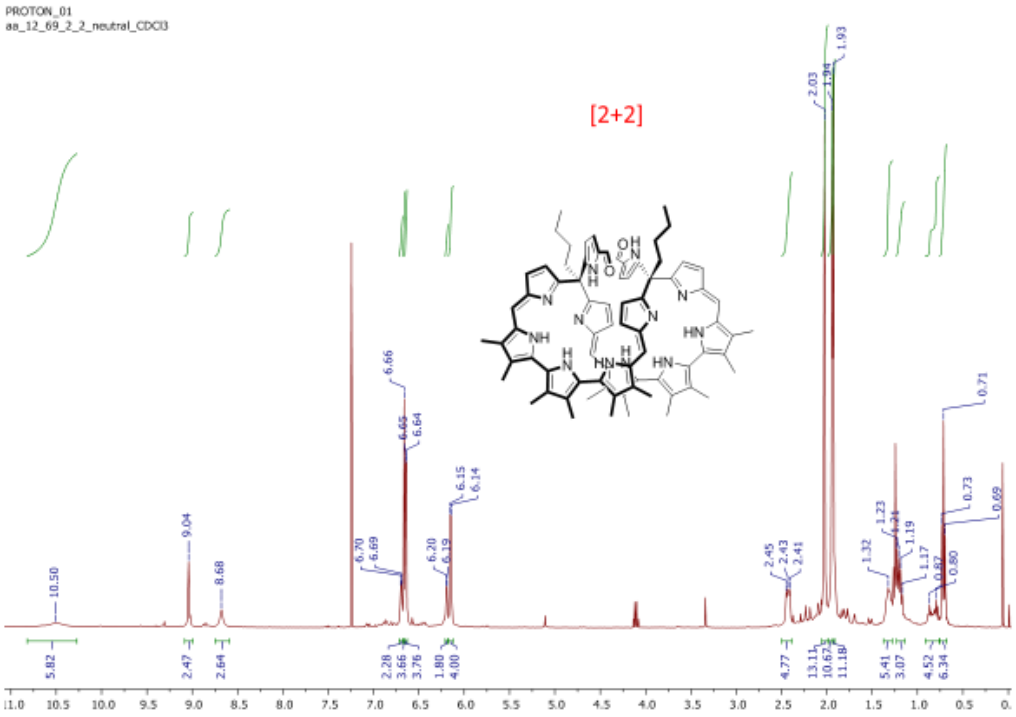

^{1}H-NMR (400 MHz, $CDCl_3$) δ 10.50 (6H, br s), 9.04 (2H, s), 8.68 (2H, br s), 6.70 (2H, br d), 6.66 (4H, s), 6.65 (4H, d), 6.20 (2H, br d), 6.15 (4H, d), 2.43 (4H, dd), 2.03 (12H, s), 1.94 (12H, s), 1.93 (12H, s), 1.37-1.16 (8H, m), 0.75-0.68 (6H, t).

[2+2] neutral adduct ^{13}C-NMR (400 MHz, $CDCl_3$)

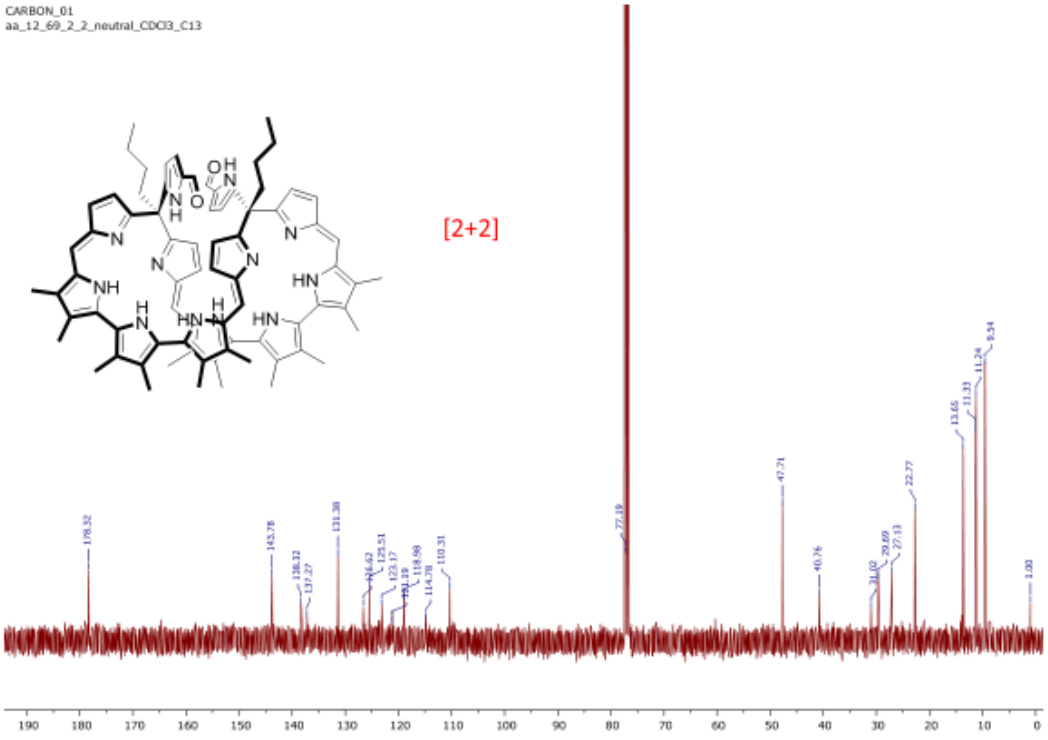

^{13}C-NMR (400 MHz, $CDCl_3$) δ 178.32, 143.78, 138.32, 137.27, 131.38, 126.62, 125.51, 123.17, 121.19, 118.98, 114.78, 110.31, 47.71, 40.76, 27.13, 22.77, 13.65, 11.33, 11.24, 9.54 ppm.

High resolution mass spectrum of the [2+2] adduct.

Data File	MSF16-3895(aa_12_87_2_2)_hrESIpos2.d	**Sample Name**	3895(aa_12_87_2_2)	**Comment**	3895(aa_12_87_2_2)
Position	P1-B3	**Instrument Name**	Instrument 1	**User Name**	
Acq Method	pos.m	**Acquired Time**	11/17/2016 12:23:22 PM	**DA Method**	KS.m

MS Zoomed Spectrum

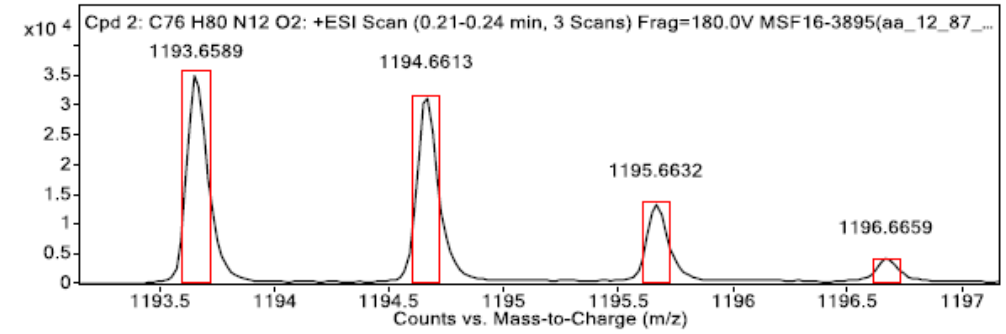

MS Spectrum Peak List

Obs. m/z	Calc. m/z	Charge	Abund	Formula	Ion/Isotope	Tgt Mass Error (ppm)
943.99290			155457.2			
1193.65890	1193.66000	1	35458.78	C76H80N12O2	(M+H)+	0.94
1194.66130	1194.66310	1	31766.2	C76H80N12O2	(M+H)+	1.5
1195.66320	1195.66610	1	13486.75	C76H80N12O2	(M+H)+	2.47
1196.66590	1196.66910	1	3922.34	C76H80N12O2	(M+H)+	2.72
1197.65310	1197.67210	1	992.45	C76H80N12O2	(M+H)+	15.92
1198.63580	1198.67510	1	328.13	C76H80N12O2	(M+H)+	32.82

--- End Of Report ---

[2+2].4HCl adduct ^{1}H-NMR (400 MHz, $CDCl_3$)

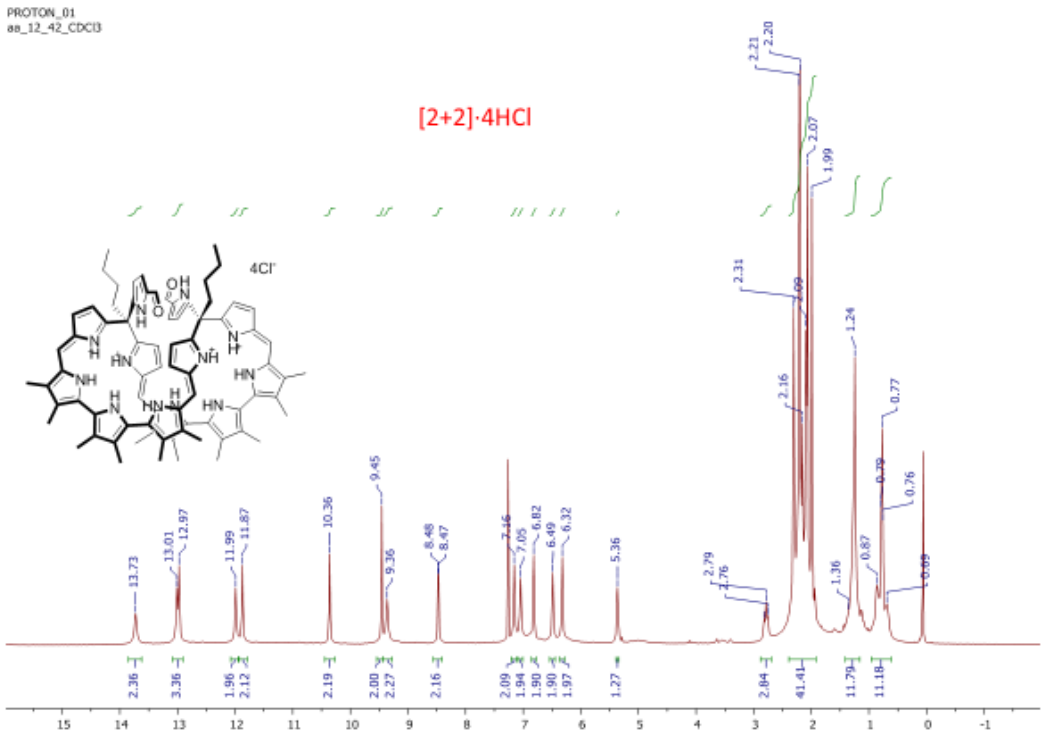

^{1}H-NMR (400 MHz, $CDCl_3$) δ 13.73 (2H, s), 13.01 (2H, s), 12.97 (2H, s), 11.99 (2H, s), 11.87 (2H, s), 10.36 (2H, s), 9.45 (2H, s), 9.36 (2H, s), 8.48 (2H, d), 7.16 (2H, s), 7.05 (2H, s), 6.82 (2H, s), 6.49 (2H, s), 6.32 (2H, s), 5.36 (2H, s), 2.79 (4H, t), 2.31 (6H, s), 2.21 (6H, s), 2.20 (6H, s), 2.09 (6H, s), 2.07 (6H, s), 1.99 (6H, s), 1.41-1.27 (8H, m under grease), 0.90-0.60 (6H, m under grease).

[2+2].4HCl adduct ^{13}C-NMR (400 MHz, CD_2Cl_2)

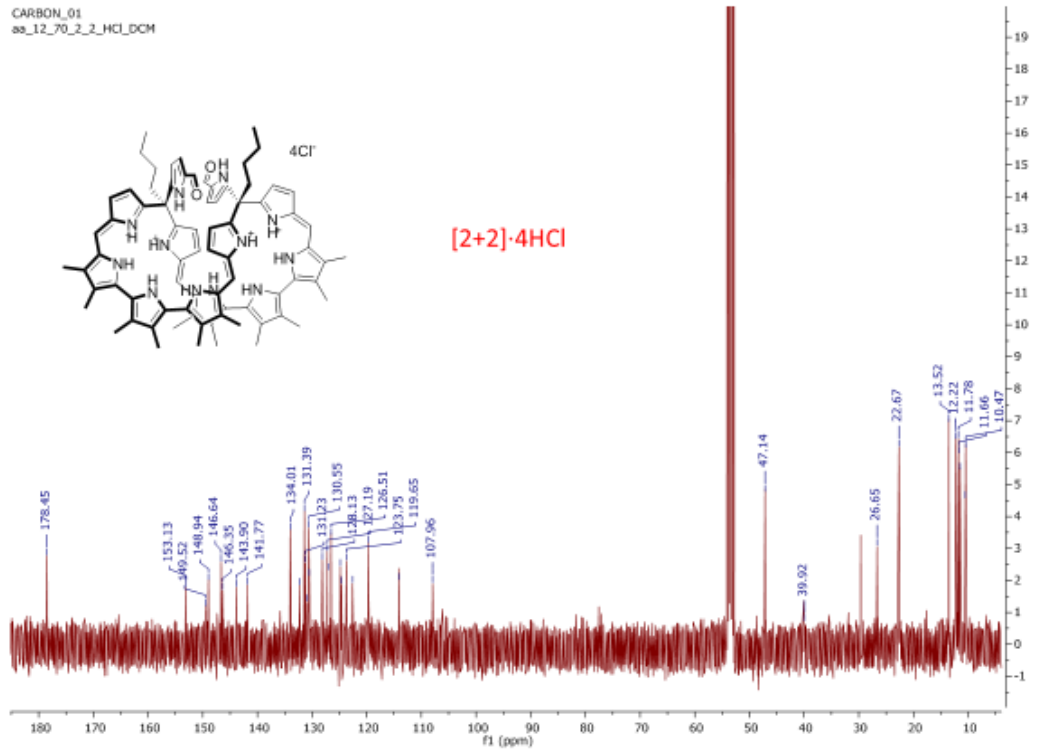

^{13}C-NMR (400 MHz, $CDCl_3$) δ 178.45, 153.13, 149.52, 148.94, 146.64, 146.35, 143.90, 141.77, 134.01, 132.25, 131.39, 131.23, 130.85, 130.55, 130.50, 128.13, 127.19, 127.09, 126.51, 124.84, 124.61, 123.75, 122.57, 119.65, 114.13, 107.96, 47.14, 39.92, 26.65, 22.67, 13.52, 12.22, 11.78, 11.66, 11.50, 10.52, 10.47 ppm.

[3+2]·6HCl adduct ^{1}H-NMR (400 MHz, CD_2Cl_2)

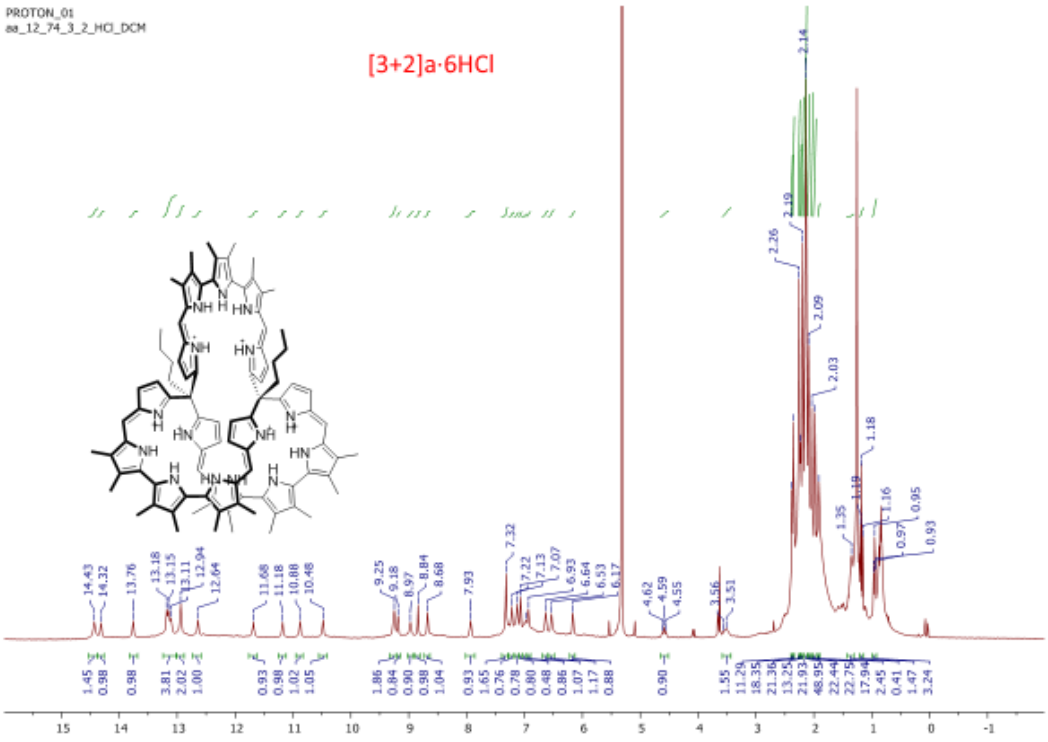

^{1}H-NMR (400 MHz, CD_2Cl_2) δ 14.43 (2H, br s), 14.32 (1H, s), 13.76 (1H, s), 13.18 (1H, s), 13.15 (2H, br s), 13.11 (1H, s), 12.94 (2H, s), 12.64 (1H, s), 11.68 (1H, s), 11.18 (1H, s), 10.88 (1H, s), 10.48 (1H, s), 9.25 (2H, br s), 9.18 (1H, s), 8.97 (1H, s), 8.84 (1H, s), 8.68 (1H, s), 7.93 (1H, s), 7.32 (2H, s), 7.22 (1H, s), 7.13 (1H, s), 7.07 (1H, s), 6.98 (1H, br s), 6.93 (1H, s), 6.64 (1H, s), 6.53 (1H, s), 6.17 (1H, s), 5.32 (1H, br s), 4.59 (1H, br t), 3.58-3.43 (2H, m), 2.51 (1H, m), 2.38 (3H, br s), 2.36 (6H, br s), 2.26 (6H, br s), 2.23 (3H, br s), 2.19 (6H, br s), 2.14 (24H, br m), 2.09 (6H, br s), 2.03 (6H, br s), 1.98 (6H, s), 1.40-1.28 (4H, m under grease), 0.98-0.80 (6H, m under grease).

[3+2] adduct ^{13}C-NMR could not be obtained due to solubility, large molecular weight. At a concentration of 35 mg/mL of $CDCl_3$ and 15,000 scans, the pyrrole aromatic carbon atoms were not observed.

High resolution mass spectrum of the [3+2] adduct.

Data File	MSF16-3896(aa_12_87_3_2)_hrESIpos4.d	**Sample Name**	3896(aa_12_87_3_2)	**Comment**	3896(aa_12_87_3_2)
Position	P1-B4	**Instrument Name**	Instrument 1	**User Name**	
Acq Method	pos.m	**Acquired Time**	11/17/2016 12:31:41 PM	**DA Method**	KS.m

MS Zoomed Spectrum

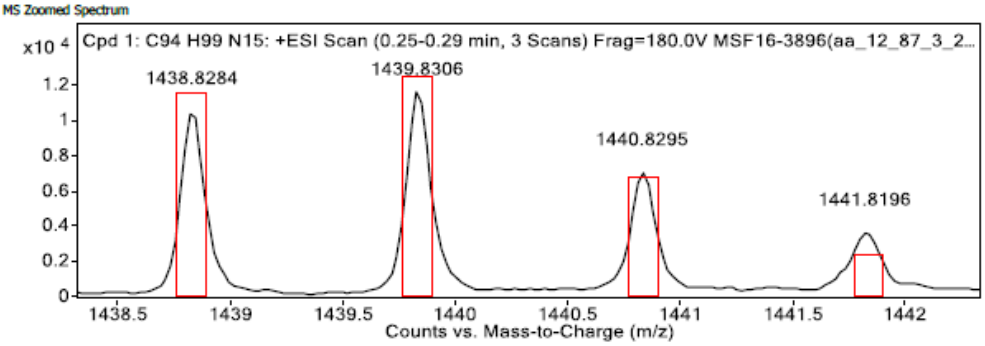

MS Spectrum Peak List

Obs. m/z	Calc. m/z	Charge	Abund	Formula	Ion/Isotope	Tgt Mass Error (ppm)
659.29020			36291.81			
1438.82840	1438.82810	1	10584.5	C94H99N15	(M+H)+	-0.23
1439.83060	1439.83110	1	11677.91	C94H99N15	(M+H)+	0.36
1440.82950	1440.83420	1	7111.4	C94H99N15	(M+H)+	3.24
1441.81960	1441.83730	1	3703.48	C94H99N15	(M+H)+	12.24

--- End Of Report ---

[3+2]·6HCl ^{1}H-NMR (400 MHz, $CDCl_3$)

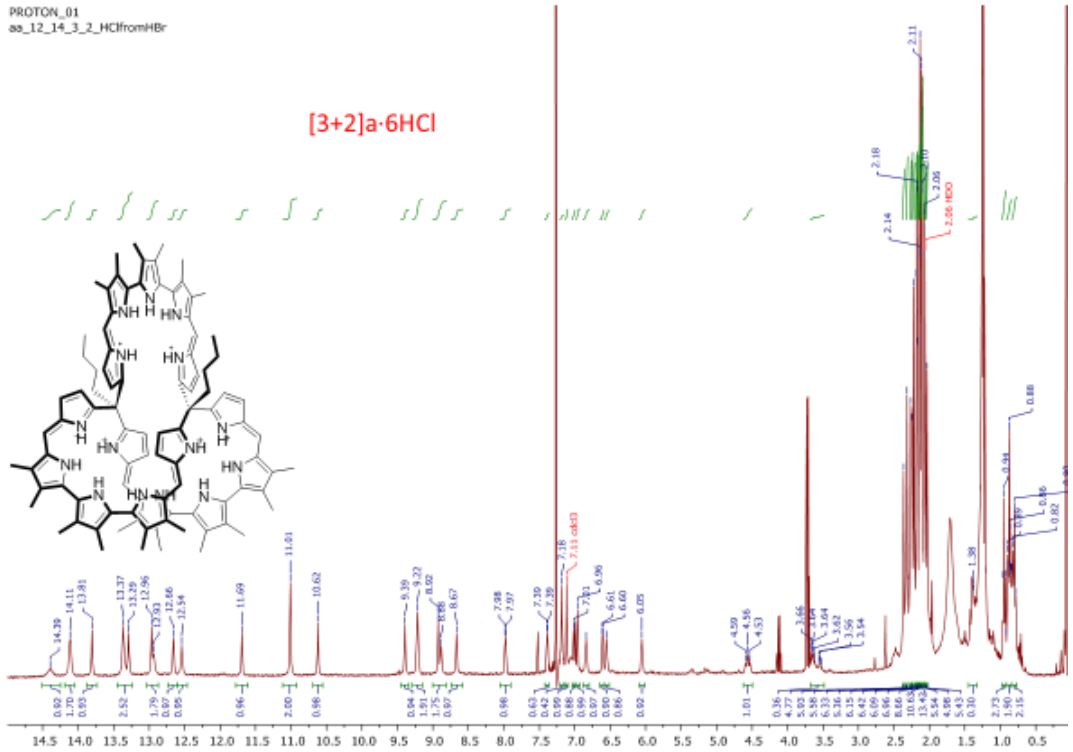

^{1}H-NMR (400 MHz, $CDCl_3$) δ 14.39 (1H, br s), 14.11 (2H, s), 13.81, (1H, s), 13.37 (2H, s), 13.29 (1H, s), 12.96 (1H, s), 12.93 (1H, br s), 12.66 (1H, s), 12.54 (1H, s), 11.69 (1H, s), 11.01 (2H, s), 10.62 (1H, s), 9.39 (1H, s), 9.22 (2H, br s), 8.92 (1H, s), 8.88 (1H, br s), 8.67 (1H, s), 7.98 (1H, d), 7.39 (1H, d), 7.18 (1H, s), 7.11 (1H, s), 7.01 (1H, s), 6.96 (1H, s), 6.84 (1H, br s), 6.61 (1H, d), 6.53 (1H, s), 6.06 (1H, s), 4.56 (1H, t), 3.68-3.49 (2H, m), 2.48 (1H, br t), 2.36 (3H, s), 2.31 (3H, s), 2.26 (3H, s), 2.24 (3H, s), 2.22 (3H, s), 2.18-2.17 (9H, m), 2.14-2.13 (6H, m), 2.11 (6H, s), 2.10 (9H, br s), 2.06 (3H, s), 2.06 (3H, s), 2.03 (3H, s), 1.45-1.2 (8H, m, under grease and ethanol), 0.98-0.69 (6H, m, under grease).

[3+2]a ^{1}H-NMR (400 MHz, CD_2Cl_2)

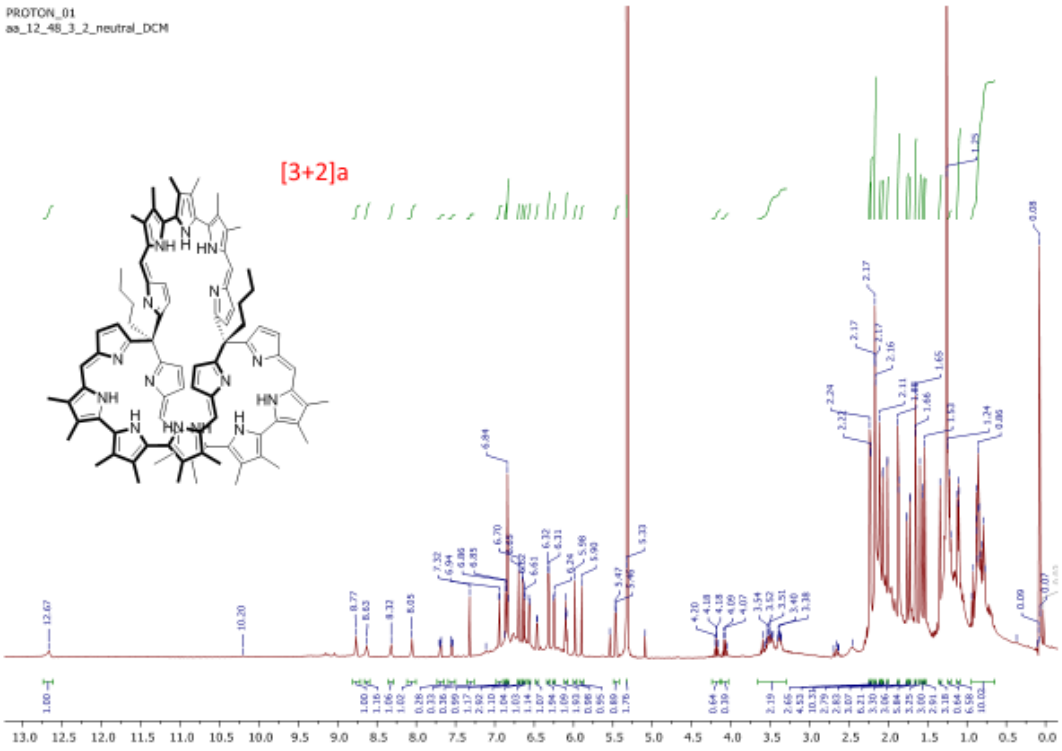

PROTON_01
aa_12_48_3_2_neutral_DCM

[3+2]a

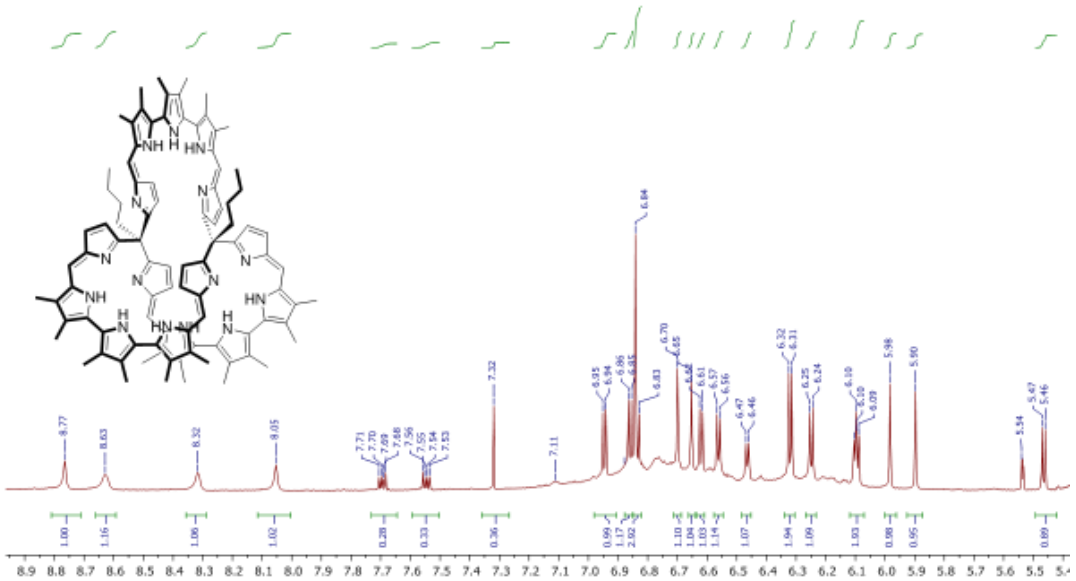

PROTON_01
aa_12_48_3_2_neutral_DCM

[3+2]a

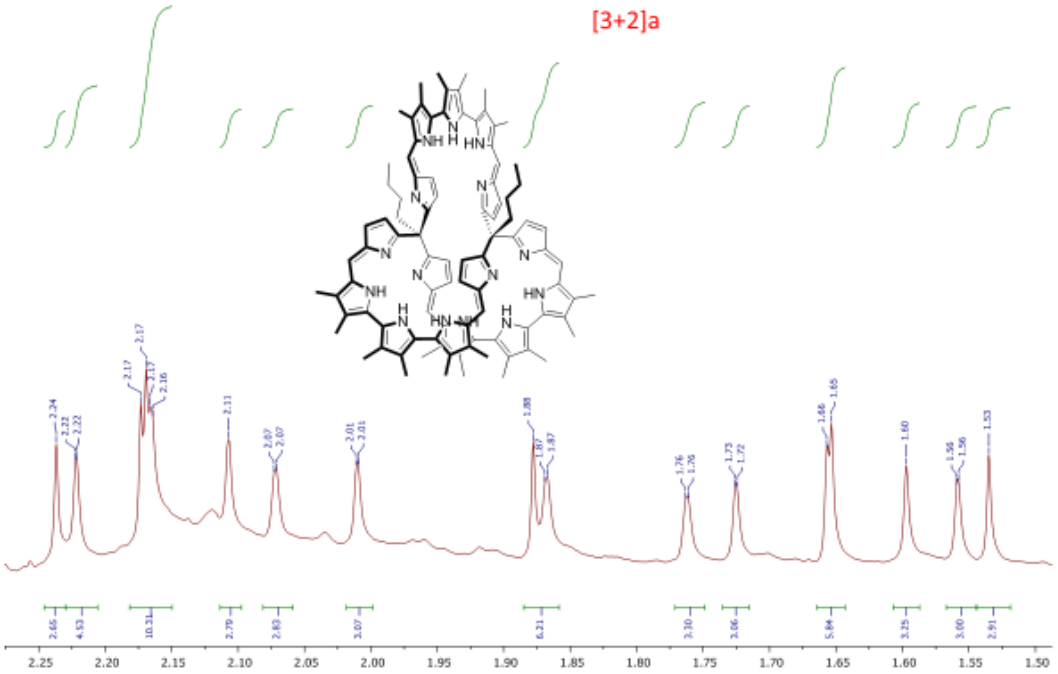

^{1}H-NMR (400 MHz, CD_2Cl_2) δ 12.67 (1H, br s), 8.77 (1H, br s), 8.63 (1H, br s), 8.32 (1H, br s), 8.05 (1H, br s), 6.95 (1H, d), 6.86 (1H, d), 6.84-6.83 (2H, s, 1H, d), 6.70 (1H, s), 6.65 (1H, s), 6.62 (1H, d), 6.57 (1H, d), 6.47 (1H, d), 6.32 (2H, d), 6.25 (1H, d), 6.10-6.09 (1H, d, 1H, d), 5.98 (1H, s), 5.90 (1H, s), 5.47 (1H, d), 3.55-3.33 (2H, m), 2.70-2.60 (1H, m), 2.54-2.40 (1H, m), 2.24 (3H, s), 2.22 (3H, s), 2.17 (12H, m), 2.11 (3H, s), 2.07 (3H, s), 2.01 (3H, s), 1.88 (3H, s), 1.87 (3H, s), 1.76 (3H, s), 1.73 (3H, s), 1.66-1.65 (6H, m), 1.60 (3H, s), 1.56 (3H, s), 1.53 (3H, s), 1.13-1.09 (8H, m), 0.94-0.77 (6H, m under grease).

Appendix

checkCIF/PLATON report

Structure factors have been supplied for datablock(s) shelx

THIS REPORT IS FOR GUIDANCE ONLY. IF USED AS PART OF A REVIEW PROCEDURE FOR PUBLICATION, IT SHOULD NOT REPLACE THE EXPERTISE OF AN EXPERIENCED CRYSTALLOGRAPHIC REFEREE.

No syntax errors found. CIF dictionary Interpreting this report

Datablock: shelx

Bond precision: C-C = 0.0060 A Wavelength=1.54184

Cell: a=12.4451(3) b=16.7853(3) c=20.1600(3)
alpha=104.881(1) beta=99.036(2) gamma=103.359(2) Temperature: 100 K

	Calculated	Reported
Volume	3853.66(14)	3853.66(14)
Space group	P -1	P -1
Hall group	-P 1	-P 1
C74.71 H82.97 N11.74		
C76 H84 N12 O2, C H2 Cl2,		
Moiety formula O1.74, 0.26(C5 H4 N O),		
H2 O		
0.74(C H2 Cl2), 4(		
C76.75 H87.49 Cl5.48 N12		
Sum formula		C77 H88 Cl2 N12 O3
O3		
Mr	1420.41	1300.49
Dx,g cm-3	1.224	1.121
Z	2	2
Mu (mm-1)	2.291	1.165

F000	1498.4	1384.0
F000'	1505.94	
h,k,lmax	15,20,25	15,20,25
Nref	15575	15128
Tmin,Tmax	0.811,0.900	0.790,1.000
Tmin'	0.705	

Correction method= # Reported T Limits: Tmin=0.790 Tmax=1.000
AbsCorr = MULTI-SCAN

Data completeness= 0.971 Theta(max)= 73.715

R(reflections)= 0.0794(11898) wR2(reflections)= 0.2320(15128)

S = 1.044 Npar= 934

The following ALERTS were generated. Each ALERT has the format **test-name_ALERT_alert-type_alert-level**. Click on the hyperlinks for more details of the test.

Alert level B

CHEMW03_ALERT_2_B WARNING: The ratio of given/expected molecular weight as calculated from the _atom_site* data lies outside the range 0.95 <> 1.05
From the CIF: _cell_formula_units_Z 2

From the CIF: _chemical_formula_weight 1300.49 TEST: Calculate formula weight from _atom_site_* atom mass num sum
C 12.01 76.75 921.84
H 1.01 87.49 88.19

N 14.01 12.00 168.11
Cl 35.45 5.48 194.28

O 16.00 3.00 48.03
Calculated formula weight 1420.46

Author Response: The program, Squeeze, in Platon98, was used to remove the contributions to the scattering due to some disordered solvent.

PLAT201_ALERT_2_B Isotropic non-H Atoms in Main Residue(s) ..... 7 Report

Author Response: The lower occupancy atoms of one of the disordered pyrrole aldehyde groups was refined isotropically.

Alert level C

DIFMN02_ALERT_2_C The minimum difference density is < -0.1*ZMAX*0.75

_refine_diff_density_min given = -1.371

Test value = -1.275

DIFMN03_ALERT_1_C The minimum difference density is < -0.1*ZMAX*0.75 The relevant atom site should be identified.

PLAT098_ALERT_2_C Large Reported Min. (Negative) Residual Density -1.37 eA-3

PLAT220_ALERT_2_C Non-Solvent Resd 1 C Ueq(max)/Ueq(min) Range 3.3 Ratio

PLAT222_ALERT_3_C Non-Solvent Resd 1 H Uiso(max)/Uiso(min) Range 4.1 Ratio PLAT234_ALERT_4_C Large Hirshfeld Difference C54 -- C55 .. 0.16 Ang.

PLAT340_ALERT_3_C Low Bond Precision on C-C Bonds ..... 0.00597 Ang.

PLAT413_ALERT_2_C Short Inter XH3 .. XHn H65B .. H70A .. 2.00 Ang.

PLAT413_ALERT_2_C Short Inter XH3 .. XHn H65B .. H70B .. 2.10 Ang.

PLAT911_ALERT_3_C Missing # FCF Refl Between THmin & STh/L= 0.600 107 Report

PLAT918_ALERT_3_C Reflection(s) with I(obs) much Smaller I(calc) . 1 Check

---

Alert level G

FORMU01_ALERT_2_G There is a discrepancy between the atom counts in the _chemical_formula_sum and the formula from the _atom_site* data.

Atom count from _chemical_formula_sum:C77 H88 Cl2 N12 O3

Atom count from the _atom_site data: C76.75 H87.48798 Cl5.48 N12.00 CELLZ01_ALERT_1_G Difference between formula and atom_site contents detected. CELLZ01_ALERT_1_G ALERT: Large difference may be due to a symmetry error - see SYMMG tests From the CIF: _cell_formula_units_Z 2

From the CIF: _chemical_formula_sum C77 H88 Cl2 N12 O3

TEST: Compare cell contents of formula and atom_site data

atom Z*formula cif sites diff C 154.00 153.50 0.50

H 176.00 174.98 1.02

Cl 4.00 10.96 -6.96

N 24.00 24.00 0.00
O 6.00 6.00 0.00
PLAT002_ALERT_2_G Number of Distance or Angle Restraints on AtSite 14 Note

PLAT003_ALERT_2_G Number of Uiso or Uij Restrained non-H Atoms ... 35 Report

PLAT007_ALERT_5_G Number of Unrefined Donor-H Atoms ..... 17 Report

PLAT041_ALERT_1_G Calc. and Reported SumFormula Strings Differ Please Check

PLAT042_ALERT_1_G Calc. and Reported MoietyFormula Strings Differ Please Check

PLAT051_ALERT_1_G Mu(calc) and Mu(CIF) Ratio Differs from 1.0 by . 96.64 %

PLAT068_ALERT_1_G Reported F000 Differs from Calcd (or Missing)... Please Check

PLAT072_ALERT_2_G SHELXL First Parameter in WGHT Unusually Large 0.11 Report PLAT083_ALERT_2_G SHELXL Second Parameter in WGHT Unusually Large 7.58 Why ?

PLAT153_ALERT_1_G The s.u.'s on the Cell Axes are Equal ..(Note) 0.0003 Ang.

PLAT174_ALERT_4_G The CIF-Embedded .res File Contains FLAT Records 4 Report

PLAT175_ALERT_4_G The CIF-Embedded .res File Contains SAME Records 1 Report

PLAT178_ALERT_4_G The CIF-Embedded .res File Contains SIMU Records 3 Report

PLAT300_ALERT_4_G Atom Site Occupancy of >O1 is Constrained at 0.595 Check

PLAT300_ALERT_4_G Atom Site Occupancy of >O2 is Constrained at 0.74 Check

PLAT300_ALERT_4_G Atom Site Occupancy of >N11 is Constrained at 0.74 Check

PLAT300_ALERT_4_G Atom Site Occupancy of >N12 is Constrained at 0.595 Check

PLAT300_ALERT_4_G Atom Site Occupancy of <O1A is Constrained at 0.224 Check

PLAT300_ALERT_4_G Atom Site Occupancy of <O1B is Constrained at 0.183 Check

PLAT300_ALERT_4_G Atom Site Occupancy of >C47 is Constrained at 0.74 Check

PLAT300_ALERT_4_G Atom Site Occupancy of >C48 is Constrained at 0.74 Check

PLAT300_ALERT_4_G Atom Site Occupancy of >C49 is Constrained at 0.74 Check

PLAT300_ALERT_4_G Atom Site Occupancy of >C50 is Constrained at 0.74 Check

PLAT300_ALERT_4_G Atom Site Occupancy of >C51 is Constrained at 0.74 Check

PLAT300_ALERT_4_G Atom Site Occupancy of >C66 is Constrained at 0.595 Check

PLAT300_ALERT_4_G Atom Site Occupancy of >C67 is Constrained at 0.595 Check

PLAT300_ALERT_4_G Atom Site Occupancy of >C68 is Constrained at 0.595 Check

PLAT300_ALERT_4_G Atom Site Occupancy of >C69 is Constrained at 0.595 Check

PLAT300_ALERT_4_G Atom Site Occupancy of >C70 is Constrained at 0.595 Check

PLAT300_ALERT_4_G Atom Site Occupancy of <N12A is Constrained at 0.224 Check

PLAT300_ALERT_4_G Atom Site Occupancy of <N12B is Constrained at 0.183 Check

PLAT300_ALERT_4_G Atom Site Occupancy of <C66A is Constrained at 0.224 Check

PLAT300_ALERT_4_G Atom Site Occupancy of <C66B is Constrained at 0.183 Check

PLAT300_ALERT_4_G Atom Site Occupancy of <C67A is Constrained at 0.224 Check

PLAT300_ALERT_4_G Atom Site Occupancy of <C67B is Constrained at 0.183 Check

PLAT300_ALERT_4_G Atom Site Occupancy of <C68A is Constrained at 0.224 Check

PLAT300_ALERT_4_G Atom Site Occupancy of <C68B is Constrained at 0.183 Check

PLAT300_ALERT_4_G Atom Site Occupancy of <C69A is Constrained at 0.224 Check

PLAT300_ALERT_4_G Atom Site Occupancy of <C69B is Constrained at 0.183 Check

PLAT300_ALERT_4_G Atom Site Occupancy of <C70A is Constrained at 0.224 Check

PLAT300_ALERT_4_G Atom Site Occupancy of <C70B is Constrained at 0.183 Check

PLAT300_ALERT_4_G Atom Site Occupancy of >H11 is Constrained at 0.74 Check

PLAT300_ALERT_4_G Atom Site Occupancy of >H12 is Constrained at 0.595 Check

PLAT300_ALERT_4_G Atom Site Occupancy of >H48 is Constrained at 0.74 Check

PLAT300_ALERT_4_G Atom Site Occupancy of >H49 is Constrained at 0.74 Check

PLAT300_ALERT_4_G Atom Site Occupancy of >H51 is Constrained at 0.74 Check

PLAT300_ALERT_4_G Atom Site Occupancy of >H67 is Constrained at 0.595 Check

PLAT300_ALERT_4_G Atom Site Occupancy of >H68 is Constrained at 0.595 Check

PLAT300_ALERT_4_G Atom Site Occupancy of >H70 is Constrained at 0.595 Check

PLAT300_ALERT_4_G Atom Site Occupancy of <H12A is Constrained at 0.224 Check

PLAT300_ALERT_4_G Atom Site Occupancy of <H12B is Constrained at 0.183 Check

PLAT300_ALERT_4_G Atom Site Occupancy of <H67A is Constrained at 0.224 Check

PLAT300_ALERT_4_G Atom Site Occupancy of <H67B is Constrained at 0.183 Check

PLAT300_ALERT_4_G Atom Site Occupancy of <H68A is Constrained at 0.224 Check PLAT300_ALERT_4_G Atom Site Occupancy of <H68B is Constrained at 0.183 Check

PLAT300_ALERT_4_G Atom Site Occupancy of <H70A is Constrained at 0.224 Check

PLAT300_ALERT_4_G Atom Site Occupancy of <H70B is Constrained at 0.183 Check

PLAT300_ALERT_4_G Atom Site Occupancy of <O2A is Constrained at 0.26 Check

PLAT300_ALERT_4_G Atom Site Occupancy of <N11A is Constrained at 0.26 Check

PLAT300_ALERT_4_G Atom Site Occupancy of <C47A is Constrained at 0.26 Check

PLAT300_ALERT_4_G Atom Site Occupancy of <C48A is Constrained at 0.26 Check

PLAT300_ALERT_4_G Atom Site Occupancy of <C49A is Constrained at 0.26 Check

PLAT300_ALERT_4_G Atom Site Occupancy of <C50A is Constrained at 0.26 Check

PLAT300_ALERT_4_G Atom Site Occupancy of <C51A is Constrained at 0.26 Check

PLAT300_ALERT_4_G Atom Site Occupancy of <H11A is Constrained at 0.26 Check

PLAT300_ALERT_4_G Atom Site Occupancy of <H48A is Constrained at 0.26 Check

PLAT300_ALERT_4_G Atom Site Occupancy of <H49A is Constrained at 0.26 Check

PLAT300_ALERT_4_G Atom Site Occupancy of <H51A is Constrained at 0.26 Check

PLAT300_ALERT_4_G Atom Site Occupancy of >Cl1A is Constrained at 0.74 Check

PLAT300_ALERT_4_G Atom Site Occupancy of >Cl2A is Constrained at 0.74 Check

PLAT300_ALERT_4_G Atom Site Occupancy of >C1A is Constrained at 0.74 Check

PLAT300_ALERT_4_G Atom Site Occupancy of >H1A1 is Constrained at 0.74 Check

PLAT300_ALERT_4_G Atom Site Occupancy of >H1A2 is Constrained at 0.74 Check

PLAT301_ALERT_3_G Main Residue Disorder ..... Percentage = 14 Note

PLAT302_ALERT_4_G Anion/Solvent Disorder ..... Percentage = 45 Note

PLAT304_ALERT_4_G Non-Integer Number of Atoms (171.16) in Resd. # 1 Check

PLAT304_ALERT_4_G Non-Integer Number of Atoms (2.86) in Resd. # 2 Check

PLAT304_ALERT_4_G Non-Integer Number of Atoms (3.70) in Resd. # 3 Check PLAT432_ALERT_2_G Short Inter X...Y Contact O1B .. C62 .. 2.85 Ang.

PLAT432_ALERT_2_G Short Inter X...Y Contact C1 .. C47A .. 1.82 Ang.

PLAT432_ALERT_2_G Short Inter X...Y Contact C1 .. C48A .. 2.83 Ang.

PLAT432_ALERT_2_G Short Inter X...Y Contact C1 .. N11A .. 2.86 Ang.

PLAT432_ALERT_2_G Short Inter X...Y Contact C2 .. C47A .. 2.64 Ang.

PLAT432_ALERT_2_G Short Inter X...Y Contact C45 .. C47A .. 3.05 Ang.

PLAT432_ALERT_2_G Short Inter X...Y Contact C46 .. C47A .. 2.55 Ang.

PLAT432_ALERT_2_G Short Inter X...Y Contact C52 .. C47A .. 2.93 Ang.

PLAT432_ALERT_2_G Short Inter X...Y Contact C55 .. C69B .. 3.08 Ang.

PLAT605_ALERT_4_G Largest Solvent Accessible VOID in Structure ... 348 A**3

PLAT720_ALERT_4_G Number of Unusual/Non-Standard Labels ..... 2 Note PLAT773_ALERT_2_G Check long C-C Bond in CIF: C1 -- C47A . 1.82 Ang.

PLAT790_ALERT_4_G Centre of Gravity not Within Unit Cell: Resd. # 8 Note

H2 O

PLAT860_ALERT_3_G Number of Least-Squares Restraints ..... 356 Note

PLAT869_ALERT_4_G ALERTS Related to the use of SQUEEZE Suppressed ! Info

PLAT912_ALERT_4_G Missing # of FCF Reflections Above STh/L= 0.600 340 Note

---

0 **ALERT level A** = Most likely a serious problem - resolve or explain

2 **ALERT level B** = A potentially serious problem, consider carefully

11 **ALERT level C** = Check. Ensure it is not caused by an omission or oversight

97 **ALERT level G** = General information/check it is not something unexpected

8 ALERT type 1 CIF construction/syntax error, inconsistent or missing data

22 ALERT type 2 Indicator that the structure model may be wrong or deficient

6 ALERT type 3 Indicator that the structure quality may be low

73 ALERT type 4 Improvement, methodology, query or suggestion

1 ALERT type 5 Informative message, check

It is advisable to attempt to resolve as many as possible of the alerts in all categories. Often the minor alerts point to easily fixed oversights, errors and omissions in your CIF or refinement strategy, so attention to these fine details can be worthwhile. In order to resolve some of the more serious problems it may be necessary to carry out additional measurements or structure refinements. However, the purpose of your study may justify the reported deviations and the more serious of these should normally be commented upon in the discussion or experimental section of a paper or in the "special_details" fields of the CIF. checkCIF was carefully designed to identify outliers and unusual parameters, but every test

has its limitations and alerts that are not important in a particular case may appear. Conversely, the absence of alerts does not guarantee there are no aspects of the results needing attention. It is up to the individual to critically assess their own results and, if necessary, seek expert advice.

Publication of your CIF in IUCr journals

A basic structural check has been run on your CIF. These basic checks will be run on all CIFs submitted for publication in IUCr journals (*Acta Crystallographica*, *Journal of Applied Crystallography*, *Journal of Synchrotron Radiation*); however, if you intend to submit to *Acta Crystallographica Section C* or *E* or *IUCrData*, you should make sure that full publication checks are run on the final version of your CIF prior to submission.

Publication of your CIF in other journals

Please refer to the *Notes for Authors* of the relevant journal for any special instructions relating to CIF submission.

PLATON version of 11/08/2016; check.def file version of 04/08/2016

Datablock shelx - ellipsoid plot

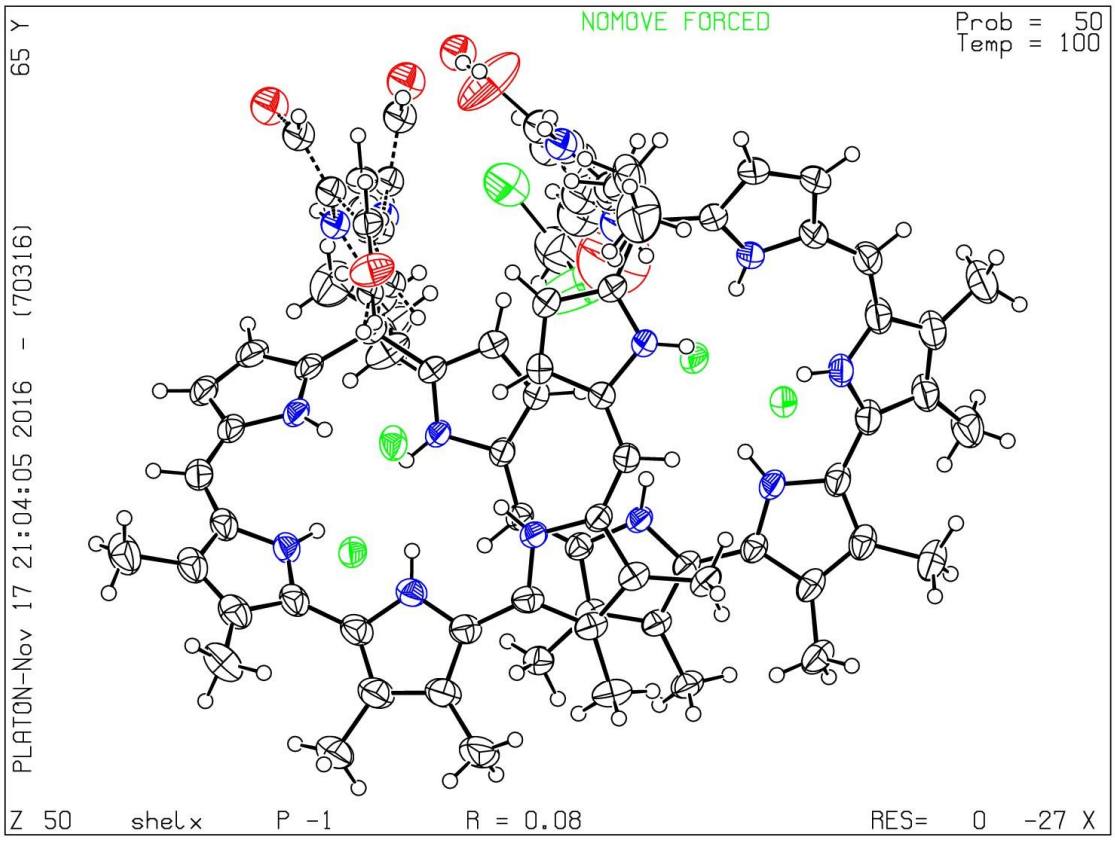

Bibliography

(1) Busschaert, N.; Caltagirone, C.; Van Rossom, W.; Gale, P. A. Applications of Supramolecular Anion Recognition. *Chem. Rev.* **2015,** *115* (15), 8038.

(2) Kunz, W.; Henle, J.; Ninham, B. W. 'Zur Lehre von der Wirkung der Salze' (about the science of the effect of salts): Franz Hofmeister's historical papers. *Curr. Opin. Colloid In.* **2004,** *9* (1–2), 19.

(3) Bose, P.; Ghosh, P. Visible and near-infrared sensing of fluoride by indole conjugated urea/thiourea ligands. *Chem. Comm.* **2010,** *46* (17), 2962.

(4) Bose, P.; Ahamed, B. N.; Ghosh, P. Functionalized guanidinium chloride based colourimetric sensors for fluoride and acetate: single crystal X-ray structural evidence of -NH deprotonation and complexation. *Org. & Biomol. Chem.* **2011,** *9* (6), 1972.

(5) Arimori, S.; Davidson, M. G.; Fyles, T. M.; Hibbert, T. G.; James, T. D.; Kociok-Kohn, G. I. Synthesis and structural characterisation of the first bis(bora)calixarene: a selective, bidentate, fluorescent fluoride sensor. *Chem. Comm.* **2004,** (14), 1640.

(6) Bazzicalupi, C.; Biagini, S.; Bencini, A.; Faggi, E.; Giorgi, C.; Matera, I.; Valtancoli, B. ATP Recognition and sensing with a phenanthroline-containing polyammonium receptor. *Chem. Comm.* **2006,** (39), 4087.

(7) Yoon, J.; Kim, S. K.; Singh, N. J.; Lee, J. W.; Yang, Y. J.; Chellappan, K.; Kim, K. S. Highly Effective Fluorescent Sensor for H2PO4. *J. Org. Chem.* **2004,** *69* (2), 581.

(8) Sanchez, G.; Espinosa, A.; Curiel, D.; Tarraga, A.; Molina, P. Bis(carbazolyl)ureas as Selective Receptors for the Recognition of Hydrogenpyrophosphate in Aqueous Media. *J. Org. Chem.* **2013,** *78* (19), 9725.

(9) Zeng, Z.; Torriero, A. A. J.; Bond, A. M.; Spiccia, L. Fluorescent and Electrochemical Sensing of Polyphosphate Nucleotides by Ferrocene Functionalised with Two ZnII(TACN)(pyrene) Complexes. *Chem. Eur. J.* **2016,** *16* (30), 9154.

(10) Singh, A. S.; Sun, S.-S. Recognition, Encapsulation, and Selective Fluorescence Sensing of Nitrate Anion by Neutral C3-Symmetric Tripodal Podands Bearing Amide Functionality. *J. Org. Chem.* **2012,** *77* (4), 1880.

(11) Metzger, A.; Anslyn, E. V. A Chemosensor for Citrate in Beverages. *Angew. Chem. Int. Ed.* **1998,** *37* (5), 649.

(12) Sokkalingam, P.; Kim, D. S.; Hwang, H.; Sessler, J. L.; Lee, C.-H. A dicationic calix[4]pyrrole derivative and its use for the selective recognition and displacement-based sensing of pyrophosphate. *Chem. Sci.* **2012,** *3* (6), 1819.

(13) Moyer, B. A.; Custelcean, R.; Hay, B. P.; Sessler, J. L.; Bowman-James, K.; Day, V. W.; Kang, S.-O. A Case for Molecular Recognition in Nuclear Separations: Sulfate Separation from Nuclear Wastes. *Inorg. Chem.* **2013,** *52* (7), 3473.

(14) Marcus, Y. *Ion prop.*; Marcel Dekker: New York, 1997.

(15) Kang, S. O.; Powell, D.; Bowman-James, K. Anion Binding Motifs: Topicity and Charge in Amidocryptands. *J. Am. Chem. Soc.* **2005,** *127* (39), 13478.

(16) Eller, L. R.; Stępień, M.; Fowler, C. J.; Lee, J. T.; Sessler, J. L.; Moyer, B. A. Octamethyl-octaundecylcyclo[8]pyrrole: A Promising Sulfate Anion Extractant. *J. Am. Chem. Soc.* **2007,** *129* (36), 11020.

(17) Borman, C. J.; Custelcean, R.; Hay, B. P.; Bill, N. L.; Sessler, J. L.; Moyer, B. A. Supramolecular organization of calix[4]pyrrole with a methyl-trialkylammonium anion

exchanger leads to remarkable reversal of selectivity for sulfate extractionvs.nitrate. *Chem. Comm.* **2011,** *47* (27), 7611.
(18) Kim, S. K.; Lee, J.; Williams, N. J.; Lynch, V. M.; Hay, B. P.; Moyer, B. A.; Sessler, J. L. Bipyrrole-Strapped Calix[4]pyrroles: Strong Anion Receptors That Extract the Sulfate Anion. *J. Am. Chem. Soc.* **2014,** *136* (42), 15079.
(19) Jia, C.; Wu, B.; Li, S.; Huang, X.; Zhao, Q.; Li, Q. S.; Yang, X. J. Highly Efficient Extraction of Sulfate Ions with a Tripodal Hexaurea Receptor. *Angew. Chem. Int. Ed.* **2016,** *50* (2), 486.
(20) Sessler, J. L.; Zimmerman, R. S.; Bucher, C.; Kral, V.; Andrioletti, B. Calixphyrins. Hybrid macrocycles at the structural crossroads between porphyrins and calixpyrroles. *Pure Appl. Chem.* **2001,** *73* (7), 1041.
(21) Král, V.; Sessler, J. L.; Zimmerman, R. S.; Seidel, D.; Lynch, V.; Andrioletti, B. Calixphyrins: Novel Macrocycles at the Intersection between Porphyrins and Calixpyrroles. *Angew. Chem. Int. Ed.* **2000,** *39* (6), 1055.
(22) Chatterjee, T.; Ghosh, A.; Madhu, S.; Ravikanth, M. Stable core-modified calixsmaragdyrins: synthesis, structure and specific sensing of the hydrogen sulfate ion. *Dalton Trans.* **2014,** *43* (16), 6050.
(23) Bernátková, M.; Andrioletti, B.; Král, V.; Rose, E.; Vaissermann, J. Synthesis of Functional meso-Aryl Porphomonomethenes and Porphodimethenes: Application to the Preparation of a Chiral Calix[4]phyrin Dimer. *J Org. Chem.* **2004,** *69* (23), 8140.
(24) Gale, P. A.; Dehaen, W. *Anion Recognition in Supramolecular Chemistry*; Springer-Verlag Berlin Heidelberg, 2010.
(25) Lehn, J. M. *Angew. Chem. Int. Ed. Eng.* **1988,** *27*, 89.
(26) Beer, P. D.; Cheetham, A. G.; Drew, M. G. B.; Fox, O.; Hayes, E. J.; Rolls, T. D. *Dalton Trans.* **2003**, 603.
(27) Fox, O.; Rolls, T. D.; Drew, M. G. B.; Beer, P. D. *Chem. Commun.* **2001**, 1632.
(28) Bucher, C.; Zimmerman, R. S.; Lynch, V.; Sessler, J. L. *J. Am. Chem. Soc.* **2001,** *123*, 9716.
(29) Bucher, C.; Zimmerman, R. S.; Lynch, V.; Sessler, J. L. *Chem. Commun.* **2003**, 1646.
(30) Setsune, J.-I.; Watanabe, K. *J. Am. Chem. Soc.* **2008,** *130*, 2404.
(31) Mateus, P.; Delgado, R.; Brandao, P.; Carvalho, S.; Felix, V. Selective recognition of tetrahedral dianions by a hexaaza cryptand receptor. *Org. Biomol. Chem.* **2009,** *7* (22), 4661.
(32) Kintzinger, J. P.; Lehn, J. M.; Kauffmann, E.; Dye, J. L.; Popov, A. I. Anion coordination chemistry. Chlorine-35 NMR studies of chloride anion cryptates. *J. Am. Chem. Soc.* **1983,** *105* (26), 7549.
(33) Motekaitis, R. J.; Martell, A. E.; Dietrich, B.; Lehn, J. M. Anion binding in macrobicyclic metal cryptate complexes: copper(II)-BISTREN. *Inorg. Chem.* **1984,** *23* (11), 1588.
(34) Jazwinski, J.; Lehn, J.-M.; Lilienbaum, D.; Ziessel, R.; Guilhem, J.; Pascard, C. Polyaza macrobicyclic cryptands: synthesis, crystal structures of a cyclophane type macrobicyclic cryptand and of its dinuclear copper(I) cryptate, and anion binding features. *J. Chem. Soc., Chem. Comm.* **1987,** (22), 1691.
(35) Dietrich, B.; Fyles, T. M.; Hosseini, M. W.; Lehn, J.-M.; Kaye, K. C. Proton coupled membrane transport of anions mediated by cryptate carriers. *J. Chem. Soc., Chem. Comm.* **1988,** (11), 691.
(36) Dietrich, B.; Lehn, J.-M.; Guilhem, J.; Pascard, C. Anion receptor molecules : Synthesis of an octaaza-cryptand and structure of its fluoride cryptate. *Tet. Lett.* **1989,** *30* (31), 4125.

(37) Grell, D.; Grell, E.; Bugnon, P.; Dietrich, B.; Lehn, J. M. Molecular Ionics of Anion Receptor Molecules: A Microcalorimetric Study. *J. Therm. Anal. Calorim.* **2004,** *77* (2), 483.
(38) Motekaitis, R. J.; Utley, W. B.; Martell, A. E. Iron(II) and sulfate binding by the binucleating ligands O-BISDIEN, O-BISTREN, and O-BISBAMP. *Inorg. Chim. Acta* **1993,** *212* (1-2), 15.
(39) Chen, D.; Motekaitis, R. J.; Murase, I.; Martell, A. E. The synthesis of binucleating polyaza macrocyclic and macrobicyclic ligands and the dioxygen affinities of their cobalt complexes. *Tetrahedron* **1995,** *51* (1), 77.
(40) Schmidtchen, F. P. Synthese makrotricyclischer Amine. *Chem. Ber.* **1980,** *113* (3), 864.
(41) Schmidtchen, F. P.; Muller, G. Anion inclusion without auxiliary hydrogen bonds: X-ray structure of the iodide cryptate of a macrotricyclic tetra-quaternary ammonium receptor. *J. Chem. Soc., Chem. Comm.* **1984,** (16), 1115.
(42) Schmidtchen, F. P. Inclusion of anions in macrotricyclic quaternary ammonium salts. *Angew. Chem.* **1977,** *89* (10), 751.
(43) Zhang, Z.; Cha, W.-Y.; Williams, N. J.; Rush, E. L.; Ishida, M.; Lynch, V. M.; Kim, D.; Sessler, J. L. Cyclo[6]pyridine[6]pyrrole: A dynamic, Twisted Macrocycle with No Meso Bridges. *J. Am. Chem. Soc.* **2014**, 7591.
(44) Thordarson, P. Determining association constants from titration experiments in supramolecular chemistry. *Chem. Soc. Rev.* **2011,** *40* (3), 1305.
(45) www.supramolecular.org.